Czech Technical University in Prague

Faculty of Nuclear Science and Physical Engineering

DIPLOMA THESIS

B-QUARK PRODUCTION IN SEMILEPTONIC DECAYS ON ATLAS AT LHC

Jaroslav Günther

Supervisor: prom.fyz. Václav Vrba, CSc.

7.5.2010

Acknowledgements

I would like to thank especially to my supervisor Václav Vrba for offering me the topic for this thesis, for his valuable guidance and providing me a lot of experience with the current physical praxis in the field of particle physics. I am very thankful to Maria Smizanska for discussions about the decay chanels with J/ψ (bound state $c\bar{c}$ quarks) one of which I tried to analyze and to Wolfgang Walkoviak for discussions about the analysis of the decay $B^+ \to J/\psi\mu^+\mu^-$. His insights helped me to solve numerous problems that came up in my analyses. I appreciate very much the aid of Pavel Řezníček and Ioannis Nomidis from whom I got valuable advices about object-oriented programming for creating B physics algorithms and about TAG analysis. I was aided particularly by James Catmore in data analysis techniques and ganga software. I should thank my colleague Pavel Jež for introducing me to the Athena framework and for useful hints about LaTeX and ROOT. I am also grateful to Guido Negri, Xavier Espinal and Jiří Chudoba for many useful discussions about GRID and for helping me with computing issues related to GRID shifts I participated in. Not least word of thanks go to Institute of Physics in Prague whereby I was allowed to spend several months in the CPPM and CERN laboratories which gives me very much, not only of the b-physics point of view. This thesis mostly rest on the experience and informations I gathered there.

Prohlášení

Prohlašuji, že jsem svou diplomovou práci vypracoval samostatně a použil jsem pouze podklady uvedené v přiloženém seznamu.

Nemám závažný důvod proti užití tohoto školního díla ve smyslu §60 Zákona č. 121/2000 Sb., o právu autorském, o právech souvisejících s právem autorským a o změně některých zákonů (autorský zákon).

Declaration

I declare that I wrote my diploma thesis independently and exclusively with the use of cited bibliography.

I agree with the usage of this thesis in the purport of the Act 121/2000 (Copyright Act).

Praha, 7.5.2010 Jaroslav Günther

Název práce:
Studium produkce b-kvarku v semileptonických rozpadech pomocí aparatury ATLAS na urychlovači LHC

Autor: Jaroslav Günther

Obor: Matematické inženýrství

Druh práce: Diplomová práce

Vedoucí práce: prom.fyz. Václav Vrba, CSc. Katedra fyziky, Fakulta jaderná a fyzikálně inženýrská, České vysoké učení technické v Praze

Abstrakt:

Čtenáři je na počátku práce předložena teorie narušení CP symetrie v rozpadech neutralních b-mesonů. Teoretický formalismus přechází v potřebu konkrétních experimentálních měření pro ověření, popřípadě dalšímu rozvoji fyzikálního pohledu na realitu. Tato pozorování jsou realizovaná detektorem ATLAS, který je následně popsán. Autor se více zabývá výhledy měření zde prezentovaných radiativních, hadronových, čistě mionových a semileptonových b-rozpadů v experimentu ATLAS. Metodika sběru dat a systém triggeru jsou popsány dále s ohledem na b rozpady. Jelikož v průbehu psaní této práce začal ATLAS s rekonstrukcí a analýzou reálných dat, jsou zde popsány aspekty této rané fáze běhu experimentu se zaměřením na semimionové b-rozpady. Systém softwarových nástrojů a postupu analýzy je načrtnut ve třetí a poslední kapitole. Na konci práce je ukázán praktický výsledek takové analýzy za použití GRIDu.

Klíčová slova: narušení CP symetrie, ATLAS, výhledy B fyziky, analýza, GRID, raná fáze ATLAS , rozpady B-mesonů, trigger

Title: **Study of B-Quark Production in decay cannels with J/ψ on ATLAS at LHC**

Author: Jaroslav Günther

Abstract:

At the beginning this thesis gives the reader a theoretical framework of the CP violation effects in neutral B meson decays. The theoretical formalism is left in order to put emphasis on concrete description of the ATLAS experiment and its major detector parts. The measurements which are performed with help of this device may confirm or eventually extend the physical view of the reality. The author is more focused on the B physics in ATLAS and so the most important tasks in sense of B decay measurements are presented. In particular one can find the prospects in radiative, hadronic, purely muonic and semileptonic B-decays in this thesis. ATLAS data aquisition and trigger system is described concerning also specifically B decays. Since recently the ATLAS started its operation, this early stage of run is discussed and devoted primarily to the semileptonic B-decays related strategies. The system of data analysis tools with all the software is briefly outlined in the third chapter and used in the last chapter which deals with the analysis of the extensive experimental data using GRID for analysis.

Key words: CP violation, ATLAS, B physics prospects, analysis, GRID, early stage of ATLAS run, B-decays, trigger

Contents

Chapter 1

Theoretical overview

Contemporary physics was growing up from its beginning in the 17th century into two parallel directions, empirical and mathematical. Each of them has its own role. Mathematical methods are used for the description of the hypothetical physical ideas and for making mathematical interferences from these hypothesis. Such mathematical interferences can be tested empirically by mechanical generation of scientific data with use remote sensors or experimental devices such as accelerators. These tests may or may not validate the theory and this is the theorist‘s motivation. After centuries of great scientific discoveries eventually in December 1951 the first steps were done to fulfill the first official proposal (1949) of Louis de Broglie to create a European laboratory, later on of the name CERN. In another almost six decades the LHC was constructed with its a possibility to explore the physics of b flavoured hadrons with large statistics. These particles offer a very fertile testing ground for the Standard Model (SM) description of electroweak interactions.

I would like to focus on some important theoretical aspects of b decays such as the phenomenon of CP violation or the study of rare b decays [1], which are loop-suppressed in the SM and thus very sensitive to new physics effects. Such a physics reaching behind our current model will manifest itself as so called short distance effects. The deviations from the SM might emerge as the level of interactions of individual quarks. Nevertheless, one has to take into account the confinement of quarks in hadrons and so the observed results will be strongly influenced by the long distance effects at the hadronic scale. Because of these long distance effects all the listed semimuonic decays present a different behaviour even though at the quark level they can all be represented by a decay $b \to s\mu^+\mu^-$ or $\to d\mu^+\mu^-$.

Flavour changing processes that we are interested occur at low energies, at scales $\mu << M_W$. Thus it shows up to be convenient to pass from the full theory of electroweak interactions to an effective theory by removing the high-energy degrees of freedom, i.e. integrating out the W boson and all the other particles with m M_W. The rare b decays can be described by the effective Hamiltonian that was derived from the SM, see [5] and

[1]Defined as flavour changing neutral current (FCNC) transitions $b \to s$ or d forbidden at tree-level in the SM and as heavily Cabibbo-suppressed $b \to u$ transitions .

which reads:

$$\mathcal{H}^q_{eff}(b \to q) = 4\frac{G_F}{\sqrt{2}} V_{tb}V^*_{tq} \sum_{i=1}^{10} C_i(\mu)\mathcal{O}^q_i(\mu) \tag{1.1}$$

where G_F stands for Fermi constant, q is an s or d quark, $V_{tb}V^*_{tq}$ represent elements of CKM matrix, $C_i(\mu)$ are so called Wilson coefficients and $\mathcal{O}^q_i(\mu)$ are local renormalized operators. The coefficients $C_i(\mu)$ can be calculated in some perturbation theory and measurement of these coefficients can show evidence of physics beyond SM if they deviate from the SM values. Although it is a SM hamiltonian it could be also valid for many of its extensions. The basis of operators $\mathcal{O}_i$ is not complete and in new theory candidates, such as those those exhibiting left-right asymmetries, the new physics can be presented in a form of new operators.

1.1 CP violation in B system

Number of processes prediced by Standard Model has not been observed yet. Heavy quark decays are central to the international effort to test the Standard Model. Comprehensive description of all aspects of CP symmetry and its violation can be found in [3]. However, for testing the SM description of CP violation in a quantitative way, the B system appears to be most promising. Since the weak eigenstates of quarks are mixtures of the mass eigenstates, the mixing of these three generations of quarks is described by the Cabibbo-Kobayashi-Maskawa matrix. Ordering the quarks by their masses, the elements of $\hat{V}_{CKM}$ are written as follows:

$$\hat{\mathbf{V}}_{\mathbf{CKM}} = \begin{bmatrix} V_{ud} & V_{us} & V_{ub} \\ V_{cd} & V_{cs} & V_{cb} \\ V_{td} & V_{ts} & V_{tb} \end{bmatrix} \begin{bmatrix} |d\rangle \\ |s\rangle \\ |b\rangle \end{bmatrix} = \begin{bmatrix} |d'\rangle \\ |s'\rangle \\ |b'\rangle \end{bmatrix}$$

Let us assume the following nonleptonic charged-current interaction Lagrangian in terms of the electroweak eigenstates:

$$\mathcal{L}^{CC}_{int} = -\frac{g_2}{\sqrt{2}}(\overline{u}_L, \overline{c}_L, \overline{t}_L)\gamma^\mu \hat{V}_{CKM} \begin{pmatrix} d_L \\ s_L \\ b_L \end{pmatrix} W^\dagger_\mu + h.c. \tag{1.2}$$

, where gauge coupling is related to the gauge group $SU_L(2)$ and the $W^\dagger_\mu$ fields describe the charged W bosons, taken from [17]. One can immediatelly see that the elements of the CKM matrix stand there for charged current couplings. The elements of this matrix describe the probability of transition $|V_{q\overline{q}}|^2$ from one to another quark q. If we do not leave the generation of the mass then the size of this transition probability is larger than in the case of transition probabilities between different generations. The remoter two generations we consider the smaller the probability is. The smallest transition probability is between first and third generation. The unitarity of the CKM matrix assures that the elementary vertices involving neutral gauge bosons (G, Z^0, γ) and the neutral Higgs are flavour conserving.Let us look at quark mixing matrix in a little bit more detaile. If we had N generations of matter that would mean N^2 arbitrary parametres in our unitary matrix.

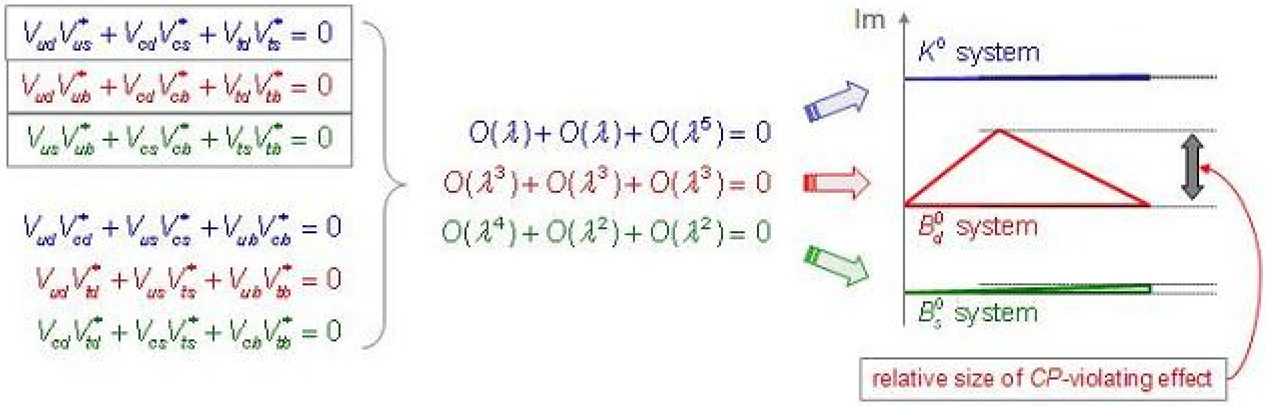

Figure 1.1: Interesting Unitary Triangles which involves different physical processes and indicate the strenght of the CP violation effect as the size of the imaginary axis and the shape of the triangle is proportional to the order of power of λ in the relevant addend of the sum.

However no all of them have physical content. Some parameters could be hidden in the field redefinition. By redefinition is meant that if one do this process no parameters go to any observable. We are allowed always to redefine the phase of any field. For example matrix $\mathbf{V_{ij}}$ is coupling up quark to down quark which if are redefined at the same time like the matrix nothing changes $u_i \to \mathrm{e}^{i\phi_i}u_i$; $d_j \to \mathrm{e}^{i\theta_j}d_j \Rightarrow \quad \mathbf{V_{ij}} \to \mathrm{e}^{i(\theta_j-\phi_i)}\mathbf{V_{ij}}$

In case of N generations there is possible to redefine in this way $2N-1$ arbitrary phases. After some careful counting one could investigate that physicaly relevant parameters are $\frac{1}{2}N(N-1) =$ moduli and $\frac{1}{2}(N-1)(N-2)$ complex phases. If there was one generation there would be nothing to mix. In case of two families there is only one parameter - moduli called Cabibbo angle but no complex phase which is essential to violate CP symmetry which is therefore exact symmetry of this two-family lagrangian. Nowdays we know 3 generations and due to sizeable CP violation e.g. in B^0 decays we know that it is the minimal number of families. There are 3 moduli (angles) and one phase. So-called Cabibbo-Kobayashi-Maskawa (CKM) matrix after parametrization $c_{ij} = cos\ \theta_{ij}$; $s_{ij} = sin\ \theta_{ij}$ or so-called Wolfenstein parametrizatiton [63] which uses 4 real parameters $\lambda = s_{12}c_{13} \approx 0.22,\ A,\ \rho,\ \eta$ looks like:

$$\hat{\mathbf{V}}_{\mathbf{CKM}} = \begin{bmatrix} c_{12}c_{13} & s_{12}c_{13} & s_{13}e^{-i\delta_{13}} \\ -s_{12}c_{23} - c_{12}s_{23}s_{13}e^{i\delta_{13}} & c_{12}c_{23} - s_{12}s_{23}s_{13}e^{i\delta_{13}} & s_{23}c_{13} \\ s_{12}s_{23} - c_{12}c_{23}s_{13}e^{i\delta_{13}} & -c_{12}s_{23} - s_{12}c_{23}s_{13}e^{i\delta 13} & c_{23}c_{13} \end{bmatrix}$$

$$\approx \begin{bmatrix} 1-\frac{\lambda^2}{2} & \lambda & A\lambda^3(\rho - i\eta) \\ -\lambda & 1-\frac{\lambda^2}{2} & A\lambda^2 \\ A\lambda^3(1-\rho-i\eta) & -A\lambda^2 & 1 \end{bmatrix} + \mathcal{O}(\lambda^4) \tag{1.3}$$

The unitarity of the CKM matrix imposes strong constraints on its elements: $\sum_{ij} V_{ij}V_{ij}^\dagger = \delta_{ij}$. This leads to a set of 12 equations, consisting of 6 normalization and 6 orthogonality relations. The latter is usually presented as 6 triangles, see Fig. 1.1, in the complex plane, which all have the same area [76]. However, only two of them agree at leading order magnitude $O(\lambda^3)$, while in the remaining ones, one side is suppressed relative to the

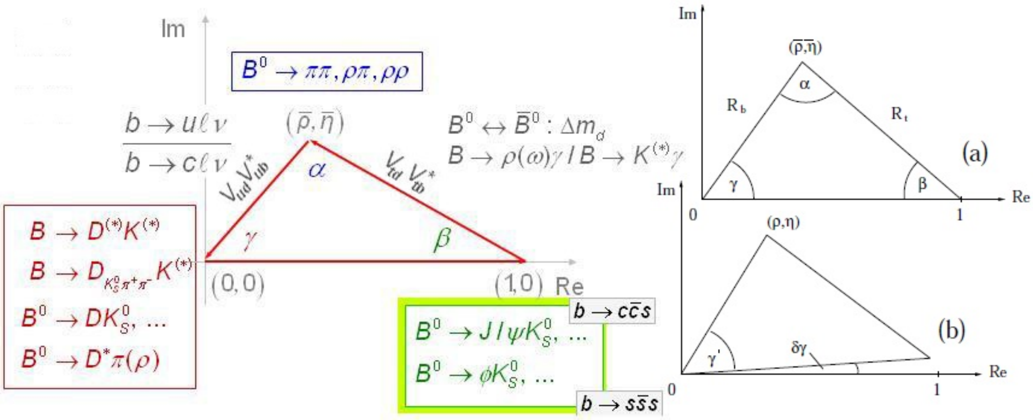

Figure 1.2: Picture of the Unitarity Triangle indicate the examples of B decay modes which give access to its angles and sides. The two non-squashed unitarity triangles of the CKM matrix: (a) and (b) correspond to the orthogonality relations $V_{ud}V_{ub}^* + V_{cd}V_{cb}^* + V_{td}V_{tb}^* = 0$ and $V_{ud}^*V_{ub} + V_{cd}^*V_{cb} + V_{td}^*V_{tb} = 0$ respectively

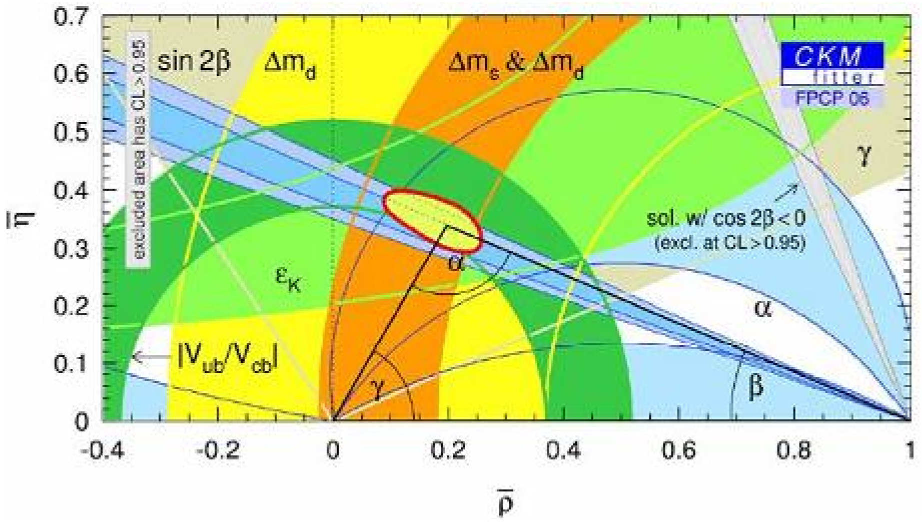

Figure 1.3: Illustration of the current experimental constraints on the CKM Unitarity Triangle.

others by $O(\lambda^2)$ and $O(\lambda^4)$. From these two triangles $V_{ud}V_{ub}^* + V_{cd}V_{cb}^* + V_{td}V_{tb}^* = 0$ and $V_{ud}^*V_{ub} + V_{cd}^*V_{cb} + V_{td}^*V_{tb} = 0$ we finally have to deal with a single triangle at this order, which is usually referred to as the unitarity triangle of the CKM matrix, see Figure 1.1. If each member of this equation is divided by the best-known one, $V_{cd}V_{cb}^*$, the most commonly used unitarity triangle arises. See the Figure 1.2. Due to the complex conjugate members we are able to test if this matrix is complex or real and also whether the CP is violated or is not. We have there many different ways how to measure these sides of the triangle with many independent observables. Up to now measurements of many decays e.g. $B^0 - \overline{B}^0$ or $B_s - \overline{B}_s$ mixing are all consistent. It was shown following picture of the behaviour of nature, see Figure 1.3. From this point of view is CP violation very rare effect whether thanks to small CP assymmetry or due to suppresed decay rates.

The experimental accuracy of ATLAS is so precise then we have to take into account even the next-to-leading order terms $O(\lambda^4)$ of the Wolfenstein expansion, and distinguish between the unitarity triangles described by $V_{ud}V_{ub}^* + V_{cd}V_{cb}^* + V_{td}V_{tb}^* = 0$ and $V_{ud}^*V_{ub} + V_{cd}^*V_{cb} + V_{td}^*V_{tb} = 0$ which are illustrated in Fig.1.2. The parameters $\overline{\eta}$ and $\overline{\rho}$ are related to the Wolfstein parameters through $\overline{\eta} = \eta(1 - \frac{1}{2}\lambda^2)$, $\overline{\rho} = \rho(1 - \frac{1}{2}\lambda^2)$. The sides R_b and R_t of the unitarity triangle shown in Fig. 1(a) are given as follows: $R_b = (1 - \frac{\lambda^2}{2})\frac{1}{\lambda}\left|\frac{V_{ub}}{V_{cb}}\right| = \sqrt{\overline{\rho}^2 + \overline{\eta}^2} = 0.41 \pm 0.07$ and $R_t = \frac{1}{\lambda}\left|\frac{V_{td}}{V_{cb}}\right| = \sqrt{(1-\overline{\rho})^2 + \overline{\eta}^2} = \mathcal{O}(1)$ [17].

There exists three ways how to violate CP symmetry, see [63]: CP violation in mixing of the neutral flavour-antiflavour systems, which is e.g. dominant mechanism for K^0-$\overline{K}^0$ systems, then CP Violation in interference between decays with and without mixing - these are called 'indirect' CP violation and the last possibility is called 'direct' - CP violation in the decay by interference of decay amplitudes with different phases. Effects of mixing of particles with their antiparticles (particle-antiparticle oscillation) and of CP violation, which are not at all synonymous, were predicted and discovered firstly in the system of the neutral strange mesons $K^0 - \overline{K}^0$, then also quite recently in the neutral B meson systems. Thus, there are also transitions to change the B_q^0 to antimeson $\overline{B}_q^0$ and conversely by exchanging W bosons between the b quarks and so the quark content is changed. see Fig. 1.4. The sum over all possible three coupling constants lead us to the unitary triangle which belong to the mixing process as in the picture 1.1. From the figure 1.4 and the fact that the B^0 and $\overline{B}^0$ decay further to fermions we have there two different interfering quantum paths (amplitudes) for going directly from B^0 to final state and the second corresponds to the transformation B^0 to $\overline{B}^0$ which then decays to the same final state. Through the interference we can be sensitive to the complex phase also investigate the CP violation.The V_{ts} has one power of λ less than the V_{td}. Moreover the frequency with which B mesons mix from one to another depends on the streght of the couplings. By the reason of that the coupling by the $B_d^0 - \overline{B}_d^0$ mixing in bigger than the one by the $B_s^0 - \overline{B}_s^0$ mixing system and the oscillation $B_d^0 - \overline{B}_d^0$ is slower. Experimentally it is difficult to decide whether the state was B^0 or $\overline{B}^0$ at the time it decayed.The cleanest but hardest way is to identify the flavor reconstructing a particular exclusive decay channel. However, in the B system the branching ratios to any final state are small and the reconstruction efficiencies are low. The other way is to use as flavor indicator the sign of the lepton in the semileptonic decay.

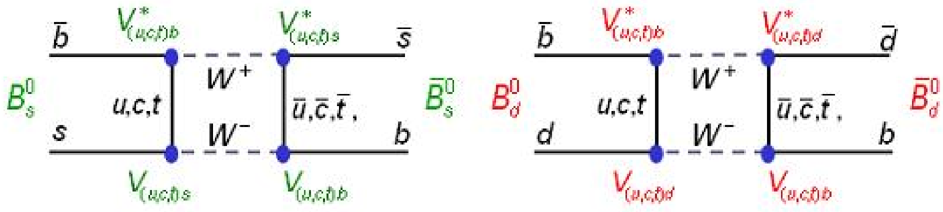

Figure 1.4: Feynman diagrams of $B^0_q - \overline{B}^0_q$ mixing , $q \; = \; d, s$

1.2 $B^0_q - \overline{B}^0_q$ oscillation

In this subsection I am not going to be concerned about details of the theory which one could find for example in the following reference [17], [5]. A state that is initially a superposition of flavour eigenstated $B^0_q = (\bar{b}q)$ and $\overline{B}^0_q = (b\bar{q})$. These states are degenerate in pure QCD. The consequent action of the operators of parity and charge conjugation on these states introduces phases that depend on the state flavour such as:

$$CP|B^0_q\rangle = e^{+i\varphi_{\overline{B}^0_q}}\,|\overline{B}^0_q\rangle \quad \text{and} \quad CP|\overline{B}^0_q\rangle = e^{-i\varphi_{B^0_q}}\,|B^0_q\rangle \tag{1.4}$$

The resulting phases are arbitrary and they does not have a physical manifest because of the flavour symmetry of the strong interaction. If CP is conserved by the dynamics, $[CP, \mathcal{H}] = 0$, then the corresponding decay amplitudes of these two states have the same magnitude and an arbitrary relative phases. The initial state as a superposition of $B^0_q, \overline{B}^0_q$ will evolve acquiring decay components that correspond to all possible final states (f_i) such as $|\psi(t)\rangle = a(t)|B^0_q\rangle + b(t)|\overline{B}^0_q\rangle + c_1(t)|f_1\rangle + ...$ In B meson mixing we are interested only in evolution of the values $a(t)$ and $b(t)$ at times much larger than the strong interaction scale then we are allowed to use simplified time evolution determined by 2×2 Hamiltonian matrix, see [17];

$$\mathbf{H} = \mathbf{M} - \frac{i}{2}\mathbf{\Gamma} = \begin{bmatrix} M & M_{12} \\ M^*_{12} & M \end{bmatrix} - \frac{i}{2}\begin{bmatrix} \Gamma & \Gamma_{12} \\ \Gamma^*_{12} & \Gamma \end{bmatrix} \tag{1.5}$$

$\mathbf{M}$ and $\mathbf{\Gamma}$ correspond to meson-antimeson transitions. The diagonal elements of both are associated with flavour conserving transitions. The off-diagonal elements of $\mathbf{M}$ arise from virtual (M_{12}) interediate states while Γ_{12} of $\mathbf{\Gamma}$ stand for a real ones, in the latter case corresponding to the same decay channels of B^0_q, $\overline{B}^0_q$. After solving the eigenvalue problem [63] we receive mutually orthogonal physical 'heavy' and 'light' eigenstates B_H , B_L respectively, corresponding to the eigenvalues $M_{H,L} - \frac{i}{2}\Gamma_{H,L}$ so that the eigenvectors of $\mathbf{H}$ have well defined masses and decay widths and the differences between their heavy and light parts reads:

$$\Delta\Gamma_q \equiv \Gamma^{(q)}_H - \Gamma^{(q)}_L = \frac{2\Re(M^{(q)*}_{12}\Gamma^{(q)}_{12})}{|M^{(q)}_{12}|} \qquad \Delta m_q \equiv M^{(q)}_H - M^{(q)}_L = 2|M^{(q)}_{12}| \tag{1.6}$$

[2] Δm_q is positive by definition and $\Delta\Gamma_q$ is under the SM defined as to have negative value for the case of B_s mesons, where the sizable width difference is expected.

[2] $\Re$ denotes the real part.

I will summarize the results characteristics of this mixing into which the reference [5] is more concerned. The relative size of plenty of contributions to this process is guided by CKM matrix elements and quark masses. Let us denote $\lambda_i^{(q)} = V_{iq}^* V_{ib}$, where i and g represent the corresponding quark. Further I will denote the magnitudes in power of the Wolfstein parameter λ we have:

$$\begin{gathered}\lambda_u^{(d)} \sim \lambda_c^{(d)} \sim \lambda_t^{(d)} \sim \lambda^3 \quad \text{for } B_d \\ \text{and} \\ \lambda_u^{(s)} \sim \lambda^4,\ \lambda_c^{(s)} \sim \lambda_t^{(s)} \sim \lambda^2 \quad \text{for } B_s.\end{gathered} \tag{1.7}$$

The amplitude of the box diagram Fig. 1.4 strongly grows with large internal quark masses $m_i >> m_b$, proporsional to the m_i^2, and it happens that the top is very heavy. For $m_i >> M_W$, it is clear, considering the above CKM hierarchy, that the top quark contribution completely dominates the dispersive part M_{12}. The remaining contributions $(i = u, c)$ are really negligible for both the B_d and B_s system. Since $m_t, M_W >> m_b, M_{12}$ can be described by an effectively local interaction already at scales far above m_b. External mass scales can thus be neglected and the resulting effective Hamiltonian is governed by a single operator and has the following form:

$$\mathcal{H}_{eff} = (V_{tq}^* V_{tb})^2 C(x_t) (\overline{q}b)_{V-A} (\overline{q}b)_{V-A} \tag{1.8}$$

, where $C(x_t)$ is the short distance Wilson coefficient [5], $x_t = \frac{m_t^2}{m_W^2}$, $V - A$ refers to the Lorentz structures $\gamma_\mu(1-\gamma^5)$ and the dispersive M_{12} has the following form:

$$M_{12} = \frac{1}{2M_B} \langle B|\mathcal{H}_{eff}|\overline{B}\rangle \tag{1.9}$$

Since the top quark contribution can not contribute to Γ_{12} due to the kinematics which forbid them (as on-shell final states of B decays), this absorptive part Γ_{12} is determined by the absorptive parts of box diagrams with u and c quarks. Actually both of them show to be important of the same way for B_d since $\lambda_u^{(d)} \sim \lambda_c^{(d)}$ and for B_s the charm quark only is of interest because of the following relation $\lambda_u^{(s)} << \lambda_c^{(s)}$. In order to calculate the Γ_{12} the heavy W- boson corresponding lines in Fig. 1.4 can be replaced contracted into a single point forming a local four-quark interaction. These u and d quarks appear to be lighter than the relevant scale of the process ($\sim$ mass of b quark) and so they can not be integrated out. This results in Γ_{12} of the form of non local product of two local Hamiltonian operators $\mathcal{H}_{eff}$ for the usual effective weak hamiltonian describing B decays (for more detailed description of the coefficients and operators involved please look into [5]), see below:

$$\mathcal{H}_{eff} = \frac{G_F}{\sqrt{2}} \sum_{q=u,c} \sum_{q'=d,s} V_{qb}^* V_{qq'} (\bar{b}q)_{V-A} (\overline{q}q')_{V-A} \tag{1.10}$$

$$\Gamma_{12} = \frac{1}{2M_B} Im \left(i \int d^4x \langle B|T\mathcal{H}_{eff}(x)\mathcal{H}_{eff}(0)|\overline{B}\rangle \right) \tag{1.11}$$

The cases $q = d$ and $q = s$ can be treated separately and have the same Wilson coefficients $C_i(\mu)$. Taking the absorptive part inside of this formal expression, the time ordered product of hamiltonians is transformed into an ordinary product of the two factors of hamiltonians and when we consider complete set of hadronic final states one may recognize the usual expression for a decay rate, generalized here to the non diagonal element Γ_{12}. We are therefore allowed to write Γ_{12} in the above expression as the absorptive part of the $\overline{B} \to B$ forward scattering amplitude.

$$\Gamma_{12}^{hadron}(B \to final\ state\ f) = \sum_f \langle B|\mathcal{H}_{eff}|f\rangle\langle f|\mathcal{H}_{eff}(0)|\overline{B}\rangle \tag{1.12}$$

Unfortunately this expression is really difficult to calculate due to the large momentum $\sim m_b >> \Lambda_{QCD}$ flowing through the u and d quark internal lines of the box diagram. Anyway, we are allowed to expand the operator product in the expression 1.11 into a series of local operators, again I will not come into detail for more please see [78].

$$\Gamma_{12}^{quark} = \frac{1}{2M_B}\sum_n \frac{C_n}{m_b^n}\langle B|Q_n|\overline{B}\rangle \tag{1.13}$$

Such an identification of exact Γ_{12}^{hadron} with the approximation Γ_{12}^{quark} could be understood also as to the assumption of local quark-hadron duality. Local now refers more to the context of the large energy scale m_b which is practically fixed value and which is not considered as a variabe that could aim us to some global averaging procedure. If we take a look at Γ_{12}^{hadron} as a function of m_b it may be discovered that there are some for increasing m_b exponencially suppressed oscillating terms that are related to some new decay channels. These terms are entirely missing in Γ_{12}^{quark}. To any finite order Γ_{12}^{quark} is a power serie in $\frac{\Lambda_{QCD}}{m_b}$ and in any case for $m_b \to \infty \Longrightarrow \Gamma_{12}^{quark} \to \Gamma_{12}^{hadron}$. For a realistic values of m_b if one omits higher power corrections then he obtains an error referred to as a violation of local duality. For more information see [5, 84, 17, 85, 86].

1.3 CP violation in neutral B meson decays

If we want to look at the CP violation for the decays of neutral B_q^0 mesons ($q \in \{d, s\}$) into CP self-conjugate final states $|f\langle$, in terms of weak phases we find it quite simple. The assumed final states have to satisfy the following equation:

$$(CP)|f\rangle = \pm|f\rangle \tag{1.14}$$

The CP asymmetry which is time dependent and is related to these decays then may be expressed as:

$$A_{CP}(t) \equiv \frac{\Gamma(B_q^0(t) \to f) - \Gamma(\overline{B}_q^0(t) \to f)}{\Gamma(B_q^0(t) \to f) + \Gamma(\overline{B}_q^0(t) \to f)} = \tag{1.15}$$

$$= 2e^{-\Gamma_q t}\left[\frac{A_{CP}^{dir}(B_q \to f)cos(\Delta m_q t) + A_{CP}^{mix}(B_q \to f)sin(\Delta m_q t)}{e^{-\Gamma_H^{(q)}t} + e^{-\Gamma_L^{(q)}t} + A_{\Delta\Gamma}(B_q \to f)\left(e^{-\Gamma_H^{(q)}t} - e^{-\Gamma_L^{(q)}t}\right)}\right] \tag{1.16}$$

, where the corresponding decay widths are presented as $\Gamma_H^{(q)}$, $\Gamma_L^{(q)}$, $\Gamma_q \equiv \frac{\Gamma_H^{(q)}+\Gamma_L^{(q)}}{2}$ and the mass difference between the B_q mass eigenstates reads $\Delta m_q \equiv M_H^{(q)} - M_L^{(q)}$ (oscillation frequency). In the above written definition 1.15 of the CP asymmetry A_{CP}^{dir} is separated from A_{CP}^{mix}, these parts have the following formulation:

$$A_{CP}^{dir}(B_q \to f) \equiv \frac{1 - |\xi_f^{(q)}|^2}{1 + |\xi_f^{(q)}|^2} \tag{1.17}$$

the direct effect A_{CP}^{dir} of violating the CP symmetry originates directly in the corresponding decay amplitudes,

$$A_{CP}^{mix}(B_q \to f) \equiv \frac{2\Im\{\xi_f^{(q)}\}}{1 + |\xi_f^{(q)}|^2} \tag{1.18}$$

and this part A_{CP}^{mix} represents the asymmetry caused by interference effects between $B_q^0 - \overline{B}_q^0$ mixing and decay processes. The above defined width difference $\Delta\Gamma_q$ di shows to be negligibly small in the B_d systems, however, it is expected to be sizeable in the B_s meson system [63, 18, 17, 20, 5] and so it provides an observable of the following prescription:

$$A_{\Delta\Gamma}(B_q \to f) \equiv \frac{2\Re\{\xi_f^{(q)}\}}{1 + |\xi_f^{(q)}|^2} \tag{1.19}$$

The $A_{\Delta\Gamma}$ is rather dependent quantity, it is bounded with the other companions A_{CP}^{mix} and A_{CP}^{dir} by the following relation:

$$\left[A_{CP}^{dir}(B_q \to f)\right]^2 + \left[A_{CP}^{mix}(B_q \to f)\right]^2 + \left[A_{\Delta\Gamma}(B_q \to f)\right]^2 = 1 \tag{1.20}$$

The only missing quantity that comprises all the important information about the CP violation and connects our experimental approach to the theory is the following:

$$\xi^{(q)} = \mp e^{-i\phi_q} \frac{\sum_{j=u,c} V_{jr}^* V_{jb} \langle f|\mathcal{Q}^{jr}|\overline{B}_q^0\rangle}{\sum_{j=u,c} V_{jr} V_{jb}^* \langle f|\mathcal{Q}^{jr}|\overline{B}_q^0\rangle} \tag{1.21}$$

, in which

$$\mathcal{Q}^{jr} \equiv \sum_1^2 Q_k^{jr} C_k(\mu) + \sum_3^{10} Q_k^{jr} C_k(\mu) \tag{1.22}$$

Q_k^{jr} are four-quark operators[3] , the label $r \in \{d, s\}$ corresponds to $\bar{b} \to \bar{d}$ and $\bar{b} \to \bar{s}$ transitions, and k distinguishes between current-current ($k \in \{1, 2\}$), QCD ($k \in \{3, ..., 6\}$) and EW ($k = \{7, ..., 10\}$) penguin operators. For more information about the Hamiltonian and operators, the following provides really good reference [5]. The ϕ_q is the $B_q^0 - \overline{B}_q^0$ related weak mixing phase and its relation to the angles of the triangle is:

$$\phi_q = +2\beta \quad \text{for} \quad q = d \quad \text{or} \quad \phi_q = -2\delta\gamma \quad \text{for} \quad q = s \tag{1.23}$$

The hadronic matrix elements accomodated in $\xi_f^{(q)}$ influence the value of this observable with uncomfortable uncertainties, see relation 1.21. However, if we measure a decay

[3] $\mu = O(m_b)$stands for a renormalization scale. The Q_k^{jr} operators also appear in the usual Hamiltonian of the corresponding b decay $\mathcal{H}_{eff} = \frac{G_F}{\sqrt{2}} \left[\sum_{j=u,c} V_{jr}^* V_{jb} \{\sum_1^2 Q_k^{jr} C_k(\mu) + \sum_3^{10} Q_k^r C_k(\mu)\}\right]$.

$B_q \to f$ which is dominated by a single CKM amplitude then the corresponding matrix elements cancel and $\xi_f^{(q)}$ turns out to be of the following form:

$$\xi_f^{(q)} = \mp e^{[-i(\phi_q - \phi_D^{(f)})]} \tag{1.24}$$

, where ϕ_D^f is a weak decay phase for which holds:

$$\phi_D^f = -2\gamma \quad \text{for dominant} \quad \bar{b} \to \overline{u} u \overline{r} \quad \text{CKM amplitudes} \tag{1.25}$$

or in case of dominant $\bar{b} \to \overline{c} c \overline{r}$ CKM amplitudes ϕ_D^f vanishes $\phi_D^f = 0$.

Chapter 2

Experiment ATLAS

Need of an apparatus of an energy and luminosity high enough ($14TeV$, $10^{34}cm^2s^{-1}$) to cover such a wide range of physics signatures that would be able to push our theory, guided the last half of the century. Eventually the LHC has came into being , working close to the limits of theoretically achievable accuracy. It is built in a circular tunnel which is buried from 50 to 175 m underground and has 26.659 km in circumference. It straddles the Swiss and French borders on the outskirts of Geneva. The LHC will collide 7 TeV protons together with a centre of mass energy of 14 TeV and a design luminosity of $10^{34}cm^2s^{-1}$. LHC accommodates especially one detector of my interest - ATLAS - which purpose is to uncover many new ways of insights into matter generation problems. Fusion of the particle detector engineering, trigger systems, software support, data handling development and physics behind the effort that was put into the collaboration of about 3000 physicist from 37 countries. That is how one could summarize our up-to-date journey in order to find the profound hypothesis that seem to govern nature. There are variety of events searched that could confirm one of possible explanations of spontaneous electroweak symmetry breaking such as Higgs boson that has decayed to two Z bosons each of which has decayed to an electron positron pair. The simulation gave us expectation about 1 event every 3 hours. The main goals are except the search for the Higgs boson and supersymetric particles, the investigation of CP violation in B-decays ,see chapter 1 as well as precise measurements of mass of heavy particles. As not least stands there the question, whether fermions are really fundamental. All these possible discoveries are planned for later times since it will take some time to understand the detectors and backgrounds. In order to explore all the tasks the ATLAS consist of many components which are able to detect the whole amount of accessible information with respect to our today's technical ability. The ATLAS detector consists of four major components, the Inner Tracker which measures the momentum of each charged particle, the Calorimeter which measures the energies carried by the particles, the Muon spectrometer which identifies and measures muons and the Magnet system that bends charged particles for momentum measurement.

Figure 2.1: On the left: readable information about particles in the detector. On the right: Inner detector layout

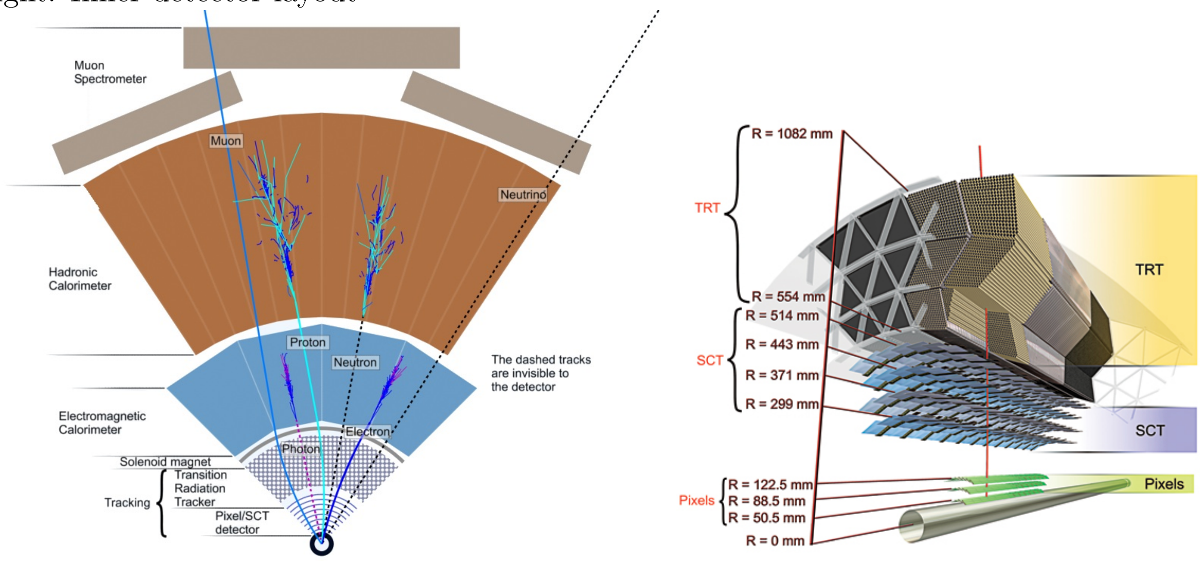

2.1 Concept of ATLAS particle identification

The ATLAS experiment consist of the detector, into which this section is focused on, meaning also the important part - trigger system. Computing and software with data handling tools are described in the next chapter. We try to identify the particles passing through the detector as shown in the Fig. 2.1.

One of the aspects of particle identification important for B-physics channel is in particular separation of kaons and pions which allow us to distinguish between the decays we are interested in from the ones with identical topologies, moreover it is crucial for tagging methods, see chapter 3.1.3

The ATLAS straw tracking system is capable to separate $e^{\pm}/\pi^{\pm}/K$ using dE/dx measurement, see further in this chapter or in chapter 4. As the track of the particle is bent by the applied magnetic field and tells us the momentum, the energy loss as a function of particle momentum can show us the mass of the particle see Fig 2.2 and [64].

2.1.1 Tracking

INNER DETECTOR (ID) is a finely segmented detector see Fig 2.1 with the purpose to record the tracks of particles. The position is measured with the accuracy in the Fig 2.3. The first two components Pixels and SCT are silicon semiconductor detectors and based on the principle of producing free charge carriers in the diode (very small voltage applied) when the particle goes through. These charge carriers drift in the electric field and induce an electrical signal on the metal electrodes.

PIXEL DETECTOR provides a very high granularity, high precision set of measurements as close to the interaction point as possible. The system determines the impact parameter resolution and the ability of the Inner Detector to find short lived particles such

Figure 2.2: On the left:Momentum vs energy loss dependence from the experimental knowledge with agreement to Bethe Bloch formula see [64] [65] and also see ATLAS performance at 900 GeV in chapter 4 . On the right: Energy losses for μ in copper - Figures taken from [63]

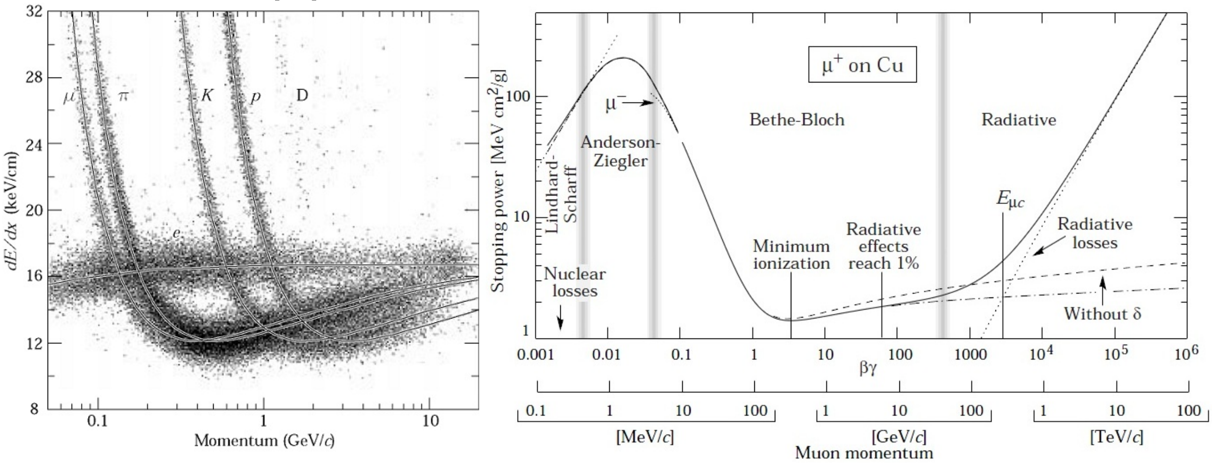

as B-Hadrons. One Pixel sensor is a 16.4 $\times$ 60.8 mm wafer (=module) of silicon with 46 080 pixels , 50 $\times$ 400 microns each. It consist of three cylindrical layers - barrels with the radial positions of 50.5 mm, 88.5 mm and 122.5 mm respectively. These three barrel layers are made of identical staves inclined with azimuthal angle of 20 degrees. There are 22, 38 and 52 staves in each of these layers respectively. Each stave is composed of 13 pixel modules. There are three disks on each side of the forward regions. One disk is made of 8 sectors, with 6 modules in each sector. Disk modules are identical to the barrel modules, except the connecting cables. Each module will be read out by 16 chips, each serving an array of 18 by 160 pixels.

SILICON PIXELS (SCT) - also called b-layer since it is vital for good vertexing (b-physics related). The SCT system is designed to provide eight precision measurements per track in the intermediate radial range, contributing to the measurement of momentum, impact parameter and vertex position. In the barrel SCT eight layers of silicon microstrip detectors are placed. Because one plate of strips can identify only which microstrip a particle has hit, two plates are placed on top of each other at a slight skew, providing precision points in the r_ϕ and z coordinates [1], using small angle stereo to obtain the z-measurement. Each silicon detector is 6.36 $\times$ 6.40 cm with 768 readout strips of 80 micron pitch. The barrel modules are mounted on carbon-fibre cylinders at radii of 30.0, 37.3, 44.7, and 52.0 cm. The end-cap modules are very similar in construction but use tapered strips with one set aligned radially. The SCT covers $|\eta| \prec 2.5$[2]. When the particle flies though the charge collection time amounts $15 - 20$ ns and current pulse of several nanoampers that is transformed into 8 bit message from each pixel is read out.

TRANSITION RADIATION TRACKER (TRT) - There exist a probability that the particle crossing the boundary between two media of different dielectric permitivity will emit an X ray photon. This detector with magnetic field of $2T$ is based on this effect of

[1]The ATLAS coordinate system is a right-handed system with the x-axis pointing to the centre of the LHC ring, the z-axis following the beam direction and the y-axis going upwards. Φ is an azimutal angle

[2]Pseudorapidity $\eta = - \ log\left(tan\ \frac{\Theta}{2}\right)$, where Θ is an angle measured from the z axis.

Figure 2.3: Resolution of the Inner detector parts in the particular directions - Figures taken from [68]

System	Element size	Resolution	η coverage
Pixels	50 $\times$ 400 μm	$\sigma_{R\phi} = 14\ \mu$m $\sigma_z = 87\ \mu$m $\sigma_R = 87\ \mu$m	$\pm$ 2.5
SCT	75 or 112.5 μm $\times$ 12 cm	$\sigma_{R\phi} = 15\ \mu$m $\sigma_z = 770\ \mu$m	$\pm$ 2.5
TRT	4 mm diameter 150 cm long	$\sigma_{R\phi} = 170\ \mu$m	$\pm$ 2.5

transition radiation turning on at ($\beta\gamma \approx 1000$) [3]. TRT is the key to distinguish between hadrons and electrons. Each track crosses 36 layers of 4 mm diameter gas-filled[4] straw tubes which act as a cathode surrounded by polyprophylen foam as a radiator. The staws are kept at high voltage of negative polarity. $30\mu m$ diameter gold-plated tungsten sense wire is centered in each of these straws. The maximum straw length is is 144 cm in the barrel, which contains about 50 000 straws, each divided in two at the center and read out at both end, to reduce the occupancy. The end-caps contain 320 000 radial straws, with the readout at the outer radius. Charged particle passing through ionizes the gas molecules which create a signal read by 420000 readout channels to measure drift time and two independent thresholds. These allow the detector to discriminate between tracking hits, which pass the lower threshold, and transition radiation hits, which pass the higher one.The barrel section is built of individual modules between 329 and 793 straws each, covering the radial range from 56 to 107 cm. Each end-cap consists of 18 wheels. The innermost 14 cover the radial range from 64 to 103 cm, while the last four extend to an inner radius of 48 cm. Wheels 7 to 14 have half as many straws per cm in z as the others, to avoid an unnecessary increase of crossed straws and material at medium rapidity. Typical TR photon energy depositions in the TRT are $810keV$, while minimum-ionizing particles, such as pions, deposit about $2keV$. For more percise measurement of the momentum TRT is combined with SCT, while the time of the TR pulse offers position resolution up to $0.17mm$.

2.1.2 Calorimetry

In contrast to the tracking strategy calorimeters are designed to absorb particle energy and prevent most of the particles to get to Muon Spectrometer. This part of the detector is designed for electromagnetic and hadron showers[5] formation when the particles get in. Finally, the energy is converted into ionization or excitation of the matter and the signal is read out as a charge directly, Cerenkov light or scintillation light both read out via corresponding photomultipliers. For neutral particles this detector system is the only tool with which we can get direct kinematic information about them.

[3] Cherenkov Radiation

[4] Xenon (70%) based which is good for X-ray absorption with the addition of CO2 (27%) and O2 (3%) to increase the electron drift velocity and for photon-quenching.

[5] Hadronic showers.are much longer and broader than electromagnetic ones.

Calorimeter is divided into several components: an electromagnetic sampling calorimeter with 'accordion-shaped' lead electrodes in the barrel and in the endcaps, a hadronic calorimeter using at copper electrodes in the endcaps, and a forward calorimeter close to the beampipe in the endcap made from copper and tungsten. In addition, presamplers consisting of one layer of LAr in front of the electromagnetic calorimeter help to correct for the energy loss in front of the calorimeter (mainly due to cryostat walls and the barrel solenoid).

The liquid argon (LAr) ELECTROMAGNETIC CALORIMETER (ECAL), see Fig.2.4, is made of lead plates as absorbers interspaced with narrow gaps of a liquid argon as the active medium. It has a spatial resolution (intrinsic) of about ≈ 11 mm at6 GeV [14]. A signal from the particles flying across the gas-gap is registered by copper electrodes and the deposited energy is measured. The size of an electromagnetic shower depends linearly on the radiation length X_0 see [64] of the calorimeter material. Pions decay directly to photons and thus also deposit their energy as electromagnetic showers. An excellent electron/jet, photon/jet and tau/jet separation is mandatory for the ATLAS electromagnetic calorimeter in order to minimize the impact of the reducible background on $H \to \gamma\gamma$ channel. Isolated high-p_T π^0 coming from jet fragmentation are a dangerous source of background and a very fine granularity of this detector is needed to distinguish between the two overlapping photons from the π_0 decay and a single isolated photon. For energy loss (in ID) measurements and correction there is a presampler consisting of an active LAr layer (with readout electrodes) with no absorbers before the electrons and photons reach EM calorimeter. This presampler is followed by 3 samling regions see Fig 2.4. The energy resolution [94] was estimated with a test beam to be $\frac{\sigma(E)}{E} = \frac{9.24\%}{\sqrt{E}} + 0.23\%$ [6] . This calorimeter is followed by the tile hadronic sampling calorimeter.

In HADRONIC TILE CALORIMETER (HCAL) the absorbing material is steel and the sensors are tiles of scintillating plastic that emit light transmitted by wavelength shifting optical fibres and converted to electrical signal by photomultiplier tubes. The tiles are arranged radially, periodically along z coordinate (direction of the beam pipe) and staggered in depth. The tiles are 3 mm thick and the total thickness of the iron plates in one period is 14 mm. Thickness of 11 interaction lengths λ at $\eta = 0$ is crucial parameter. There has to be enough material for the shower production and also reduce punch-through into the muon system to a minimum. The size of hadronic showers depends linearly on the interaction length λ see [64]of the material which is always longer than the radiation length. 10λ of active calorimeter together with the large η coverage the calorimeter ensures good resolution for high energy jets and $E_T^{missing}$ measurements important for possible supersymmetric particle signatures.Test beam energy resolution [94] for single hadrons was estimated to be $\frac{\sigma(E)}{E} = \frac{65\%}{\sqrt{E}} + 5\%$.

HADRONIC END-CAP LAr calorimeters (HEP) covers ($1.5 < |\eta| < 3.2$) is built in ATLAS as two independent wheels with outer radius 2.03 m. As an absorber copper plates are used, 25 mm thick in the upstream wheel and the second wheel farther from the interaction point accommodates 50 mm plates. In these are 8.5 mm liquid argon

[6]Energy resolution of a calorimeter reads: $\frac{\sigma(E)}{E} = \frac{a}{\sqrt{E}} + b + \frac{c}{E}$ where first is the stochastic term followed by constant term (inhomogenities, bad cell intercalibration, nonlinearities) and finally there is a noise term (EM noise, radioactivity, pile up)

Figure 2.4: On the left: Sketch of accordion structure of EM LAr calorimeter and barrel granularity. General ATLAS layout on the right. Figures taken from [110]

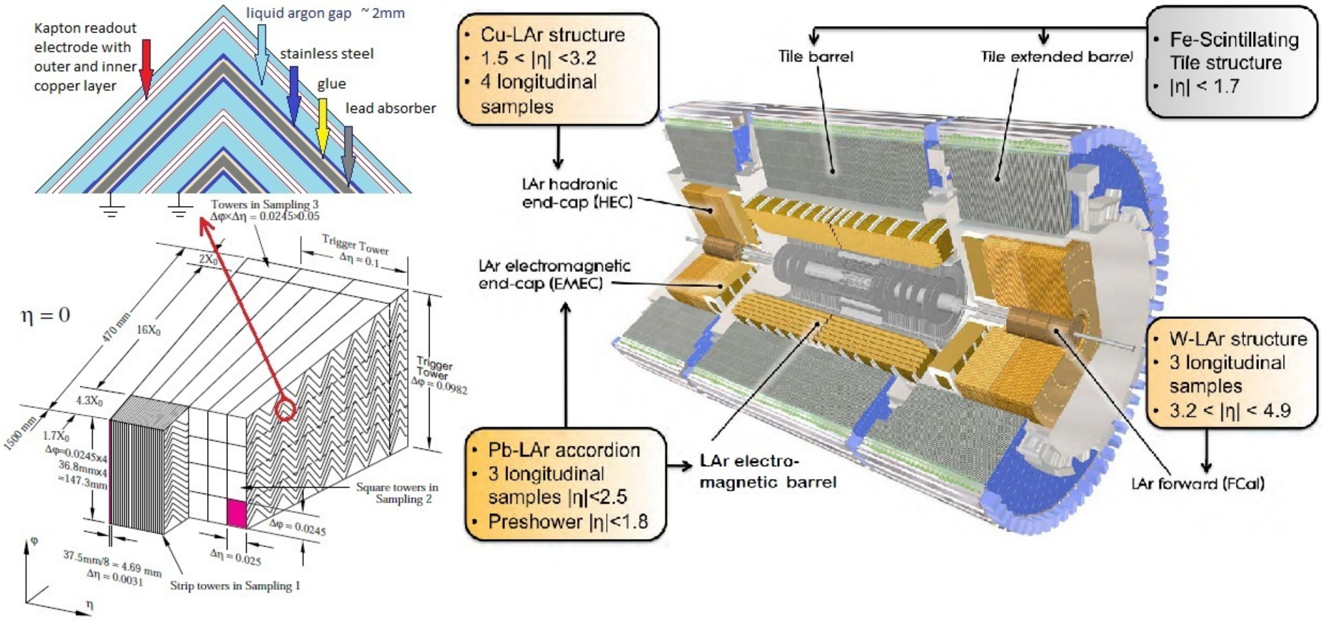

gaps between each two copper plates. The gaps are splitted with three parallel electrodes into four 1.8mm drift chambers. The central electrode serves as a readout channel and the other two layer printed circuits on either side serve only as a high voltage sources. GaAs preamplifiers mounted along the perimeter of the wheel gives the experimentator the optimal backgroung noise/signal rate.

LAr FORWARD CALORIMETER is exposed to a high level radiation doses. FCAL is integrated into the end-cap cryostat 4.7m from the interaction point. It aims to reduce the radiation background levels in the muon spectrometer. Copper forms the first section while tungsten is the material used in the other two sections of this calorimeter. These parts have a layout of metal matrix with regularly spaced longitudinal channels filled with concentric rods (positive high voltage) and tubes (grounded). Sensitive medium in the gaps is again liquid argon.

2.1.3 Muon Spectrometer

MUON SPECTROMETER forms outer part of the whole ATLAS detector. Since muons are the only charged particles that have the chance to pass through the calorimeter this part of the detector does not care about their absorption. Large air-core superconducting toroid magnets deflect muon tracks that recorded in muon chambers. The magnetic field is set to be perpendicular to the muon trajectories, while minimizing the degradation of resolution due to multiple scattering. The spectrometer is equipped with separate trigger and high-precision tracking chambers see below and chapter 3. Muon flight is noticed

Figure 2.5: Monitored drift tubes

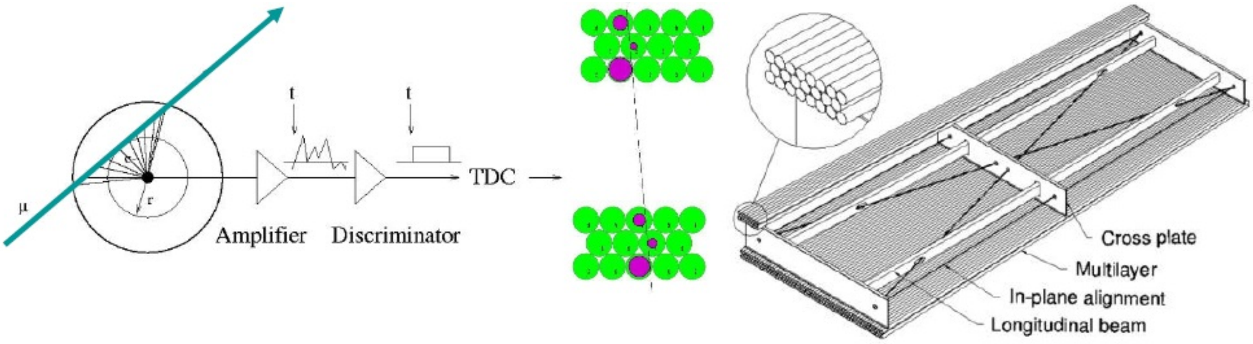

by drift tubes, an array of gas-filled tubes $r = 1.5cm$ tubes with anode wires along their axes. By measuring the time for electrons produced by ionization to drift to the wires, muon position can be determined up to $80\mu m$.

MONITORED DRIFT TUBES (MDT) - the MDT chambers are aluminium tubes of $30mm$ diameter and $400\mu m$ wall thickness, with a $50\mu m$ diameter central WRe wire. The MDT chambers are formed by 24 mono-layers of drift tubes for the inner station and 23 mono-layers for the middle and outer stations. Each drift tube is read out at one end by a low-impedance current sensitive preamplifier, with a threshold five times above the noise level. see Fig.2.5

At large pseudorapidities and close to the interaction point CATHODE STRIP CHAMBERS can be found . The CSCs are multiwire proportional chambers with cathode strip readout and with a symmetric cell in which the anode-cathode spacing is equal to the anode wire pitch. Due to the avalanche formed on the anode wire the charge induced on the segmented cathode is measured offering the precision spatial resolution ($50\mu m$) measurements. A measurement of the transverse coordinate is obtained from orthogonal strips, i.e. oriented parallel to the anode wires, which form the second cathode of the chamber. The CSC gas in a mixture of 30% Ar, 50% CO2 and 20% CF4. Read out is coped with charge sensitive preamplifier driving pulse-shaping amplifier is followed by analogue storage of the peak cathode pulse height during the Level-1 trigger latency.

2.1.4 Trigger Chambers

TRIGGER CHAMBERS offer fast signal response (on account of decreased resolution precision) and serves for filtering the information about the collision are housed in the muon spectrometer. In the barrel area (small η) Resistive plate chambers (RPC)) are used while Thin gap chambers (TGC) in the areas with large η .

RESISTIVE PLATE CHAMBERS (RPC) use the resistive bakelite plates placed in front of the metal electrodes.Two such a plates form a narrow gas gap (tetrafluoroethane (C2H2F4) with some small admixture of SF6). The primary ionization electrons are multiplied into avalanches by a high, uniform electric field of typically $4.5kV/mm$. The primary ionization electrons are multiplied into avalanches by a high, uniform electric field of typically $4.5kV/mm$. The method of read out is capacitive coupling of metal strips on both sides of the detector.Construction of the trigger chamber are rectangular shaped layers, each one read out by η strips parallel to the MDT wires and providing the bending view of the trigger detectorand the MDT orthogonal ϕ strips, orthogonal to the MDT wires, providing the second-coordinate measurement for the offline pattern recognition.This detector provides a spacetime resolution of $1cm \times 1.5ns$.

THIN GAP CHAMBERS (TGC) are designed similar to the multiwire proportional chambers. The difference is that the anode wire pitch is larger than the cathode-anode distance. The anode wires parallel to MDT wires are the signal carriers and offer the trigger information together with readout strips arranged orthogonal to the wires. These readout strips are also used to measure the second coordinate. The gas mixture is highly flammable. The gas gap thickness or equivalently cathode-cathode distance is $2.8mm$ and a wire diameter is $50\mu m$. The operating high voltage is $3.1kV$. In order to fulfill the requirement of short drift time and thus to cover time resolution less then $5ns$, optimal electric field setup was introduces together with small wire distance. The inner station of TGC has one doublet chamber with another seven chamber layers in the middle station are arranged in one triplet and two doublets serving the trigger and measuring the coordinates. Copper strips located on the cathode plates facing the center plane of the chamber provide the readout of the azimuthal coordinate.

2.1.5 Magnet system

The CENTRAL SOLENOID has a length of 5.3 m with a bore of 2.4 m. The conductor is a composite that consists of a superconducting cable located in the center of an aluminum stabilizer with rectangular cross-section. It is designed to provide a field of 2 T in the central tracking volume with a peak magnetic field of 2.6 T. To reduce the material build-up the solenoid shares the cryostat with the liquid argon calorimeter.

The TOROID MAGNET system consists of eight Barrel coils housed in separate cryostats and two End-Cap cryostats housing eight coils each. The End-Cap coils systems are rotated by 22.5^0 with respect to the Barrel Toroids in order to provide radial overlap and to optimise the bending power in the interface regions of both coil systems.

2.2 b-physics prospects in ATLAS

In the central section of ATLAS ($\eta < 2.5$) at a center of mass energy of 14 TeV more than $\approx 10^5$ $b\bar{b}$ pairs per second will be produced with a large inclusive cross section about 500 μb, see [2]. Although LHCb is one of the experiments dedicated mostly to b-physics, ATLAS is able to bring us the same quality of decay information about channels like semileptonic, rare and very rare B-decays are. ATLAS is focused on decays with two muons in the final state so called semi-muonic decays among which six channels will be measured (B_d, B_s, Λ_b) see Tab.2.1 The study of the whole B-meson family allow us to

Main strands of b-physics in ATLAS

Int. luminosity	Expected Decays	'Duties'
$<\ 10\ pb^{-1}$	J/ψ and Υ	Validation of ATLAS detector ID/alignment/tracking/trigger used for data quality monitoring
		Performance studies continue...
$20\ -200\ pb^{-1}$	$b\bar{b} \to J/\psi,\ pp \to J/\psi,$ $B+ \to J/\psi K^+$ $\Upsilon \to \mu^-\mu^+$	Measurement of production cross sections for B-hadrons and quarkonia (J/ψ,Υ) to test QCD predictions
		Main B-decay data collecting starts ...
$200\ pb^{-1}\ -\ 1fb^{-1}$	$(B^+, B_s, B_c, \Lambda_b$ + h.c.) $B_c^+ \to J/\psi\pi^+$ $B^0_{s,d} \to hadron^+hadron^-$	Contibuting to world averages on B-hadron properties. Setting limits on rare decay branching ratios.
		Approaching precise measurements of ...
$1\ fb^{-1}\ -\ 30fb^{-1}$	$B_s^0 \to D_s^-\pi^+$, $B_s^0 \to D_s^- a_1^+$ $B_d^0 \to J/\psi K_s^0$ $B_s^0 \to J/\psi\Phi^0$ $B_s \to \Phi\gamma$, $B_d \to K^{*0}\gamma$	$\to \Delta m_s$, BSM[7] CP-violating effects $\to sin(2\beta)$. Weak B-hadron decays $\to$ weak phase Φ_s. Rare decay searches. $\to \|V_{ts}\|$, $\|V_{td}\|$. Exclusive radiative decays. Quarkonia and Λ_b polarization studies.
		Coming to high luminosity period of LHC ...
$>\ 30\ fb^{-1}$	$B^0_{s,d} \to \mu^+\mu^- X$ $\Lambda_b \to \Lambda\mu^+\mu^-$, $B_d \to K^{*0}\mu^+\mu^-$ $B^0_{s,d} \to \mu^+\mu^-$, $B^0_{s,d} \to \gamma\mu^+\mu^-$ $B_d \to \rho\gamma$, $B_d \to \Phi\mu^+\mu^-$	Rare dimuon decays searches. Forward-backward asymmetry A_{FB}. Searches for rare B-decays. Exclusive radiative decays. and $\to A_{FB}$

Table 2.1: b-physics prospects on ATLAS

Figure 2.6: LHC schedule on the left. The schedule is not up-to-date, since ATLAS broke down shortly after its opening in 2008. Since 2008 ATLAS has been ramping up operations to catch up this delay. However the 'duties' stays the same. Expected mass spectrum of $B \to \pi^+\pi^-$ candidates on the right.

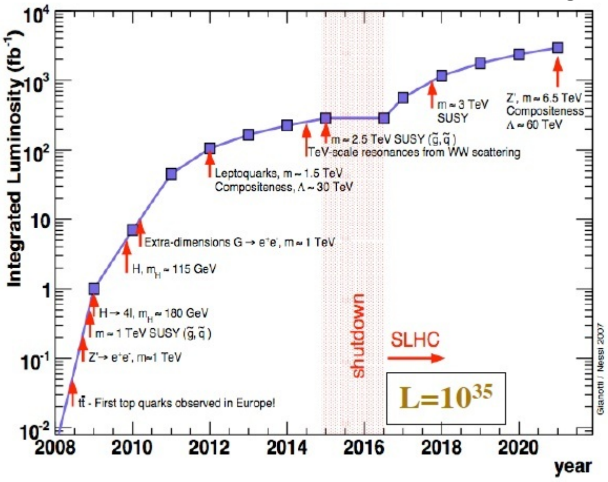

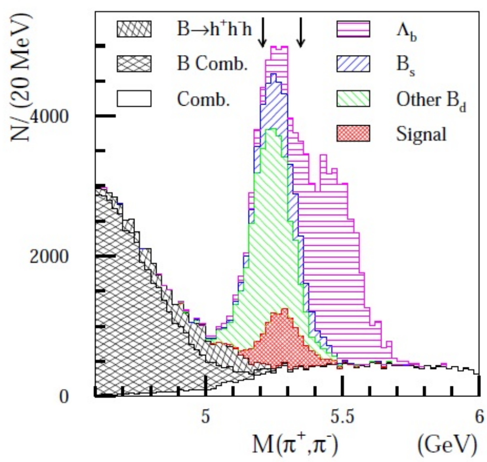

check SM predictions in a high perturbative order, look for 'new physics' , to constrain the CKM matrix elements and to provide a new information on long distance QCD effects in matrix elements of the tensor currents see chapter 1 or [63, 17]. The estimated schedule for ATLAS may be found in Fig. 2.6.

2.2.1 Radiative B-decays

Both of the radiative penguin decays $B_s \to \Phi\gamma$ (could be seen for the first time) and $B_d \to K^{*0}\gamma$ visible for ATLAS will be important for the investigation of CKM matrix element $|V_{ts}|$. Moreover, the value of photon penguin contributions is going to be also uncovered and will serve for the extraction of the physics beyond the SM from the rare semi-leptonic decays, see further. Clear observation of radiative B-decays is possible during this first year of running. The requirement of high photon identification efficiency while keeping a good ability to reduce π^0 background from the latter decay is essential. This is ensured by fine granularity in the barrel region of the ECAL. Simulation of these decays in ATLAS detector shows that after $20fb^{-1}$ for ATLAS and $2fb^{-1}$ for LHCb we shall be able to reconstruct about 9300$\times$ $B_s \to \Phi\gamma$ and 35000$\times$ $B_d \to K^{*0}\gamma$ in LHCb and 2300$\times$ $B_s \to \Phi\gamma$ and 5700$\times$ $B_d \to K^{*0}\gamma$ at ATLAS, see [10]. So we expect to be more successful at LHCb than at ATLAS in this case. The main difference comes from the trigger approach which is much more efficient thanks to no muon needed at the first LHCb level trigger, vertex trigger and no pile-up appearance. In comparison to LHCb, ATLAS will use a L1 trigger in which both the muon signal and the ECAL cluster are identified. However, ATLAS is still competitive experiment to LHCb outcome with which the cross check will be performed. Finally I would like to mention that these decays together with for example $B_d \to \rho\gamma$ decay are much easier to access experimentally in constrast to the theoretically more transparent [5] inclusive $B^0_{s,d} \to \gamma X_{s,d}$ decay[8]. Theoretical uncertainties impacting the predicted branching ratio really cancel when doing CP or isospin violation measurements. Nevertheless, these for the first sight small uncertainties could be largely enhanced by BSM theories. Not to forget that decay like $B^0_{s,d} \to \gamma\mu^+\mu^-$ with an SM extremely small branching ratio $< 10^{-9}$ might be also observed.

2.2.2 Hadronic two-body B-decays

With decays such as $B^0_{s,d} \to \pi^+\pi^-$, $B^0_{s,d} \to K^+K^-$ or $B^0 \to \rho^+\rho^-$ we have observed a signs of CP asymmetries in BaBar and other experiments. These decays can show us constraints on the α and γ angles of the unitary triangle. With a large background coming from all two body decays of b-hadrons see Fig 2.6 ATLAS copes thanks to the precise tracking system of the inner detector that provides the K/π separation. The resolution on the amplitudes of the CP asymmetry is expected to be around 0.1 ,see [11] in $B^0_{s,d} \to \pi^+\pi^-$, $B^0_{s,d} \to K^+K^-$ decay channels offering the observation of $B^0_{s,d} - \overline{B}^0_{s,d}$ oscillations and for both the direct and mixing-induced asymmetries. The final accuracy of the measurement of the CKM angles is sensitive on how well the penguin contributions are known and also

[8]With these inclusive decays I mean decays which final state is defined by its flavour content, for example for B_d all final states without charm and strange particles that rely on the quark transitions ($\bar{b}(d) \to \overline{u}u\overline{d}(d)$ or $b(\overline{d}) \to u\overline{u}d(\overline{d})$)

on the value of the angle see [59]. The CKM angle α can be measured with helps of the time dependent analysis of B meson decays dominated for example by tree level $b \to u\bar{u}d$ amplitudes. One possible experimental approach is to look at the interference between the direct tree decay (such as $B^0 \to \rho(/\pi)^+\rho(/\pi)^-$) carrying the weak phase - angle γ - information and the decay after $B^0_{s,d} - \overline{B}^0_{s,d}$ mixing. The outcome of this is the time dependent decay rate asymmetry which depends on the angle $2\beta + 2\gamma = 2\pi - 2\alpha$. Another interensting hadronic decay that will be searched is $B^+ \to K^+K^+\pi^-$. Its branching ratio is regarding to the SM predictions $< 10^{-11}$, however, some extentions of the SM predicts several magnitudes greater and therefore promising branching ratio. This gives ATLAS the possibility to make this decay visible or exclude it with a confidence exclusion limit (C.L.) of 95 percent when reaching $30fb^{-1}$, see [11].

As mentioned above the mixing of $B^0_{s,d} - \overline{B}^0_{s,d}$ meson states will be one of the fields of interest of ATLAS experiment. There exist two signal channels discussed below, which are most promising to observe $B^0_s - \overline{B}^0_s$ oscillation with the ATLAS detector. The transitions $B^0_s \to \overline{B}^0_s$ and $\overline{B}^0_s \to B^0_s$ occur as the consequence of the non-conservation of flavour in weak current interactions. The flavour eigenstates $B^0_s, \overline{B}^0_s$ are linear combinations of the two mass eigenstates H (heavy) and L (light). At lowest order this oscillations are described by box diagrams involving two W bosons and two up-type quarks see [17]. The best approach to measure the mass difference Δm_s between the mass eigenstates of the $B^0_s, \overline{B}^0_s$ system is to investigate the oscillating behavior of the proper time distribution of flavour tagged B_s mesons decaying to a flavour-specific final state. Therefore, the oscillation frequency is proportional to $\Delta m_s = m_H - m_L$. [9] If we denote $p_+(t)$ [10] as the probability for an initial pure B^0_s state produced at time $t = 0$ to be measured as B^0_s after some time t, this probability regarding to [63] reeds:

$$p_{\pm}(t) = e^{-\Gamma_s t}[cosh(\frac{\Delta\Gamma_s t}{2}) \pm cos(\Delta m_s t)]\frac{\Gamma^2 - \Delta\Gamma_s^2}{2\Gamma} \tag{2.1}$$

Finally the measurements of the following asymmetries can determine Δm_s:

$$\frac{p_+(t) - p_-(t)}{p_+(t) + p_-(t)} = \frac{cos(\Delta m_s t)}{cosh(\frac{\Delta\Gamma_s t}{2})} \tag{2.2}$$

The meaurement of the mixing frequency parameter Δm_s in these decays $B^0_s \to D^-_s\pi^+$ or $B^0_s \to D^-_s a^+_1$ is an important input parameter for the determination of other B^0 parameters from for example $B^0_s \to J/\psi\Phi^0$ using the lifetime difference $\Delta\Gamma_s$ and the weak phase Φ_s. The former decay mode followed then by $D^-_s \to \Phi(\to K^+K^-)\pi^-$ and the latter mode followed by $a^+_1 \to \rho^0(\to \pi^+\pi^-)\pi^+$ may be used to determine the Δm_s sensitivity. There arose a question how to measure the maximum value of the oscillation frequency. Since it may be proved that the naive maximum likelihood fit in a time space fails in general to give correct confidence levels (in case of limits) a new method was introduced in 1996 called the amplitude fit method [53]. This method combines Fourier analysis with the power and simplicity of a maximum likelihood fit. Monte Carlo simulations (Pythia

[9] For a more detailed description of the oscillation mechanism see [63]

[10] and $p_-(t)$ to be found as $\overline{B}^0_s$

Figure 2.7: On the right: The B_s^0 oscillation amplitude fit results as a function of Δm_s for an integrated luminosity of $30 fb^{-1}$, using the dimuon trigger $p_T(\mu_1) > 6GeV,\ p_T(\mu_2) > 3GeV$. The 'data' points show the results of an experiment with the statistics and the resolutions of ATLAS done once. Repeating such simulation gives an average fitted amplitude consistent with 0 and the values of σ_{stat} (statistical errors only) and σ_{total} (with an estimate of systematic errors added) increasing with Δm_s.Taken from [52]. On the left: CDF experimental result.

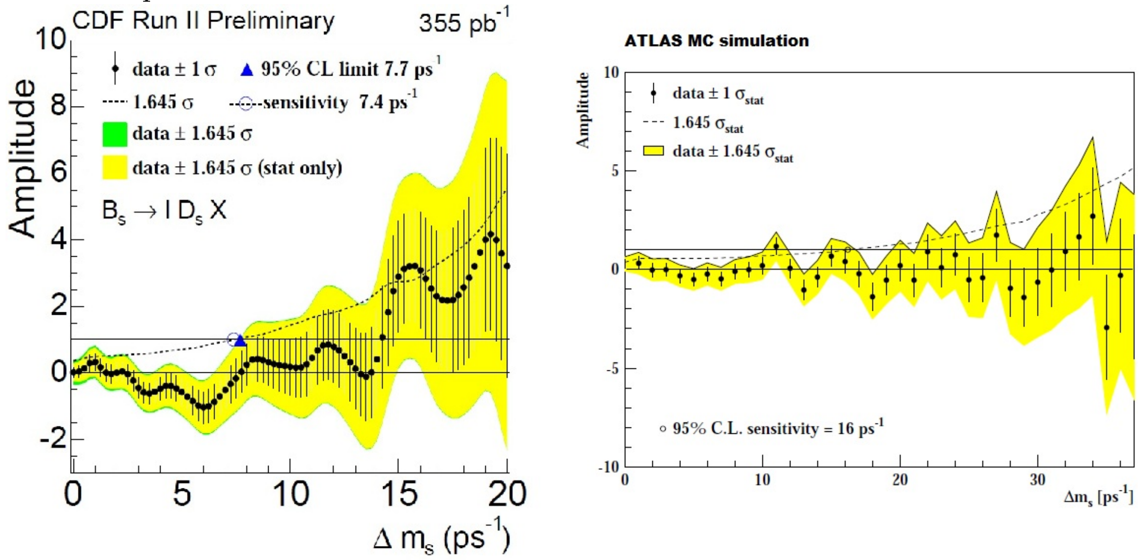

6.203) show how we expect to see this effect in ATLAS detector, see 2.8. We also expect to get ≈ 3300 fully reconstructed samples already on the $10 fb^{-1}$.

2.2.3 Purely muonic rare B-decays

The past experiments were not capable to deal with search for so rare decays as $B_{s,d}^0 \to \mu^+\mu^-$ are. Among the decays to two tau leptons or electrons the decay to two muons is the most promising one since it has the largest branching ratio (BR). The interesting observable for this decay is the BR which strongly depends on the ratio of the vacuum expectation values for charged and neutral Higgs bosons. If there appear some yet unknown particlen in the loop it will definitely bring this information to the changed BR value. The Standard Model predicts the BR of $B_s^0 \to \mu^+\mu^-$[11] to be

$$BR(B_s^0 \to \mu^+\mu^-) = 3.5 \times \frac{|V_{ts}^* V_{tb}|^2}{2.2 \times 10^{-3}} \times 10^{-9} = (3.42 \pm 0.52) \times 10^{-9} \tag{2.3}$$

and today experimental evidence confirmed the limit on this BR to be less then $< 4.5(5.3) \times 10^{-8}$ at 95% CL regarding to $5 fb^{-1}$ of data from Tevatron and less then $< 5.8 \times 10^{-8}$ at 95% CL regarding to $2 fb^{-1}$ of data from CDF experiment, see [21]. If ATLAS tell us that the BR is a significantly different from the one predicted we have a

[11]Branching ratio of double leptonic B- decays is proportional to the square of the final state lepton masses ('helicity suppresion') and so e.g.: the BR of $B_d^0 \to \mu^+\mu^-$ is $\approx 40\times$ smaller, see [114] and the BR of decays to electrons is of order 10^{-15}

sign of new physics effects. ATLAS will reach the SM sensitivity in this particular case in 4 years of running. Thus the decay will be used to test SM to high perturbative orders. So far simulations of many events in ATLAS detector showed that after $30fb^{-1}$ of data we could select about 21 signal of this kind with an expected additional 60 background events. Moreover after reaching $100fb^{-1}$ of data at high luminosity running we may gain 92 signal with 900 background events[6].

If want to make any conclusions about such a rare decay we have to get the knowledge about the proper (in this case significant) background rejection. Sources of background in this case are, see [50]:

- The combinatorial background from the semileptonic b and c quark decay processes $\bar{b}b(\bar{b}b\bar{b}b, \bar{b}b\bar{c}c) \to \mu^+\mu^- X$.
- The decays of similar topology such as hadronic two body decays: $B \to K^{\pm}\pi^{\mp}$, $B \to K^{\pm}K^{\mp}$, $B \to \pi^{\pm}\pi^{\mp}$, $B \to K^{\pm}\mu^{\mp}\nu$, where hadrons are misidentified as muons [12]. And an important contribution from $B \to \mu^{\pm}\pi^{\mp}\nu$ followed by a subsequent decay in flight of the final state π producing another muon.
- The rare exclusive decays $B^+ \to \mu^+\mu^- l^+\nu_l$, $B_c^+ \to J/\psi(\mu^+\mu^-)l^+\nu_l$ and $B^+ \to J/\psi(\mu^+\mu^-)K^+$.

The estimations are that these are the most important constituents of the background. With help of the ATLAS dimuon trigger, excellent muon identification efficiency and high beauty production cross section we may try to preserve the rare signal events as much as possible while rejecting the background. monte carlo simulations showed the appropriate cuts that will be applied during the first phase of search and tuned throughout the lifetime of the experiment. At L1 trigger the topological di-muon trigger cuts are applied. For all events passing the dimuon trigger, oppositely charged muons with $p_T > 6, 4GeV$, $4GeV < M_{\mu\mu} < 7GeV$ are at L2 trigger (vertex and tracking algorithms) fitted to a common vertex with a cut $\chi^2 < 10$, see [19]. Event filter then spatially isolates muons in the inner detector as the fraction (> 0.9) of p_T of the dimuon over the p_T sum of all other tracks with $p_T > 1GeV$ within a cone $\Delta R = \sqrt{\Delta\eta^2 + \Delta\Phi^2} < 1$ around the momentum vector of the $\mu\mu$-pair. A cut is made also on the transverse decay length $L_{xy} > 0.5$ of the B-candidate vertex. And finally the pointing angle between the dimuon summary momentum and the direction defined by the primary and secondary vertex, $\alpha < 0.017\ rad$. The overall efficiency of all trigger levels combined in terms of signal preservation is estimated to be 46% [50].

To measure the BR of this decay we need control channels when dealing with a real data. We are not allowed to determine the luminosity with a high precision and so the number N_b [13]of B-mesons produced in the experiment has to be normalized by the $B+ \to J/\psi K^+$ reference channel. With this decay we may reduce the uncertainty in the efficiency. The ratio between efficiencies of $B+ \to J/\psi K^+$ and $B_s^0 \to \mu^+\mu^-$ is gained with a accuracy of a few percent with help of another reference channel $B^+ \to J/\psi K^{*0}(K\pi)$. For tuning the

[12]Although the probability to misidentify K or π as μ is of the order of $\approx 0.5\%$ the extremely small BR makes us to take these decays into consideration.

[13]The number of signal events observed is given by $N_(\mu\mu) = 2N_b \times f_s \times BR_{\mu\mu} \times \epsilon_{tot}$

Figure 2.8: At the simulation of the first $10fb^{-1}$ of expected number of events, the invariant mass of the signal selected by the L1 trigger along with backgrounds is shown in picture (a) and after applying all cuts (b). Taken from [50].

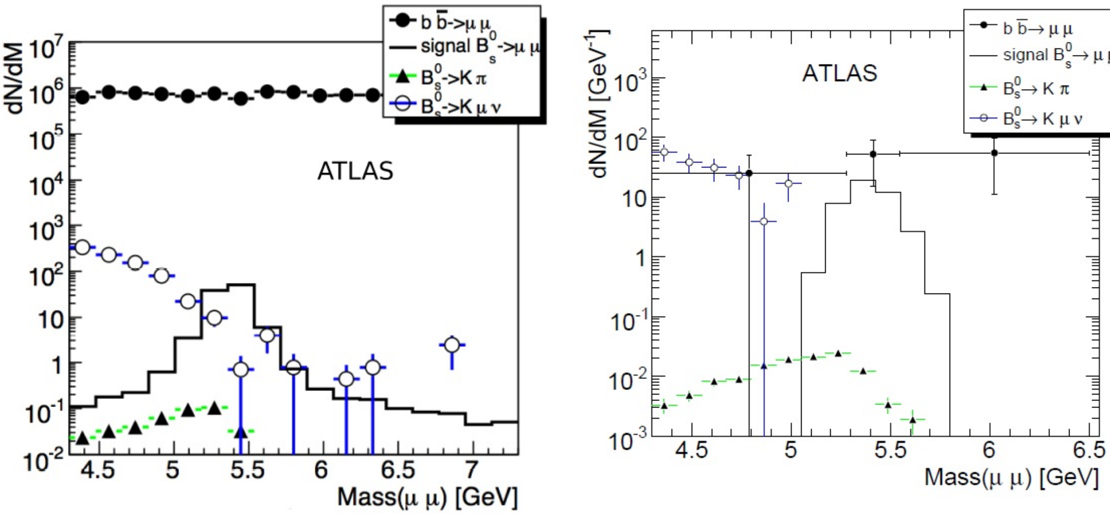

(a) (b)

probability distribution function of the signal on real data the $B^0 \rightarrow hadron^+hadron^-$ channels will be used. BR measurement then reads:

$$BR_{\mu\mu} = \frac{N_{\mu\mu}}{N_{J/\psi K^+}} \times \frac{f_u}{f_s} \times BR_{J/\psi K^+} \times \frac{\epsilon^{tot}_{J/\psi K^+}}{\epsilon^{tot}_{\mu\mu}} \tag{2.4}$$

where $N_{J/\psi K^+}$ is the number of observed events of the type $B+ \rightarrow J/\psi K^+$ and $Br_{J/\psi K^+}$ is the corresponding branching ratio, f_s [14] is the fragmentation fraction for a B-hadron to fragment into B_s, f_u is the fragmentation fraction for a B-hadron to fragment into B_u and ϵ^{tot}_* are the the *corresponding total efficiencies due to acceptance, reconstruction, selection and trigger. The ratio of the fragmentation factors gives us the largest source of systematic uncertainty. The second above mentioned source is the ratio of the efficiencies due to the presence of K^+ and so the acceptance of $B+ \rightarrow J/\psi K^+$ is reduced by that. It is also more difficult to recognize the phase space differences between these two decays and therefore the reconstruction efficiency is also affected. The sensitivity to errors in the efficiency could be also be reduced by involving an additional ratio of control channels in order to probe explicitly the efficiency for reconstructing an extra track in the final state. The channel used for this strategy is then the above mentioned $B^+ \rightarrow J/\psi K^{*0}(K\pi)$ see [29].

Since this thesis is supposed to be focused more into **semileptonic decays** which form the last family of b-decays on this paper is concerned in. In the chapter 4 I will describe some of the expected properties of semileptonic decays of b-hadrons connected to the first years of ATLAS observation.

[14]The fragmentation fractions depend on QCD parameters and the event energy scale.

Chapter 3

ATLAS Data Aquisition

3.1 ATLAS Trigger

Dispose of more than 90 million readout channels sort over 1 billion collisions per second and offers amongst other information a track of the objects that interacts with our detector. The raw information about each collision (23 events every $24.95ns$) is stored in pipeline memories. Current computer processors operate at a few GHz so it is neccesary to focus on the really engrossing information to be able to manage such amount of raw information from the detector.Therefore ATLAS employ 3 level trigger system see Fig 3.1. Level 1 as a hardware trigger and Level 2 with Level 3 (also called Event Filter) form High Level Trigger (HLT). Finally 1-4 percent of information is processed to the physical analysis. Small bunch crossing period, less than time of the flight (ToF), is also much less than scintillator times and drift times. If we consider the total inelastic cross section of p-p collisions at $14TeV$ to be $\approx 70mb$, multiply it by the estimated luminosity of $10^{-34}cm^2s^{-1}$ we have the event rate of $7 \times 10^8 Hz$. With this and with the time gap between bunches of $25ns$ we see that there is going to be also roughly 23 so called pile up minimum bias events with about 1700 particles per bunch crossing (so called pile-up effect). Most physics events are high p_T QCD jets. All the restrictions put on particles'tranverse momentum, energy etc. were firstly simulated using developed simulation techniques see below in this chapter; and then carefully checked in the initial run and in these days they are finely tuned every day with a better efficiencies for the corresponding physics requirements.

Digital highspeed pipelined electronics was developed to serve synchronous system - LEVEL-1 TRIGGER (L1). It aims is to select from the raw 40.08 MHz bunch-crossing event rate the significant information flow of 75,000 event candidates per second. he system look for high-energy signatures such as the existence of a muon is to regions of interest Level 1 has the duty to manage to make the decision in less then $2.5\mu s$ and identify Regions of Interest (RoI) see Fig 3.2.The identification is made by high-energy signatures such as the existence of a muon in given region. It uses coarse granularity from muon trigger chambers and sum of all calorimeter towers. There is no information about tracking. Central Trigger Processor (CTP) sends the information to the Trigger Timing and Control (TTC) that distribute Level 1 signal to subdetectors and synchronize it with

Figure 3.1: 3 Level ATLAS trigger system. Many of the physics processes of interest at the LHC have very small cross-sections and so the ATLAS detector is designed to produce $p-p$ interaction rate of about 1 GHz. The requirements of our recording limits are about 200 Hz

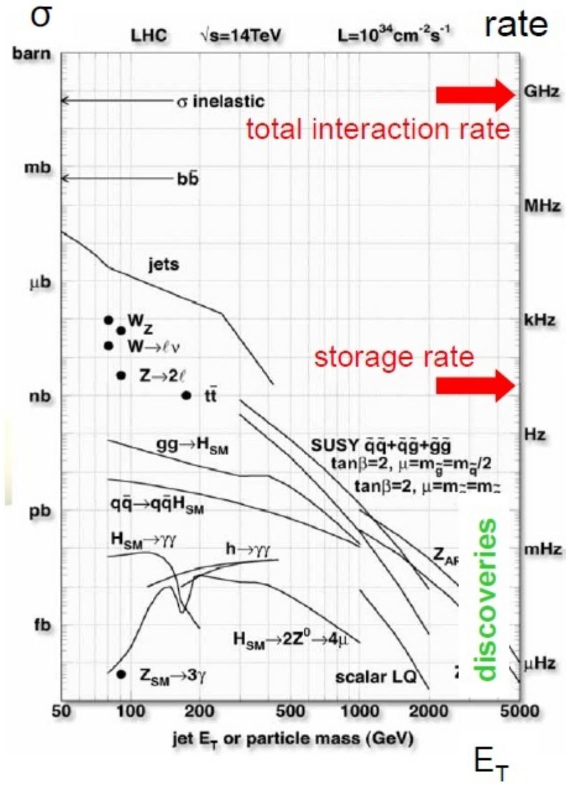

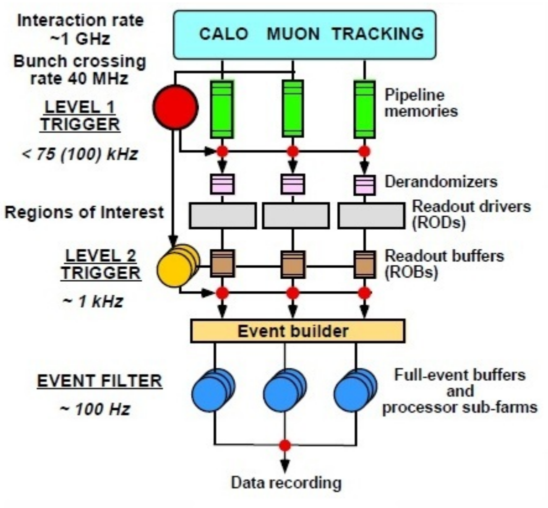

Figure 3.2: Regions of Interest selected by Level 1 trigger. Block diagram of the level 1 Trigger. Calorimeter triggers consist of analogue E_T preprocessor sending information to Jet/Energy-sum processor ($E_T, E_T^{jet}, E_T^{miss}$ sums) and Cluster processor (multiplicities of e/ γ, τ/hadrons) to pass the (8 p_T) thresholds.the information is also send to the RoIBuilder. Muon trigger analyses barrel RPCs and end-cap TGCs to process the informations Muon-CTP interface(multiplicities of μ for $6p_T$ tresholds) to Central Trigger processor and RoIBuilder.

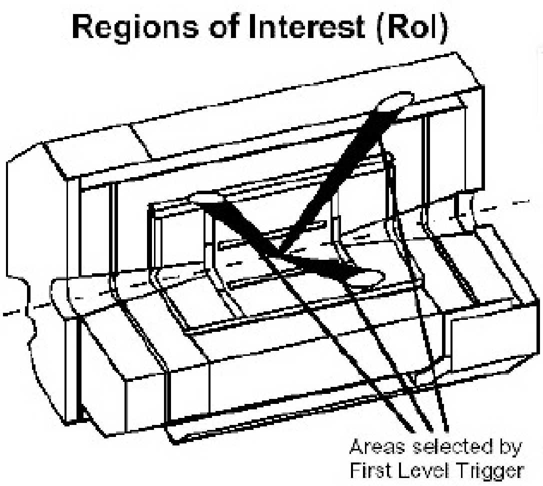

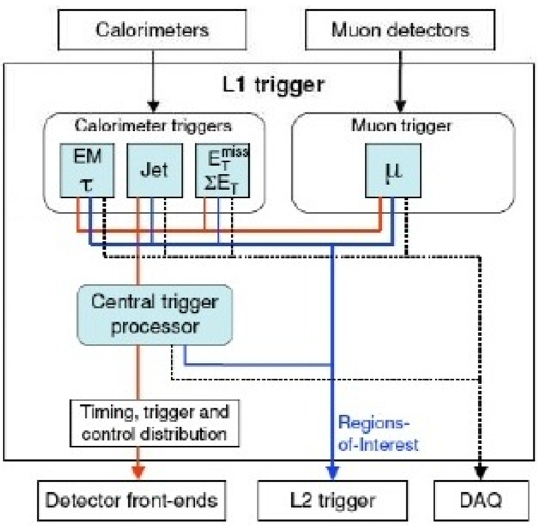

the LHC clock. Region of Interest Builder (RoIB) concatenates RoI fragments (6 $\times$ calo, 1$\times$ muon, 1$\times$ CTP) into one and sends to Level 2 processing). Finally the data are read out, preprocessed (calibrated) and are stored in readout buffers (ROBs) for use by the HLT.

To refine the selection of all the ATLAS information LEVEL-2 TRIGGER (L2) is used as a high-capacity switched network of several thousand PC's with access to the whole detector. The rate is reduced to approximately $3.5kHz$ within about $40ms$. Use seeding by RoIs from L1 trigger with full granularity in the particular RoI to reduce data access and processing time. This trigger reconstructs physics objects in stages by a sequence of fast specialized algorithms requesting data as needed. It does not execute the rest and rejects early if it is not necessary. L2 trigger may expand the confirmed RoI's features by search of them in ID what is done for muons, EM clusters and RoI's themself. Jet RoI's are only processed in the calorimeters, but b-jet tagging demands tracking detectors to evaluate the impact parameters of tracks. Only one muon reconstructed for each muon RoI. This trigger uses tracking information while requiring that all tracks originate at the centred interaction point. Muons that originate from neutral particles that decay far from the interaction point fail this standard L2 trigger. This algorithms are still under development. Problem is with the jets from late decays which do not have normal energy deposition and in many cases of interest the jet energy is not very high. Moreover, decays in different parts of the detector such as decays from end of HCAL to the first muon trigger plane, decays in the calorimeters, decays in ID beyond pixel layers to end of TRT, decays in the beam pipe and pixel layers, all these require different strategies. Decays that should also pass the test are the ones in or beyond ECAL that gives E_{HAD}/E_{EM} ratio larger than observed for jets originating at interaction point. We are also interested in decays near the end of HCAL and before the first muon trigger plane that give hadron clusters in small $\Delta R(\Delta\eta, \Delta\phi)$ region of muon spectrometer and Level 1 muon trigger returns multiple RoIs in this small region. The key signatures are: cluster of 3 or more Level-1 RoI's in a cone of $\Delta R = 0.4$, no jets in a cone of $\Delta R = 0.7$ centered on muon RoI cluster, no inner detector track for jets with $p_T > 1TeV$ in $(\Delta\eta, \Delta\phi)$ region of (0.2x0.2) and finally large energy deposition in HCAL in comparison to deposition in ECAL.just to notice, after this procedure we still have the flow of 5 GB/s.

The EVENT FILTER (EF) is the last stage trigger that confirms and refines L2 trigger with access to fully built events on a full granularity level through the whole detector and also uses alignment and calibration information. Analysis algorithms performs its analysis in approximately $1-4s$ to achieve the final storage rate of about 200 Hz.The RoI's from Level 2 are checked again in more detail using some of the same algorithms as will be used later for off-line analysis. HTL works with full granularity and precision of calorimeter and muon chamber data as well as Inner Detector tracking data. Particle ($e^{+}e^{-}\gamma$...) identification is facilitated by track reconstruction and better energy-deposition data improves threshold cuts. The final data of about 1.3 MB per event is sent on to the central computer center for storage and distribution to researchers around the world. It has to be noticed that 10% of the events selected by the triggers are done with minimum bias, meaning there are actually few selection criteria. This is to make sure that the researchers have not missed anything beyond what they are looking for.

Figure 3.3: L1 muon trigger scheme - taken from[62]

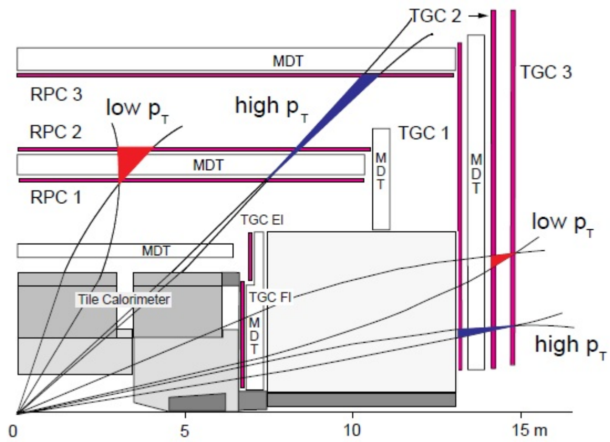

Further in the text the description of Level 1 Calorimeter Trigger as well as the description of majority of High Level triggers is omitted. I concentrate more at triggers extensively used for b-physics analysis even if the other triggers definitely also significantly contribute to get rid of the background.

B-HADRON EVENTS PROCESSING is not the same with the standard RoI processing. These events are triggered by low-p_T single muon at L1 trigger. If this muon was confirmed at L2 (muon spectrometer+ ID), a full track search is executed to allow decisions based on semi-exclusive B-event hypotheses. The strategy is to search for tracks in the TRT with very low p_T thresholds. The reconstructed TRT tracks are used to define additional L2 RoIs that lead the trigger to extend the track searches in the SCT. The SCT tracks provide information for calculation of invariant masses, that are extrapolated into the calorimeter or Muon Systems to confirm low-p_T lepton candidates, in conjunction with the TRT signals in the case of electrons.

3.1.1 Level 1 Muon Trigger

L1 muon trigger uses detectors described in section 2.1.4. TGCs (moderately fast, capable of end-cap high noise withstanding) and RPCs (very fast detection in barrel region) are required for fast detection of moderate muon p_T and bunch identification with a small dead time. The angle of deflection of muon tracks depends on the magnetic fields applied, moreover the track is effected also by the energy-loss fluctuation for low-p_T $(6 - 10GeV)$ and coulomb scattering in the material traversed. As one can see in the picture, the triggering is performed in three stations of two detector planes each (except the innermost TGC station having 3 planes). Two stations serve the $low - p_T$ triggering and the third is for high-p_T triggers (treshold 8-35 GeV) .We require to trigger these muons with the efficiency $> 90\%$. Two orthogonal projections η and ϕ read out by the detector planes will be referred further as 'bending' and 'non-bending' projection (even though there is a bending in ϕ). How much the p_T is cut by the trigger depends mainly on the 'bending' projection coordinate. The 'non-bending' information gives the L2 trigger the track candidate localization in space, second coordinate for offline reconstruction of muons and limits the background trigger rate from noise hits of low-p_T γ, n and other charged particles in the chambers. In both projections, space coincidence is required (time range $25ns$) since the applied p_T thresholds set up the width of the road.To trigger low-p_T there has to appear the hits in 3 out of 4 layers in the inner two stations . For High-p_T hits in at least one of the two layers in each of the two projections of the third station are required in addition. In the endcaps (third station) of the TGCs three active detector layers appear in the bending plane, and a two-out-of-three prompt is issued. To summarize that, there are 6 p_T independently programmable thresholds applied, 3 associated with the low and 3 with the high p_T trigger. The optimalization of the signal trigger efficiency versus the background rejection is developed every day with respect to the physically interesting events searched. Real muons from a number of sources: decays of bottom and charm quarks, decays of W and Z particles and decays in flight of charged pions and kaons together with the luminosity and center of mass energy tell us acceptable restrictions on the muon momentum. The trigger has to ensure that some percent of the selected muons will have the true value as the treshold applied. When the trigger threshold is set to 20 GeV, at least 25% of the muons selected by the trigger should have true p_T greater than 20 GeV.

Triggering muons today follows the following procedure. Hits on the middle RPCs/TGCs are found, linearly extrapolated to the interaction point and the coincidence window is defined on the first station in the following sense: one hit in this 'window' and hits in both planes and views for at least one station for low-p_T and the same plus coinciding hit in outermost station for $high - p_T$ trigger. MuCTPI resolve double counting for muons traversing both regions and forward multiplicities to CTP. This is important because we require a low-pT dimuon trigger also maintained at high luminosity. Because of that, the threshold on the dimuon trigger is kept at about $6GeV$ [1] per muon for luminosity equal to $10^{34}cm^{-2}s^{-1}$, while the threshold for the single-muon trigger will have to be about $20GeV$ for an acceptable trigger rate.Muon p_T distribution is a steeply decreasing function and it it therefore rare that muons should be double counted (in areas of overlapping chambers for example).However, it is required that about 10% of the dimuon triggers is due to doubly-counted single muons.

3.1.2 *b*-physics trigger

About 1% of collisions produce $b\bar{b}$. Most of the b physics will be measured at the luminosity $10^{33}cm^{-2}s^{-1}$. Nevertheless at $10^{34}cm^{-2}s^{-1}$ hides high-p_T discoveries and rare B decays. L1 trigger + flavour tagging [2] already gives us a clean signature about $b \to \mu$ decay. The main background is from K or π decays in flight [3] is removed mainly by the L1 low-p_T threshold. L2 reconstruction of the b event in ID employs enlarged L1 RoI (to find for example $J/\psi \to \mu^+\mu^-$), informations about RoI from the L1 calorimeter trigger (EM, Jet) and full detector scanning to select the tracks and find the decay vertices apply invariant mass cuts etc. . HLT combines the tracks reconstructed in the Inner Detector

[1] $< 6GeV$ muons are sorely detectable especially in the barrel region

[2] so called b-tagging procedure attempting to determine whether the decay is from a B or an anti-B

[3] Graph as cross section vs p_T would show us $6GeV$ lower threshold

Figure 3.4: Left column is solely di-muon triggers strategy related. Right column corresponds to increased coverage for lower luminosities.

Trigger	$2 \times 10^{33}\,\mathrm{cm}^{-2}\mathrm{s}^{-1}$ LVL2	$2 \times 10^{33}\,\mathrm{cm}^{-2}\mathrm{s}^{-1}$ EF	$1 \times 10^{33}\,\mathrm{cm}^{-2}\mathrm{s}^{-1}$ LVL2	$1 \times 10^{33}\,\mathrm{cm}^{-2}\mathrm{s}^{-1}$ EF
$B_{d,s} \to \mu^+\mu^-(X)$	200 Hz	small	100 Hz	small
$J/\psi \to \mu^+\mu^-$		10 Hz		5 Hz
$D_s^+ \to \phi\pi^\pm$	–	–	60 Hz	9 Hz
$B \to \pi^+\pi^-$	–	–	20 Hz	3 Hz
$J/\psi \to e^+e^-$	–	–	10 Hz	2 Hz
Total	**200** Hz	**10** Hz	**190** Hz	**20** Hz

and the Muon System signatures. One strategy, called STACO is based on the statistical combination of two independent measurements using the parameters of the reconstructed tracks and their covariance matrices. Another MUID and COBRA strategies aim the same but were developed to fit the global muon track using the hits from the two detectors which were found and used separately by the standalone reconstructions.

B physics trigger accept rates are shown in the figure 3.4 see [61] . The simulation predicted low momentum threshold $6GeV$ may be lowered for the low rates as $p_T > 5GeV$ (for the barrel region) and $p_T > 3GeV$ for endcaps. At the peak luminosity of $1 \times 10^{-34} cm^{-2}s^{-1}$ di-muon L1 trigger rate is going to be below $1kHz$ for a $p_T > 6GeV$. The heavy flavoured decays prevade over all the others in this case . In this region one has to be careful on large uncertainities due to sensitivity on low-p_T muons in the endcaps and a small fraction of single muon events that sudder from double counting. Di-muon triggers perform selection of decays such as $B^0 \to J/\psi(\mu^+\mu^-)K_S^0$ and $B_{d,s} \to \mu^+\mu^-(X)$.

At L2 muon triggers are firstly confirmed using the MDT chambers information. More percise track following offers tighter threshold which [4] considerably reduces the trigger rate. ID extrapolation then has the same effect on the trigger rate, rejects muons from pions and kaons and improves prompt muon p_T resolution - see Figure 3.5. L2 trigger rate at the luminosity $10^{33}cm^{-2}s^{-1}$ with $6GeV$ low p_T threshold and $|\eta| < 1$ was simulated given $2kHz$. About half of this rate originates in the remaining pion/kaon decays and heavy flavour decays. When one would extrapolate this result to the full detector there would be a $\approx 5kHz$ rate. Offline quality track reconstruction, vertex fitting and mass cuts are the tasks done later by EF trigger [5].

NOTE ON L1 CALORIMETER TRIGGER (L1CALO trigger) $\approx$ 7000 calorimeter 'towers' are read out by L1CALO trigger . The resolution is 0.1×0.1 in $\Delta\eta \times \Delta\phi$. ECAL and HCAL are two layers of this calorimeter trigger. 4×4 towers builds the so called window of **electron/photon trigger** in the region $|\eta| < 2.5$. There are four elements

- 2×2 ECAL cluster for position of RoIs identification from local E_T maximum

[4] Muon p_T spectrum is steeply decreasing.

[5] selects for example events like $J/psi \to \mu^+\mu^-$

Figure 3.5: L2 MuFast algorithm uses data from precision chambers (MDT) and rejects $low - p_T$ background. Then the track is extrapolated to ID and muons from MDT are combined with the ID tracks - see on the right the efficiency.

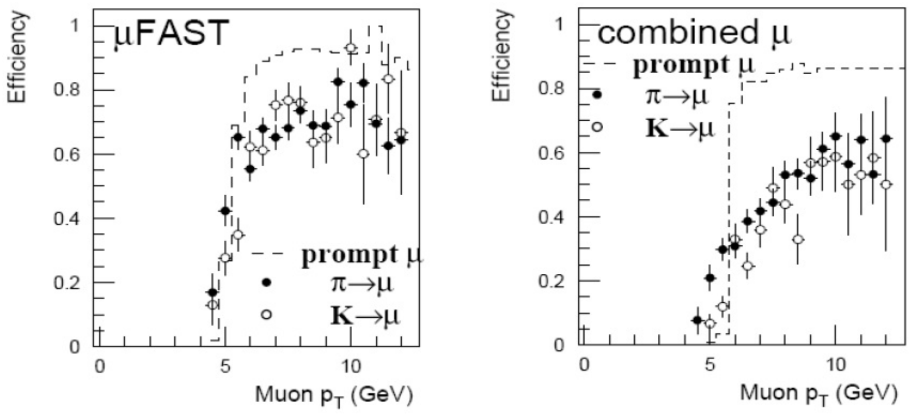

- Highest EM shower's E_T evaluating 2×1 or 1×2 ECAL tower cluster, 4 such regions in each RoI cluster
- 12 EM tower ring of clusters around the clusters mentioned above serving to isolation test in the ECAL
- HCAL isolation issues the 16 hadronic towers behind the EM clusters with the corresponding isolation ring

The window slides in steps of one trigger tower in both directions.The e^+e^-/γ can contribute to the L1 trigger in the following ways. When one of the singnals above is above a given threshold then the event is accepted and then these particles serve as inclusive triggers. To distinguish the multiplicity of e^+e^-/γ , for example as di-electron/di-photon triggers and together with other triggers they may serve to find electron and missing-ET events or electron plus muon event.

L1 τ/hadron trigger has the same input channels and very similar logic as the e^+e^-/γ trigger. The initial towers are taken the same by 4×4 with the query that the inner 2×2 contains more transverse energy than any other of the 8 possible 2×2 clusters inside the same window. The small block sides by 0.1 in both directions (η, ϕ). The E_T^{core} is defined as 2×1 block in the EM trigger within the 2×2 area plus the 2×2 hadronic cluster.

12 trigger towers surrounding the 2×2 smaller cluster are used for isolation that separately sum the towers in the ECAL and HCAL. It was observed that the EM isolation is much more effective than the hadronic one so it is widely used.

Events in a muon trigger feature some average multiplicity of L1CALO trigger and jet RoI. This is very important for B-trigger decision because these regions are exactly the ones that have to be read out. Simulations[6] on a monte carlo generated sample of $b\bar{b}$ event with a $p_T > 6GeV$ muon showed that for a jet threshold $E_T > 5GeV$ there are on

[6]with a detailed calorimeter description and L1 trigger electronics were taken into account

Figure 3.6: L1CALO clusters on the left.On the right is a picture of L1 trigger triggering electron candidates on two isolated EM clusters with $p_T > 20GeV$ (possible signature of $Z \to e^+e^-$).

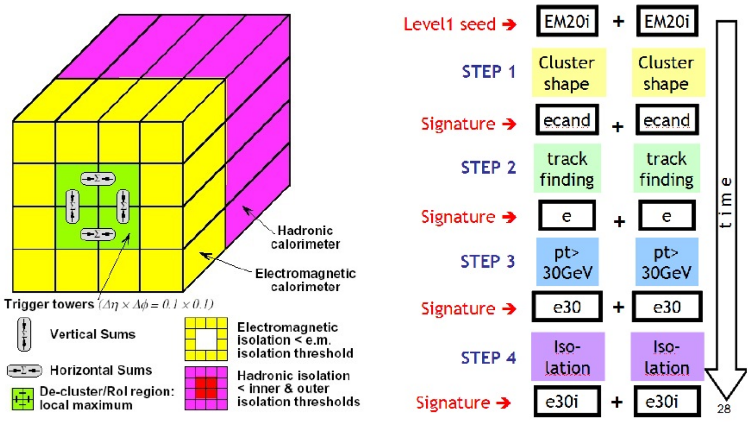

average 2 RoIs per event while EM cluster threshold of $E_T > 2GeV$ results in 1 RoI per event.

B-trigger on hadronic final states is pointed to the track information from the SCT and pixel detector by the RoI as a guide or works with a full-scan strategy. It leads to B-decay reconstruction such as $B \to hadron^+hadron^-$ and $D_s^+ \to \phi\pi^\pm$. Simulation told us that the RoI strategy is efficient for B-hadron decays with $p_T > 15GeV$. L2 trigger then makes the kinematic and topology cuts to reduce the combinatorial background. EF refits the track and uncovers the vertex more accurately. The rate can be then reduced by sharper mass, assumed decay length or vertex-quality cuts applied.

To trigger the muon electron final states meaning the channels $B^0 \to J/\psi K_s^0$ with $J/\psi \to \mu^+\mu^-$ or $J/\psi \to e^+e^-$ with opposite side electron or muon tag respectively, electron identification is required. To trigger an electron there are two strategies. RoI as a guiding tool to find SCT tracks leaded by EM RoIs or the second methodology is to perform a full reconstruction of tracks in the TRT without any guides. 0.3 percent of the full ID is reconstructed with the much faster RoI-guided method. unfortunately the lowest threshold possible in the calorimeter with acceptable RoI multiplicity is $2GeV$ what is not powerful until a higher energy then the minimum threshold possible with a full scan of the TRT. At this point I would like to mention something interesting from the chapter 2.1: as an electron crosses the material it introduces distortions to the track which cause the resolutions of the fitted parameters to be degraded and the reconstructed parameters to be biased. The above mentioned algorithms are able to cope with this to a good efficiency so that for example the efficiency to find a separate RoI for both e^+ and e^- with $p_T > 3GeV$ is about 80 percent.

3.1.3 b-tagging

To identify the b-quark decay one could be curious about how to identify the b quark related jets. Since b quark is much heavier than everything what it might decay to,

Figure 3.7: Impact parameter can be defined for each track individually by the distance between reconstructed track and primary vertex

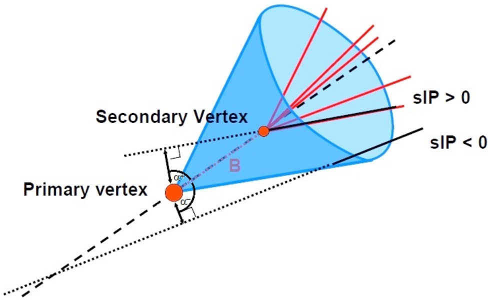

Figure 3.8: Track impact parameter resolution versus track p_T , for several bins in the track pseudo-rapidity.- taken from [60]

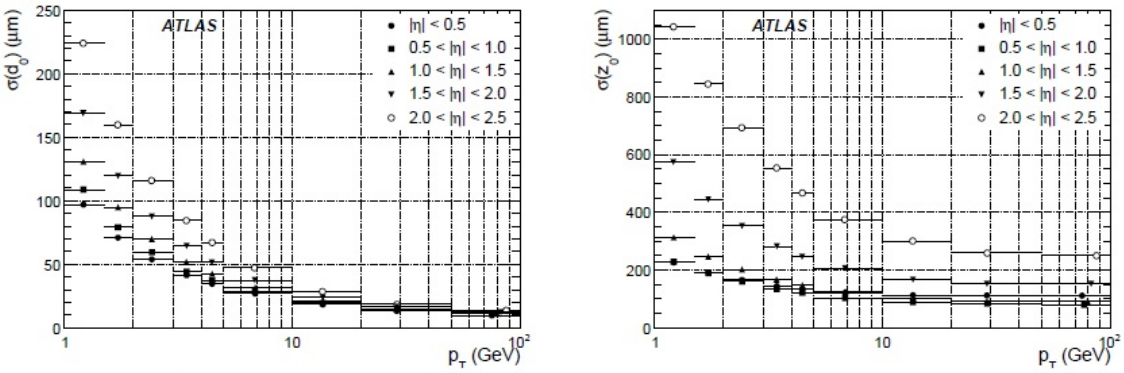

(a) Transverse impact parameter

(b) Longitudinal impact parameter

Figure 3.9: Signed transverse impact parameter d_0 distribution (left) and signed transverse impact parameter significance d_0/σ_{d_0} distribution (right) for b-jets, c-jets and light jets.- taken from [60]

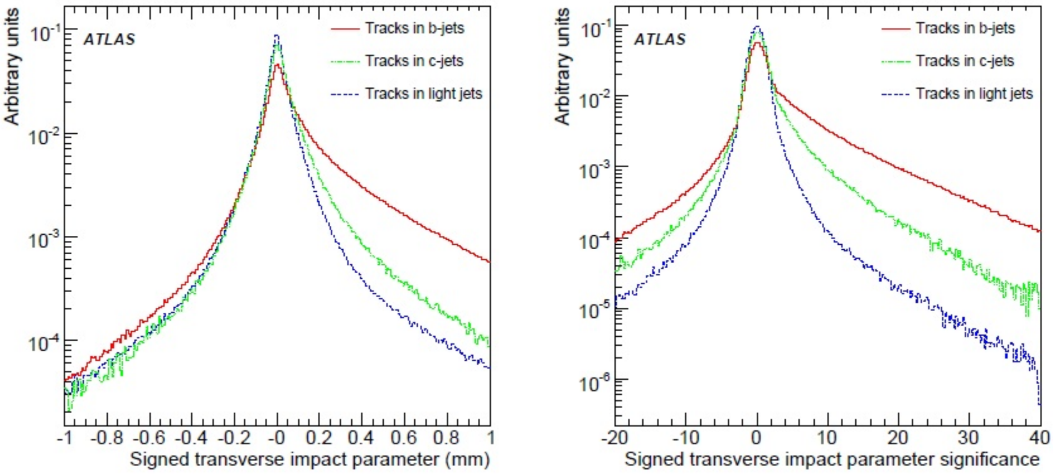

Figure 3.10: Secondary vertex variables: invariant mass of all tracks in vertex (left), energy fraction vertex/ jet (center) and number of two-track vertices (right) for b-jets and light jets.- taken from [60]

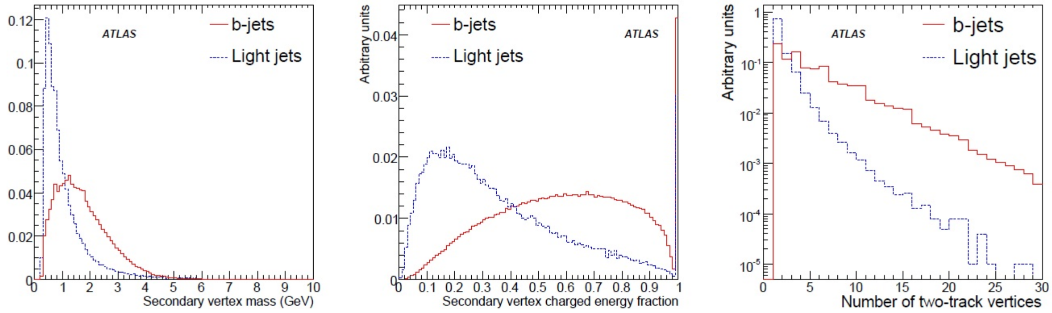

the products have high-p_T and belong to the rich high-p_T physics programm of ATLAS experiment. Some strategies have been developed in the last decades and they might be useful also for rare τ jet identification or SM of supersymmetric particle studies like Higgs bosons coupling to heavy objects. The tagging of a b-quark gives direct hints about the underlying (primary) process before hadronization occurred. In this chapter I want to briefly review the algorithms used for this tagging. The basic question is, how one could distinguish between the lighter hadronic jets[7] and the b-jet ? There is one advantageous property of b-hadrons; the relatively long lifetime $\approx 1.5\ ps$. Thus the particle flight is measurable with a millimeter ruler ($c\tau \approx 400\mu m$ or $4mm$ for $50GeV$ particles ($\beta\gamma\tau c$) in ATLAS) until it decays and we are allowed to measure the displacement of this subsequent b-hadron decay as a impact parameters of the tracks coming from the *secondary vertex*.

The *Impact parameter* (IP) is defined as a distance of the track from the point of closest approach of the track to the interaction vertex. The IP is a signed quantity, it is positive if the point of closest approach lies upstream with respect to the jet direction and negative in the other case. The IP depends on the resolution of the detector and precision of each measurement so for the purpose of b-tagging we define a dimensionless variable called create a new 'track significance' as $S = \frac{IP}{\sigma_{IP}}$, where the σ_{IP} denotes the resolution of the detector in the direction of IP measurement see Fig 3.8. Distribution of this significance was estimated (by monte carlo simulations) to be Gaussian with tails. Integrating such a distribution for a given significance of a given track and multiplying so obtained track probabilities (to be a b-track), one may conclude the probability of the jet to be the b-jet or light jet.

Secondary vertex itself may be reconstructed explicitly. Different methods for vertex fitting are available, however, due to to cascade decays more than one secondary vertex may be reconstructed in a jet what is useful to improve the rejection of c-quark jets. Finally the mass at the secondary vertex can be estimated by summing up the estimates masses of the particle tracks assigned to the secondary vertex. In a c-jet the mass is limited by D-meson ($\approx 1.8GeV$) see Fig. 3.10.

Most of the tagging methods in based on the likelihood ratio called the jet weight as

[7]Other jet-types (lighter quarks /cquarks/gluons) are much harder or not distinguishable in the detector.

a discriminating variable. This comes from the need of optimal selection that for all the given tracks that we labeled as b-jet tracks we ensure to choose the ones with the most suppressed background. Such a requirement is statistically best fulfilled by the above mentioned jet weight as a monotonous function of the ratio of probabilities; to be a b jet track over the probability to be a light jet track. see Fig **??** . As one can see on the picture - the b jet weight distribution is distinguishable from the light jet distribution and so we are entitled to make a cut in our analysis to reject the background noise from other processes. This cut has an impact on the b-tagging efficiency (identified b-jets/all b-jets). It also determines the rejection rate of light-jets. Both of these quantities strongly depend on η and p_T of the jet for a given cut on the jet weight.

There are two main algorithms to tag a b-jet the **spatial taggers** incorporate strategies employing lifetime information like impact parameters and decay vertices; and the **soft-lepton taggers** use lepton reconstruction in case of the semileptonical b- hadron decays. These leptons have a considerably large p_T as well as a large transverse momentum relative to the jet axis p_T^{rel}. These parameters are well comprised in the corresponding algorithms. I will just briefly mention some algorithms that are about to be tested and tuned on the real data in these days. The JetProb algorithm prompts tracks with the negative side of the transverse IP significance distribution and then estimates the probability of the tracks pointing to the primary vertex. More robust tagging algorithms calculates the distribution of the IP significance in the transverse plane (IP2D) and or in addition in the longitudinal projection (IP3D). Then we have also the secondary-vertex taggers (SV1/2) that try to fit inclusive secondary vertices and build the jet weight from several one or more-dimensional variable distributions see Fig 3.10. JetFitter is a tagger that fits the decay chain of b-hadrons. It fits a common b/c-hadron flight direction along with the position of additional vertices on it. The jet weight is obtained similarly to SV1/2, but in this particular case taking different decay topologies into account. To all these the collaboration tries to develop two soft-lepton algorithms. One of them utilises soft muons and one or two dimensional reference histograms of the muons p_T and the muons p_T^{rel}. The second one works with electrons and tries to pick up the relevant soft electrons from such a b-jets.

Finally let me note that in order to recognize CP asymmetry it is indispensible to know exactly the flavour of the particular B meson at our production. With that I mean which of b and $\bar{b}$ was a building stone of our B meson before it decayed. For that purpose we have three **b-flavour-tagging approaches** [8]:

- **lepton tag** - uses the semileptonic decays of the other b quark or in another words lepton tag performs an opposite side b quark weak decay tag by the charge of the high p_T lepton, see diagrams 3.11. In B physics code this is in the BFlavourTagger class which scanns the lepton (muon) collection in the dataset.
- **jet 'charge'** - relies on a combination of charges of particles reconstructed alongside the jet of the corresponding B- meson. This charge is correlated with the flavour of the B mesonas shown in the diagrams 3.12. . In B physics code this is implemented as a BFlavourJetChargeTagger class which picks up the tracks inside the predefined cone sin the surroundings of the B hadron.

[8] I discussed this also in my bachelor thesis [66], but much detailed description can be found in [17]

Figure 3.11: Feynmann diagrams for lepton tagging algorithm.

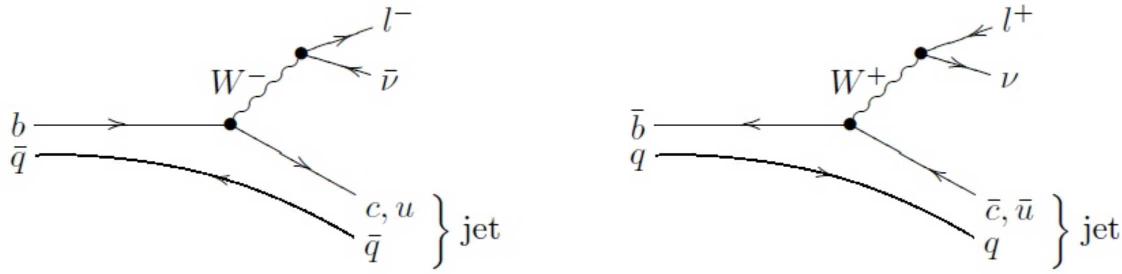

Figure 3.12: Feynmann diagrams for jet tagging algorithm.

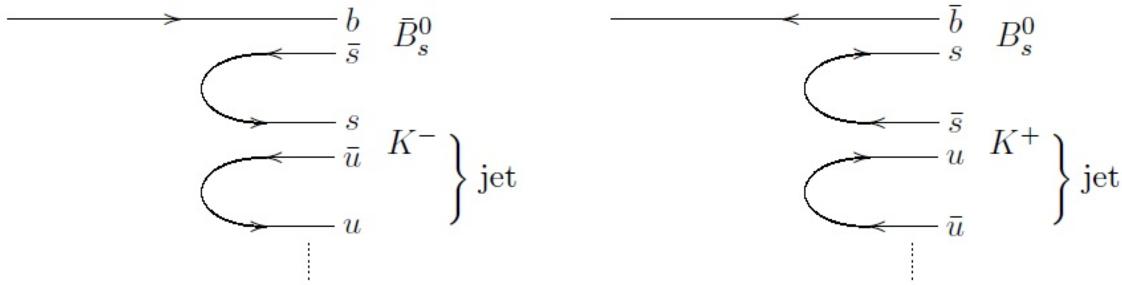

- **'$B - \pi$' tag** - the charge of a π quanta produced close to fully reconstructed B meson mediates us the information about the B meson flavour - same side tag

When we deal with decays that include the consequent decay of $J/\psi \to \mu^+\mu^-$ the most powerful methods seem to be the same-side tagging strategies. Since the muon is required at the L1 trigger it has been found that almost all simulated events had $b \to \mu X$ decay for the second b quark if the decay of interest comprised $J/\psi \to e^+e^-$. For this reason opposite side tag is the most effective one.

b-tagging is a crucial strategy for hunting many interesting physics espetially for example the SM Higgs boson in the $\bar{t}tH \to \bar{b}b$ decay where b-tagging can help to get rid of large background coming from the τ, W^+ jets. Further we could mention the top quark mass measurements etc. The performance is being tested and the critical parameters limiting the efficiency of this approach such as misalignments in the ID , dead sectors etc. are taken into account.

3.2 Data Handling and Analysis

The sections above described the basic ideas of the approach to the data collecting in such an experiment as ATLAS is. To summarize what happens until one gets to an analysis capable dataset; From more than 1600 readout driver modules (ROD) the data flow through the optical links offering information from within the RoIs to L2 . Finally they build up the event passing all the trigger criteria. All such events are then handed to EF and eventually stored on a permanent storage. Up to this moment all the software that has been run was an online software upon which the so called Data Aquisition (DAQ) service has been taking control. The DAQ monitors, configures and controles the entire

ATLAS detector during the data taking. Nevertheless, DAQ is not capable of managing some of the functions such as detector hardware operation - power and gas systems etc. For this the Detector Control System (DCS) has been developed. I will use some of the terminology described in my bachelor thesis such as the GRID terminology see 5.1. Tier-0 (CERN) reconstruction software runs on the raw data streams and produces the Event Summary Datasets (ESD) of about 500 kB per event [9]. ESD contains all the information necessary for track refitting, jet-finding, particle identification etc.. This reprocessing, done by the offline software - described later in this section - yields 100kB/event Analysis Object Dataset (AOD) most used for the purposes of common analysis.At last the so called Derived Physics Data (DPD) of about 10kB/event tells us the event story as filtered AOD's or eventually the Tag Data which amount 1kB/event allowing fast selection of events with certain signatures. CERN distributes all these reconstructed datasets with 10 percent of the raw data to each of 10 Tier-1 sites. Tier-1 then escalates this data to more than 60 Tier-2's for user analysis in their countries and institutes etc who produce the derived physics data D2PD (as ESD/AOD/DPD) or D3PD as a flat ntuples [10]. From them we are able to plot our concluding histograms.

3.2.1 ATHENA framework

I guess than many people including myself are curious what is really happening in such a beutiful materialization of human efforts to hunt the nature mysteries as LHC really is. Collaboration is neccesary and we need some common tools to be sure that the results may be reproduced by another man with the same questions put on the same pieces of information from the detector. Software framework is a good solution of this problem and it also enables us to build different views and approaches since everyone has the same abstract interfaces and write their own algorithm. In case of ATLAS such a frameworks is called ATHENA and gives all the people the common tools and uses the same data sourcing approach (transition from raw data to all the above mentioned types of data). ATHENA has been build up on the basis o LHCb experiment (so called Gaudi architecture) and now is a common ATLAS-LHCb project. It is based on object oriented programming language C++ and some python scripts that may setup some parameters of the algorithms. The actual code is provided in form of shared libraries. The framework consist of 9 major components:

- Application Manager, there is one such instance that manages and coordinates the activities of the other components of the whole framework
- Algorithms and Sequencers share a common interface to perform a fully programmable pre-event processing . A sequencer is a sequence of algorithms each of which might be another sequncer. Algorithms are invoked by athena if scheduled at certain points of the run/event loop.
- Tools operate similarly on input data and produce output data but they may be executed multiple times per event and they can not be manipulated freely since

[9]These are the is the target sizes, by now these files (ESD,AOD) amount a bit more.

[10]ntuples are files to be read out by the ROOT software code - similar to C++ code written by the user see below

they do not share a common interface. Each instance of a tool belongs under either Algorithm, Service or by default AlgToolSvc.They are invoked by Algorithms to compute specific tasks and are scheduled by a Service called ToolSvc

- Transient Data Stores event, detector conditions data are each managed by another store instance and threated with different approaches regarding their lifetime in the system etc.
- Services gives the opportunity to the Algorithms to approach to event or conditions detector data, the internal data store (StoreGate) and are designed to fulfill all the physicist's requirements. There is a message reposting service, random number generators and other services with different persistency . For example there is a Job Option Service. The JobOptionSvc is a catalogue of user-modifiable properties of Algorithms, Tools and Services.
- Selectors make selection of events or transient data for the application manager.
- Converters convert objects form one type to another - for example transient object to a persistent one .
- Options to Algorithms and Tools are coded in so-called properties which can be set in C++ (default) and in the Python steering files.
- ATHENA has also implemented some Utilities as a C++ classes that provide general support for another parts of the framework.

Most transient data classes come with a reflex dictionary that binds them to Python or CINT and so athena Algorithms and Tools can be written in Python too. Interactive analyses from Python or root have access to all transient ATLAS data. All the people in the collaboration team may install the full athena release as a kit of typical size of 6 GB on their privite computer with Scientific Linux environment. One would say - the simpler is better approach, therefore there exist several frameworks on top of the ATHENA framework such as AthenaROOTAccess, EventView, EWPA (Every Where Physics Analysis) and the new PyAthena framework in Control/AthenaPython improves the way python algorithms are treated in ATHENA. Each of these offer several advantages. Nevertheless all the plots and results that are supposed to undergo the approval for publications (at least in B-physic group) by these days has to be threated by the C++ code for ATHENA framework and ROOT code for the final decorations.

3.3 Offline analysis within ATHENA framework

Scientists want to compare the real results with the estimations of the whole experiment performance made by the monte carlo simulations and the physical assumptions of our theory. This need arose actually even before the experiment was running and had become a crucial tool for the construction and optimal discovery design of ATLAS. There exist a 'chain' of how one may proceed the Athena offline software. First one requests some reasonable data to look at. When there is no detector the Simulation comes into the play. Generators such as Geant and many other monte carlo generators aim to produce this bunch of outgoing particles together with their momenta originating from some particular physical process. We may apply this for more complicated processes and repeating collisions for a given conditions thanks to the parton distribution (probabilistic) functions. The simulation then amounts all the information about the detector (material, geometry etc.) and all the initial conditions of the state of colliding particles. The output of this particular process is a record of all the hits in the particular detectors, the energy deposition and some other parameters. The qualitative efficiency of the simulation is highly sensitive on the initial conditions that means for example the significant parameter of realistic granularity. Digitization then copes with the response of the detector to the particular hits dealing with the finite resolution of the machine and some possible misalignments etc. These data then may be compared to the real data because they offer the very same parameterized output. That is how we test our generator algorithms and tune also our analysis - the truth data from the generator are stored with the digitized data for reference and we may point to them in our algorithms. The raw data RDOs then are reconstructed to find the interesting tracks and pre-identify the particles [11]. Reconstruction builds containers with the informations like muon container with all the muon candidates, tracks, jets etc. in the form of C++ object data called ESD - event summary data or more tuned AOD - analysis object data. Another data objects like small simple TAG file about the event for event pre-selection or specific Ntuple files may be prompted from the reconstruction algorithm. The handling with them may be then proceed again with Athena software or more widely used ROOT.

- ROOT is an object-oriented framework in which we can write scripts little bit similar to the C++ programming. Since it is a framework there are provided services and macros to use directly. ROOT is important tool to solve the data analysis challenges of high energy physics experiments. It provides a wide variety of objects like histograms, fitting scripts, etc. Only the basic knowledge of C++ programming and little experience should suffice to the physicists to write a code and analyze the data. The often used documentation is available at [120]

- Pythia is a program for the generation of high-energy physics events, i.e. for the description of collisions at high energies between elementary particles such as e^+, e^-, p and $\overline{p}$ in various combinations. Together they contain theory and models for a number of physics aspects, including hard and soft interactions, parton distributions, initial and final state parton showers, multiple interactions, fragmentation and decay. They are largely based on original research, but also borrow many formulas and other knowledge from the literature. This description is taken from [118]

- Atlantis is a very nice tool aimed to display events happened in the ATLAS detector. The primary goals of the program are the visual investigation and the understanding of the physics of complete events. Secondary goals are to help develop reconstruction and analysis algorithms, to facilitate debugging during commissioning and to provided a tool for creating pictures and animations for publications. For more information see [117].

[11]TRT, muon chambers used

Chapter 4

Semileptonic decay channels at early stage of ATLAS run

4.1 Early stage of ATLAS run

ATLAS was ready since 2008 when some commissioning, initial calibration and performance studies started using cosmic ray data recorded until the first successful pilot run. The December 2009 was the happy month during which ATLAS begun to capture minimum bias events at center of mass energy of $900GeV$ and later $2.36TeV$. In this month the detector triggered out almost 400 000 events ($\approx 9\mu b^{-1}$) at $900GeV$ with high quality calorimeter and tracking information. For the consequent calorimeter studies the energy $2.36TeV$ ($\approx 0.7\mu b^{-1}$) was used resulting in about 36 000 of events[26]. These datasets do not include many high p_T objects as one expects to be the case of ATLAS designed environment full utilization. Despite of non optimal conditions for the low energy particles studied and of the early stage of run, its data confidence was found to be remarkably good.

Initial beam conditions and detector state has not been optimal and the efficiency of each sub-detector varied between 84 to 100 percent. Problems with luminosity estimation appeared as well as the variable beam related background. The understanding to the at that time incomplete detector (middle pixel layer missing) was crucial, unfortunately DAQ processing capacity and bandwidth was still limited. Together with the requirement on robust trigger with respect to noise, misalignment and effectiveness b physics had to wait until the luminosity studies dropped a bit of trigger capacity this was delivered to B-physics triggers.

Chiefly K_s^0 meson properties were utilized in some investigations on momentum scale, energy loss and tracker resolution.The tracking system of the ID provides a time-over-threshold measurement for the signal which can be used to extract the specific energy loss dE/dx. Studies of tracks (more than 1 pixel hit) and the mean dE/dx is found for each after to be as the distribution presented in Fig.4.1. Readable bands correspond to different particle species.

Among another processes compared with the simulations I would mention the sec-

Figure 4.1: Distribution observed in the data. Bands corresponding to different particle species are clearly visible see also 2.1.2.

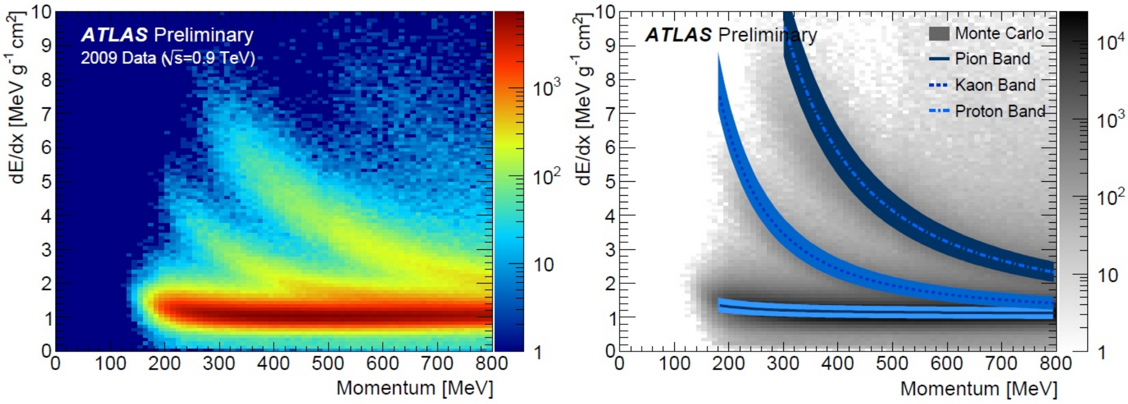

ondary vertex tagging which is essential for indentification of heavy flavour hadrons. Further the track selection for the b-tagging algorithms which was designed to select particles of interest and reject not well measured tracks, tracks from long lived hadrons (kaons) and particles arising from material interactions such as photon conversions or hadronic interactions. Performance of all these algorithm rejections were observed in a good agreement with the monte carlo simulations.

The significant muon signals in the first datasets were triggered with help of the air-core torroid magnet system and end-cap magnets with generated average field of 0.5 Tesla. Thanks to this field muons were free of the multiple scattering effects. Due to only partially functional toroid system, the datasets offering muon analysis were not so extensive as it was the case by the other studies during the early run. The muon trigger described in the last chapter of my thesis has a limited acceptance for the lower p_T muon tracks reconstructed offline. During this pilot run in 2009 38 muons in the endcap regions were triggered at L1 by the TGC and about 12 muons in the barrel. 10 muons were accepted at L1 by the RPC 1 of which with the correct timing during the timing adjustment phase. The other 2 muons of the 12 were outside the trigger acceptance. Only one muon passed the full trigger chain up to the EF combined trigger after applying the $p_T > 4GeV$ cut. The muon momenta and directions measured by the L2 and EF are in good agreement with the offline measurement. The muon spectrum was as expected soft and strongly peaked in the forward direction and so it was hard for them to cross the forward calorimeter since the minimum of $p_T = 3.2GeV$ is required for that, see [12].

During the pilot run the calibration of signals generated by hadronic final states or particle jets was done. The input was formed by electromagnetic energy scale signal with incoming particle energy as a calibration reference. Finally an extension in form of parton level calibration was done. With this I mean the effort to calibrate out particle level inefficiencies like losses in magnetic field etc. and correct acccidental contributions from background activity with use of real data or with help of monte carlo simulations. The pilot run at $900GeV$ continued until the end of March 2010 improving the detector performance. It has the $b\bar{b}$ related fraction of the total cross section smaller than at it is estimated to be at the designed $14TeV$. This together with the low luminosity of $10^{29}cm^{-2}s^{-1}$ results in really a few (tens/month) b events.

4.1.1 7 TeV strategy and changes

These seven-trillion-electronvolt monitored collisions, that is what we have observed for the first time on 30th of March 2010 and what initiated intensive phase of ATLAS performance. In the first $6.8\mu b^{-1}$ or 369673 events containing a 25 total of 3769168 tracks that passed final event selection till April 2010, twice as many tracks as in $900GeV$ are present, see [23]. The increasing center of mass energy leads also to a rising number of charged particles per event as expectations based on simulations told us. Improvements to the trigger threshold and to the track reconstruction settings had to be applied for this new data. In order to improve the efficiency, the threshold for the p_T of the track reconstruction algorithm was more convenient to lower from 500 MeV to 100 MeV. It removed the 'turn on effect' due to the algorithm cut being at the same p_T as the analysis cut.

One of the main features of the $7TeV$ run is the primary vertex reconstruction approach. The one used at $900GeV$ neglected the multiple proton-proton interactions inside the same bunch crossing. This may not be omitted and therefor an iterative adaptive finder algorithm has been developed to reconstruct multiple primary vertices. This algorithm also takes into account the condition that the reconstructed vertices must be consistent with the beam-spot. In view of this 'new' constraint the requirement of being at least three tracks in the vertex was removed. The algorithm has an acceptance of a minimum of 2 tracks per vertex by now. Some changes have been made to the so called Minimum Bias Trigger Scintillator (MBTS) detector (triggers events for readout). To get a better triger signal to noise separation, voltages and the counter thresholds were tuned. After all these changes verification was necessary and so the $900GeV$ results were re-reconstructed with this new setup and compared to the earlier published results.

The selection of events consist of the following conditions that have to be fulfilled for the event to be collected. All inner detector sub-systems are supposed to be at nominal conditions. The event of interest is then supposed to pass the Level 1 MBTS single counter trigger with the origin in the primary vertex. Further condition is the pile-up veto meaning that second primary interaction in the same bunch crossing is forbidden. Thus events that have a second vertex with 4 or more tracks are not qualified for subsequent analysis. At least one good track included finally features also the rejection of an event. Good track is a track with a minimum of one Pixel and six SCT hits, transverse and longitudinal impact parameters calculated with respect to the event primary vertex $|d0| < 1.5mm$ and $|z_0|sin\theta < 1.5mm$, respectively and track p_T threshold as mentioned above.

To handle the beam backgrounds on this data, the MBTS timing difference between the two sides of the detector is used and comparison of the results from a single beam and collision events. The residual backgrounds were found to be below 0.1%.

The increase in the number of pixel hits was found due to the fact that more modules were operational in the 2010 data collecting process. Since in one phase space the reconstruction efficiency (function of $|\eta|$, p_T) should not depend on the centre of mass energy this has been also studied in the real data from $900GeV$ and $7TeV$. Anyway since the p_T spectrum is harder at $7TeV$ center of mass energy the average efficiency over the whole sample of data increased by and so 0.6%. From the track p_T and $|\eta|$ coordinate correlation imply that this increase can be more noticable in certain regions of $|\eta|$. The number of tracks as a function of$|\eta|$ is now quite well understood up to some small inconsistencies at high $|\eta|$ most likely due to unaccounted material.

4.1.2 b-decays related "duties" in timeline range 10-200 pb-1 of data

The beauty production is mediated by gluon-gluon fusion and $q\bar{q}$ annihilation [1], flavor excitation [2] and gluon splitting [3]. It is of an importance to measure the b-hadron p_T spectra within large range so that we are advised how to disentangle the contributions of these production parts. Before we come to that point we have to validate the detector and objects performance (alignment/ tracking/trigger) with the cumulating data collection utilizing the well known processes such as B-decays recognized it. SM signatures understood in ATLAS will form a background for later searches of new phenomena.

To sum up the B-physics program mentioned already in the chapter 2.2, with early data this comprises:

- B-physics trigger calibration with J/ψ, Υ and exclusive B-channels as a tester. Alignment, material, field, reconstruction checkup.
- Heavy quarkonia physics.
- Measurement of production cross sections with continuing performance studies with B-hadrons and quarkonia ($b\bar{b} \to J/\psi/\Upsilon$, $pp \to J/\psi/\Upsilon$)
- B masses and lifetime measurements of well known B-physics quantities to test and monitor the detector performance, with the prospect to improve precisions of these later (with increasing integrated luminosity).
- Starting to collect information on total and differential cross sections of exclusive channels since the large total cross section in ATLAS allows extraction of these channels serving as reference channels for the muonic rare decays .
- Polarization measurements.

The charmonium events resulting in J/ψ which occurs also in plenty of B decays share with them a common detection strategy. In order to distinguishing these prompt J/ψ with the origin at the pp interaction point and the B-hadron decays to J/ψ ATLAS uses to the radial displacement of the two muon track vertex from the beam line. Production mechanism of quarkonium has many features that still remain unexplained, nevertheless we already know that heavy quarkonium production promise to will reveal problems in detector alignment or non-uniformities of the magnetic field with the first year of

[1]Flavor creation in hard QCD scattering corresponds to lowest-order, two-to-two QCD $b\bar{b}$ production diagrams.

[2]Semi-hard process in which a $b\bar{b}$ pair from the quark sea of the proton is excited into the final state due to one of the b quarks undergoes a hard QCD interaction with a parton from the other proton.

[3]Processes in which the $b\bar{b}$ pair arises from a $g \to b\bar{b}$ splitting in the initial or final state - soft process

Figure 4.2: Efficiencies of cut on proper time in order to separate indirect/prompt J/ψ.Pseudo-proper decay time distribution (left-bottom) for reconstructed prompt J/ψ and the sum of prompt and indirect J/ψ from b-decays results in mutual BG forming between J/ψ from b-decays and quarkonia decays (right-bottom).

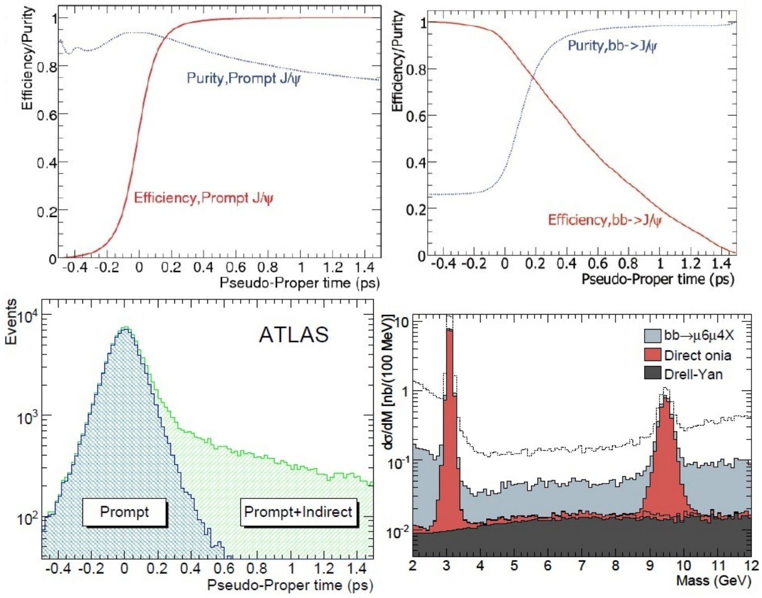

data. Many physics proceses at LHC feature significant quarkonia background (large predicted rates) and its investigation will constantly continue as inevitable tool for initial calibrations of the ATLAS detector and software. J/ψ and B-decays form significant background to each other see Fig. 4.2. Therefore well justified question is: How do we separate these two processes ? The strategy is based on proper time of zero characteristic of prompt J/ψ , while those from B-decays have positive proper time and so we may apply a cut in our dataset analysis. [4]

To proceed with all the quarkonia duties at the early stage I will mention now what is interesting and useful to look at with this production. Firstly the p_T dependence of σ for both J/ψ and Υ is measured reasonably for p_T up to $10-50GeV$ for $10pb-1$ and then up to $100GeV$. Prompt pp over indirect $b\bar{b}$ J/ψ cross-section ratio and prompt $J/\psi \rightarrow \mu^-\mu^+$ and prompt $\Upsilon \rightarrow \mu^-\mu^+$ differential production cross-sections were inspected. Quarkonium spin alignment measurements at ATLAS will help us to make the various production models of quarkonium more legible. Moreover the measurement of cross section contribution to these from χ_c (with $> 10pb^{-1}$, $\rightarrow 30\%$ of prompt $J/\psi(\mu\mu)\gamma$) and χ_b (with $> 100pb^{-1}$) cross-section contributions to J/ψ and Υ by their radiative decays. Polarization of quarkonium may vary with p_T with the consequence that different polarization states influence the overall acceptance (and thus cross-section). Correlations between measured efficiencies and polarization state an important consideration especially at high p_T muon region and so it will be studied also in the future.

In April 2010 invariant mass distribution of muons has been studied at $7TeV \approx 195\mu b^{-1}$

[4]Pseudo-proper time $= \frac{L_{xy}\ M_{J/\psi}}{p_T(J/\psi)\ c}$ where $M_{J/\psi}$ and $p_T(J/\psi)$ represent the J/ψ invariant mass and transverse momentum, and L_{xy} is the transverse decay length of the meson. The estimated resolution in the pseudo-proper decay time is $0.110ps$ for the low p_T charmonia and late 0.07 ps for higher p_T .

Figure 4.3: J/ψ mass from opposite side muon candidates (chosen with MUID/STACO strategy) reconstructed from the first 7TeV data. Each of the muons is in the region $|\eta| < 2.7$ with $p_T > 2.5GeV$, $E > 3GeV$ and impact parameter less than $20mm$, SCT hits > 5. Vertex fit was applied (VKalVrt algorithm).

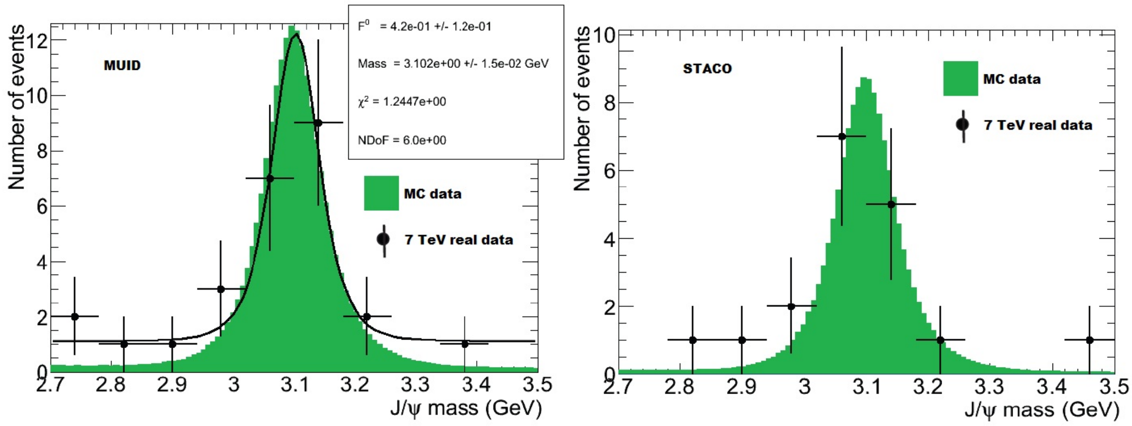

of real data. Excess of events at the expected J/ψ mass has been seen. Since the muon detector does not improve any measurements so far [5], we can recover with help of the tag of ID tagging algorithms. Though we can recover them we need at least a segment of the track in the muon sector and so we must not apply p_T cuts in order to have a chance to capture these muons in the spectrometer. When the same analysis was performed earlier the invariant mass of J/ψ was found to be similar to the found one today see Fig. 4.3. However, on the $7TeV$ real data a wider peak may be observed with a statistical limitations (STACO $\sigma = 94 \pm 26MeV$, MUID $\sigma = 94 \pm 26MeV$ [6]).

As corresponds to the above knowledge, at low p_T the J/ψ cross section is heavily dominated by direct QCD production. At $195\mu b^{-1}$ with the assumptions as taken for histograms 4.3 we see about 14 candidates in the real data in comparison to about 87 proposed by MC simulation. It is important to notice that this may be caused by single muon efficiency and/or polarisation effect. moreover one must not forget that monte carlo simulations also does not have to be correct.

To close the description of quarkonia interests I would like to mention some other measurements on which the early b physics is being based at these days. For example one of the really important reference channels' $B^+ \to J/\psi K^+$ cross section was measured with $10pb^{-1}$ with 5% precisiion (differential cross section with 10%). This particular measurement and its improvement with time will reduce the uncertainties in the overall $b\bar{b}$ cross section estimation. In additon, this decay represents one of the reference channels for other analyses namely of very rare B-decays. With the first data fit simultaneously mass and lifetimes of B_s and B_d mesons are measured using $B_d^0 \to J/\psi K_s^0$ and $B_s^0 \to J/\psi \Phi^0$ decays. After $10pb^{-1}$ the precision of B_d lifetime is expected to reach 10% and similar for B_s mean lifetime after $150pb^{-1}$, see [121]. After this sensitive tests of the detector performancen the precise B-physics at higher integrated luminosity is expected to be

[5]Muon needs at least $3GeV$ of energy to fly through the calorimeter and so many muons do not leave the full muon detector associated track

[6]SACO and MUID are reconstruction algorithms mentioned in the second chapter of this thesis.

explored. In this next step a muon threshold will rise from $4GeV$ to $6-8GeV$. At the designed luminosity, only dimuon trigger will be employed.

4.2 Semileptonic b-decays

The envisaged investigation of events induced by transitions $b \to s(d)\mu^+\mu^-$ is widening the discovery potential which was not accessible to B-factories till LHC era. Such semileptonic decays have a typical branching ratio about 10^{-6} and feature favorable properties providing the probe of perturbative QCD theory. In the later stage of ATLAS run we will proceed to collect a good statistics on the hunted 'Higgs decays' of which the semileptonic decays form the main background. ATLAS has a sensitivity to measure $sin(2\beta)$ comparable to LHCb detector and also with these decays it will contribute to measure $B^0-\overline{B}^0$ mixing. Another interesting new physics related measurements are forward-backward asymmetry which is sensitive to new physics, dimuon mass spectrum, measurements of total and differential cross-sections or angular correlation between the two quarks in $b\bar{b}$ events. The cross section can be made by using the exclusive decays as well as using more inclusive samples such as $b \to J/\psi X$ decays or also even more inclusive technique of tagging b-jets.The angular correlation enables the checking of next-to-leading order or higher contributions to the b-quark production cross section. Among all the variables, the azimuthal separation of $b\bar{b}$ can offer an comprehensive decay information.

As mentioned in the last section, ATLAS to be capable of exclusive b decay perceptiveness has to grasp the response of the detector to all the inclusive J/ψ events. It has been shown with a good agreement with the real data so far that for the J/ψ events selected with p_T thresholds at $6GeV$ and $4GeV$ for the harder and the softer muon respectively, the pseudo-proper time cut $> 0.15ps$ gives $b\bar{b} \to J/\psi X$ selection efficiency of 80% contamined with prompt $J\psi$ on the rest 20%. In earliest data the performance of the detector and reconstruction algorithms have not been well understood and therefore no cuts on the secondary vertex displacement were applied in the b trigger system (topologically similar backgrounds were admitted to the analysis) and so the reconstruction shows the optimal overall precision then. At high luminosity, a secondary vertex cut at the trigger level may have to be introduced to remove the background from direct J/ψ production.

Since all the semi-leptonic rare B-decays have similar topologies the analysis strategy is almost the same. I decided to bring up skeleton of it at this point. I will use a decay $B_d^0 \to J/\psi K^{*0}$ as an example Two oppositelly charged muons are triggered to a common vertex and vertex quality and invariant mass cuts are applied on J/ψ candidate. Also the reconstruction of K^{0*} candidates is done from the $K^{0*} \to K^{\pm}\pi^{\mp}$ decay by forming the corresponding double track vertices and applying vertex quality, invariant mass and transverse momentum cuts. After this the B_d candidates are searched by combining dimuon and K^0 vertices to make up their primordial particle parents as four-track vertices, then again some vertex quality, invariant mass, transverse momentum and proper decay length cuts are applied.

In the following subsections I will describe some properties of the following decays that are the milestones of the early run guiding us to high luminosity at these days. The decays : $B^+ \to J/\psi K^+$ [4] , $B_d^0 \to J/\psi K_s^0$ [7], $B_s^0 \to J/\psi \Phi^0$[21, 25], $B_d^0 \to K^{*0}\mu^+\mu^-$ [9] and

Figure 4.4: Schematic representation of the $B_s^0 \to J/\psi\Phi^0$ decay showing the definitions of the angles Θ_1, Θ_2, χ in the coordinate system used by ATLAS. The list of g_k terms taking this coordinate system into account and corresponding to the angular distribution function see [25] is shown also.

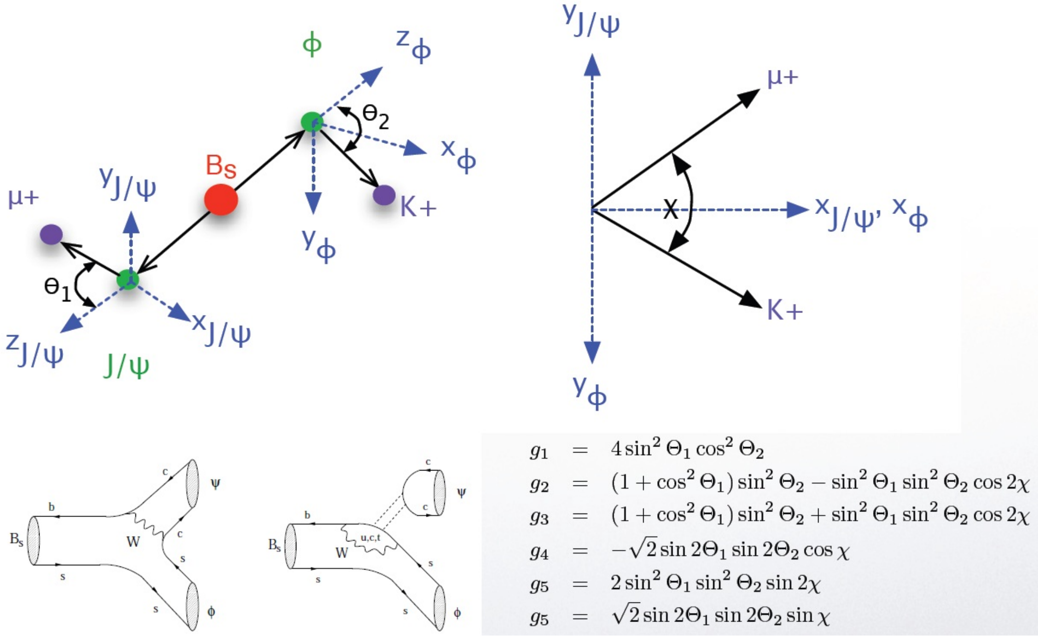

finally $\Lambda_b \to \Lambda(\to p\pi^-)J/\psi(\to \mu^+\mu^-)$ [9, 6] are mentioned in more detail.

4.2.1 $B_s^0 \to J/\psi\Phi^0$

$B_s^0 \to J/\psi\Phi^0$ is topologically identical to the decay discussed further $B_d^0 \to K^{*0}\mu^+\mu^-$. However, the decay $B_d^0 \to K^{*0}\mu^+\mu^-$ is expected to yield 15 times more statistics and together with the other $b\bar{b} \to J/\psi X$ channels form the primary (15%) background to this channel . This decay is sensitive to $B_s^0 - \overline{B}_s^0$ mixing induced CP violation which is characterized by the mass difference Δm_s of the 'heavy' B_H and 'light' B_L mass eigenstates and by a CP violating mixing phase $\Phi_s \approx arg(\frac{V_{cs}^* V_{cb}}{V_{cs} V_{cb}^*})$. The ATLAS sensitivity on the CP asymmetry in this channel is predicted to be of the same order as the small asymmetry predicted in the Standard Model. The weak phase , which in the SM is very small $\Phi_s = -0.0368 \pm 0.0018$, may be enhanced by BSM processes whilst satisfying all existing constraints like measurement of Δm_s at the Tevatron: $\Delta m_s = 17.77 \pm 0.10$ (stat.) ± 0.07 (syst.)ps^{-1} (implicates larger weak phase than the one predicted by SM). This decay leads to three final state helicity configurations and their linear combinations are CP eigensates with different CP parities. On condition that the helicity amplitudes are not separated we are not able to gain the desired weak phase Φ_s. The angular analysis has to be performed to disentangle the amplitudes see Fig 4.4. In the experiment we observe three independent angles, the B_s^0 proper time of this decay and the tagged flavour of B_s^0 (opposite side tag or jet tag).

The time dependent angular distribution, see [25] of this decay depends on 8 physical parameters: two independent transversity amplitudes and their phases $|A_\perp|$, $|A_\parallel|$, $\delta_\perp$, $\delta_\parallel$,

Figure 4.5: Distributions of the reconstructed B_s^0 mass and decay time expected with $150pb^{-1}$ in ATLAS

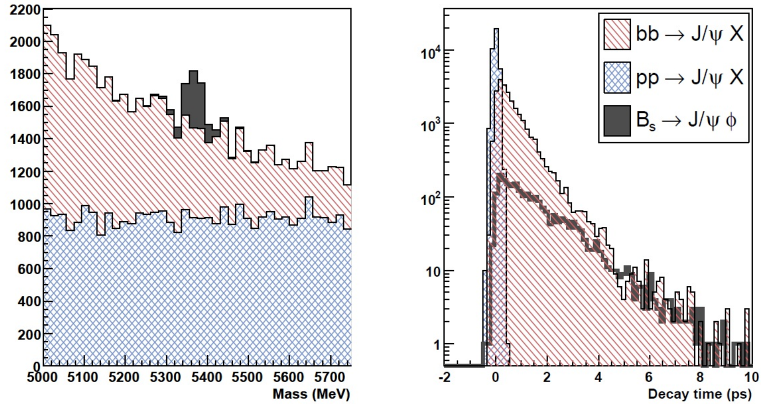

oscillation frequency Δm_s, width difference and mean width $\Delta\Gamma_s = \Gamma_{B_L} - \Gamma_{B_H}, \Gamma_s$ and weak mixing phase Φ_s. New physics has no way of how it could significantly influence $\Delta\Gamma_s$, however extracting it from data is helpful as it provides constraints on the ratio $x_s = \Delta\Gamma/\Delta m_s$, which is free of most theoretical uncertainties.It is good to consider that while all parameter are independent in the theoretical models, the experimental resolution causes some to become highly correlated despite the enormous ATLAS statistics and the well controlled background see Fig 4.5. To avoid unreasonable fit in results results due to Δm_s and Φ_s the parameter x_s is assumed to be measured in $B_s^0 \to D_s\pi$ and $B_s^0 \to D_s a_1$ events and taken as fixed. For each of the above mentioned parameters there are observables that we are allowed to see. These are proper decay time τ and uncertainty $\delta\tau$, three angles Θ_1, Θ_2, χ , the tag of the initial flavour of B meson ϵ, mass m and transverse momentum p_T and some parameters as mistag fraction w_{tag} or the acceptance corrections that are determined by simulations. The value of $\Delta\Gamma_s$ can be determined with a relative error of 12% at $30fb^{-1}$ and the precision of Φ_s observation depends on x_s and on proper time resolution. Ability to resolve the weak phase rapidly drops as the lifetime resolution gets worse. ATLAS expect a mean lifetime resolution of $83fs$.

With sufficient statistics all 7 remaining physics parameters can be determined simultaneously in the maximum likelihood fit which is done in two stages. Firstly the fit to all events with to fix background parameters and secondly fit to all events with fixed background parameters.

The reconstruction itself can be devided into two stages. The first stage is the same as for the $B_d^0 \to K^{*0}\mu^+\mu^-$ decay. Formation of the J/ψ candidate by vertexing pairs of oppositely charged muons with probability of the fit $> 1\%$. 4 GeV di-muon trigger is used by now later. As the luminosity increases invariant mass cuts and increased cuts on the muons $p_T > 4, 6GeV$ will be used to keep a sensible event rate. The invariant mass is assumed to fall within 3σ ($\sigma = 58MeV$) of the nominal value with vertex fit $\chi^2 \leq 6$. And at the end of the first stage the algorithm fits oppositely charged non-muon tracks (kaons) ($p_T > 0.5GeV, \eta < 2.5$) to vertex (Φ). [7]The second part searches the B_s meson by vertexing ($\chi^2 \leq 6$) a J/ψ candidate with an additional pair of oppositely

[7] J/ψ trigger (wrong tag fraction) efficiency after 3 years of running was estimated to be at 72%

charged tracks. The J/ψ mass constrained to nominal value ($1009.2 < M < 1029.6MeV$) during this process and the vertex is assumed to point in the primary vertex direction (probability of the vertex fit required again to be $> 1\%$, $\chi^2 \leq 6$). We require the p_T of a Φ candidate to not be smaller than $2.6GeV$ and similarly to J/ψ, the mass have to be within 3σ ($\sigma = 5MeV$) of the nominal value. Then the cut on $p_T > 10GeV$ of the meson is applied. After this processall the candidate is identified as B_s meson with the decay $B_s^0 \rightarrow J/\psi(\rightarrow \mu^+\mu^-)\Phi^0(\rightarrow K^+K^-)$ With these reconstruction cuts ATLAS expects to have 200000 fully reconstructed signal events with an integrated luminosity of $30fb^{-1}$ (3 years) with a signal event selection efficiency calculated to be about 30% after all cuts. The background is believed to be about 30% of the samples after all cuts, dominated by $b\bar{b} \rightarrow J/\psi X$ and $B_d^0 \rightarrow K^{*0}\mu^+\mu^-$.

As mentioned in the text above we also need an information about the type of the meson. In has been reveald that decay lepton's charge tagging has a very low wrong tag fraction, but is effective only in $\approx 5\%$ of events to decide if the B is B_s or $\overline{B}_s$. Therefore jet charge tagging ('same side tag') stands for most of the events as the most appropriate tool in spite of its higher wrong tag fraction. All the tracks in a jet cone (ΔR) around B_s decay are used to calculate the Q_{jet} quantity.

$$Q_{jet} = \frac{\sum_i q^i p^{\kappa}_{i_{L/T}}}{\sum_i |p^{\kappa}_{i_{L/T}}|} \tag{4.1}$$

More studies showed that the longitudinal momenta of the ith track $p^{\kappa}_{i_L}$ gave the best results in comparison to the transversal one $p^{\kappa}_{i_T}$. κ denotes a tuning parameter in the formula and q_i is a charge of the particular track. 3 parameters are for the early run adjustable with the best efficiency with the values $\kappa = 0.8$, $|Q_{jet}| > 0.2$ and $\Delta R = 0.6$.

During the first run ATLAS produced more than $200pb^{-1}$ of data which corresponds to around 1000 reconstructed signals of this decay. The main focus of these is a fit to simultaneously access the mean mass and lifetimes of the B_s and B_d mesons. Thus the purpose is to get familiar with the detector performance.

4.2.2 $B_d^0 \rightarrow K^{*0}\mu^+\mu^-$

With this decay we have also access to very large field of observables which may open windows to new physics and non-standard model values of Wilson-coefficients, see chapter 1, extending our current view. If our theory is correct we may investigate the value of $|V_{ts}|$ element of the CKM matrix . The latter purpose of ATLAS is also the forward-backward asymmetry search as a phenomenon independent of CKM matrix elements. Due to extremely small event numbers the CERN accelerator system is the first factory enabling the study of this asymmetry in this channel.

The following reactions are considered to stand as an example of background for this decay: $B_d^0 \rightarrow J/\psi K_s^0$, $B_d^0 \rightarrow \omega^0\mu^+\mu^-$, $B_d^0 \rightarrow \rho^0\mu^+\mu^-$. A mentioned above this decay is of the same topology as $B_s^0 \rightarrow J/\psi\Phi^0$ and is also challenging since its angular and mass distribution can be studied only at LHC. The reconstruction process is parallel as by the $B_s^0 \rightarrow J/\psi\Phi^0$ channel. The only difference starts at the last part of the first stage (see

Figure 4.6: Distributions of the reconstructed B_d^0 mass and decay time expected with $10pb^{-1}$ in ATLAS

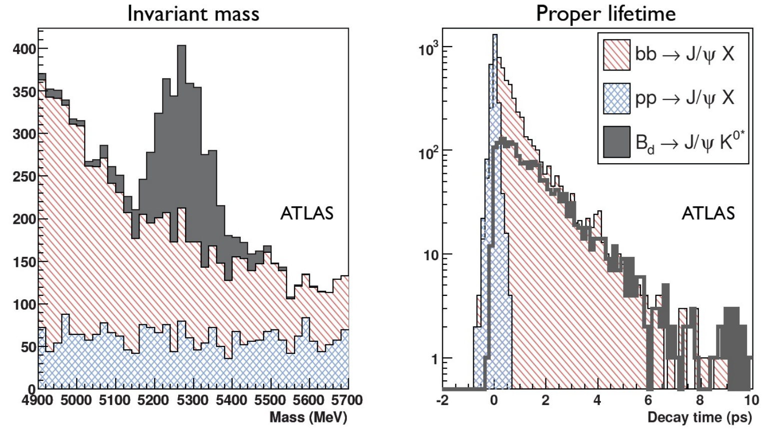

4.2.1) where the algorithms fit oppositely charged non-muon tracks, in this case kaons, pions ($K^{0*} \rightarrow K^{\pm}\pi^{\mp}$) with cuts $p_T > 0.5GeV$, $\eta < 2.5$ to the vertex $\chi^2 \leq 6$. In the second part a candidate ^{0*} is formed by cut on the invariant mass $790 < M < 990\ MeV$ and $p_T > 3\ GeV$. The ^{0*} and J/ψ candidates are then fitted to a common vertex of $p_T > 10\ GeV$, $\chi^2 \leq 6$. If the mass of the vertex lies within a mass window of $\pm 12\sigma$ around the B_d^0 mass this candidate is labeled as B_d^0 meson. In early data, loose cuts will be used with no vertex and displacement cut. The distributions of the reconstructed B_d^0 mass was simulated in Fig 4.6 assuming integrated luminosity of $10pb^{-1}$.For extracting the signal simultaneous likelihood fit is applied to mass and decay time. It has been learned that the mass of B_d^0 should be measured with a precision of 10^{-3} and the average lifetime can be measured with a certainty of 90% at $10pb^{-1}$ of data.

In the early data phase of running the experiment, this self-tagging decay serves as the calibrator of the jet charge tag for jets containing a B_d^0 meson. When tagging performance is well understood, the fragmentation modeling for $B_s^0 \rightarrow J/\psi\Phi^0$ decays may be improved. Validated Monte Carlo models for fragmentation will be used firstly to determine the tagger quality[8] for $B_s^0 \rightarrow J/\psi\Phi^0$ channel.

As noticed similarly to $B \rightarrow \mu^+\mu^-$, the semimuonic decay $B_d^0 \rightarrow K^{*0}\mu^+\mu^-$ self-tagging manly due to manifestation of two muons with high pT in the final state. The quite large branching ratio of this decay channel $= 1.5 \times 10^6$ provided possibility to test sensitively the tracking system before this was checked and better tuned by $B_s^0 \rightarrow J/\psi\Phi^0$ decay.

The partially integrated branching ratio[9]:

$$\Delta B_i = \int_{q^2_{min}}^{q^2_{max}} \frac{dB(B \rightarrow X_i\mu^+\mu-)}{dq^2} dq^2 \tag{4.2}$$

where i stands for s or d quark and $q^2_{min} =\ 1\ GeV^2$, $q^2_{max} = 6\ GeV^2$ ives us a tool to

[8]Tag efficiency $= \epsilon_{tag} = \frac{N_r+N_w}{N_t}$, Wrong tag fraction $= w_{tag} = \frac{N_w}{N_r+N_w}$, Dilution $= D_{tag} = 1 - 2w_{tag}$ and finally the tag quality $= Q_{tag} = \epsilon_{tag}D^2_{tag}$

[9]Branching ratio is defined as fraction of all decays leading to that particular final state.

extract the ratio of the CKM elements which reads, see [10]:

$$< \Delta B_i >= \frac{\Delta B_i + \Delta \overline{B}_i}{2} \Longrightarrow \frac{< \Delta B_d >}{< \Delta B_s >} = \frac{|V_{td}|^2}{|V_{ts}|^2} + corrections \tag{4.3}$$

The corrections in the above stater ratio are of the order of about one percent. The measurement of this ratio thus offers competitive value to the one given by B_s oscillation measurement. Moreover it is possible to come to this CKM element also via another decay using only B_d meson, see [17]:

$$\frac{< \Delta B_d(B \to \rho^0 \mu^+ \mu-) >}{< \Delta B_d(B \to K^{*0} \mu^+ \mu-) >} = \frac{|V_{td}|^2}{|V_{ts}|^2} + corrections \tag{4.4}$$

Unfortunately, this is theoretically much more complicated case due to contributions to Wilson coefficients originating from light quark loops and associated with the presence of low-lying resonances (ρ). These contributions are CKM-suppressed in the case above.

The inclusive parameters of the K^{*0} meson and muons almost are not affected by the matrix elements which is essential for interaction with the trigger. Nevertheless, the spectrum in the dimuon mass and the forward-backward asymmetry is noticeably influenced by them. The forward-backward asymmetry is phenomenologically interesting and will be measured in the experiment as:

$$< A_{FB}(s_1, s_2) >= \frac{< N_F >_{(s_1,s_2)} - < N_B >_{(s_1,s_2)}}{< N_F >_{(s_1,s_2)} + < N_B >_{(s_1,s_2)}} \tag{4.5}$$

where $< N_F >_{(s_1,s_2)}$ and $< N_B >_{(s_1,s_2)}$ are the numbers of all (BG) positively charged moving in the forward (F) and backward (B) directions of the B meson, respectively, in the range of the mass $s \in (s_1, s_2)$ (s represents dimuon mass squared, q^2). The A_{FB} effect disappears in all the dimuon invariant mass spectrum in the SM framework. The effect takes place in some beyond SM theories as shown in Fig. 4.7 which are characterized by the possibility that the Wilson-coefficients C_7^{eff} or C_9^{eff} are allowed to change sign with respect to the SM, this effect is discussed in much more detail in [17].

Finally the prospects for this channels after trigger and offline analysis cuts and considering a 75% first level trigger efficiency amounts 1500 signal events are expected at $30 fb^{-1}$ integrated luminosity.

4.2.3 $B_d^0 \ \to \ J/\psi K_s^0$

If one would like to measure the angle

$$\beta = arg\left(-\frac{V_{cd}V_{cb}^*}{V_{td}V_{tb}^*}\right) \tag{4.6}$$

of the unitary triangle in the picture 1.2 it is needful to find the process that involves the to the β corresponding CKM matrix elements. From the Feynman diagram 4.8 of the golden decay is obvious that we are not able to built the ratio like this $V_{cd}V_{cb}^*$ but this decay alone is proportional to $V_{cs}V_{cb}^*$. If we consider the B^0 meson mixing first defore it

Figure 4.7: Dimuon invariant mass spectrum in several theoretical models on the left and dimuon forward-backward asymmetry (solid line SM, dotted line MSSM $C_7^{eff} < 0$, dashed lines MSSM $C_7^{eff} > 0$) for $B_d^0 \to K^{*0}\mu^+\mu^-$ after obtaining $30^{fb^{-1}}$ on the right.

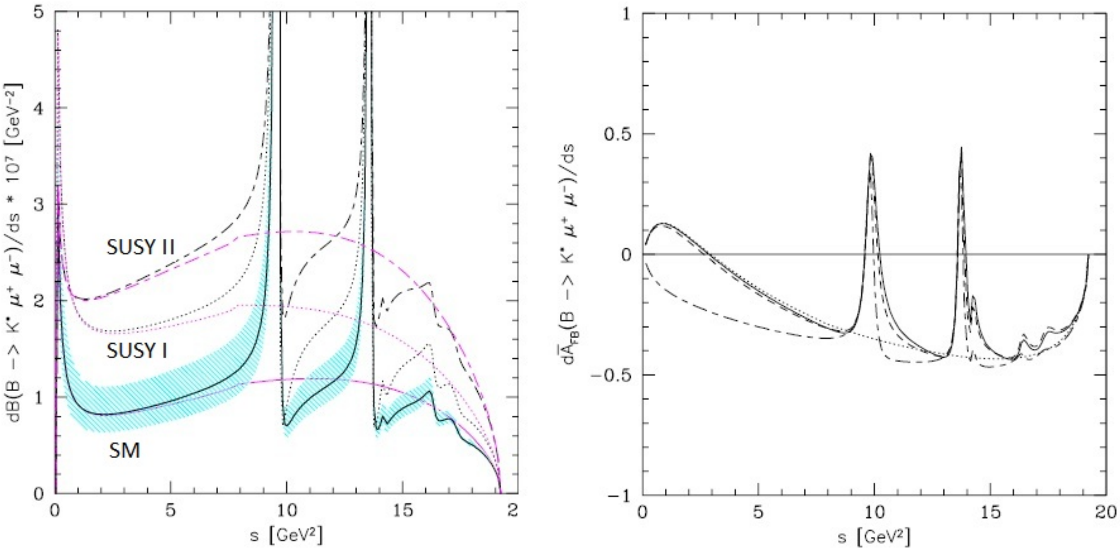

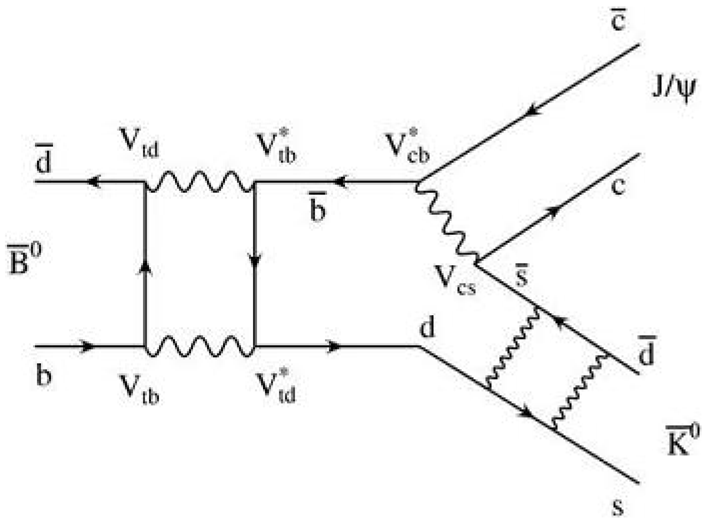

Figure 4.8: Feynman diagram of the golden decay $\overline{B}_d^0 \to J/\psi \overline{K}_s^0$, where the $K^0 - \overline{K}^0$ is taken into account.

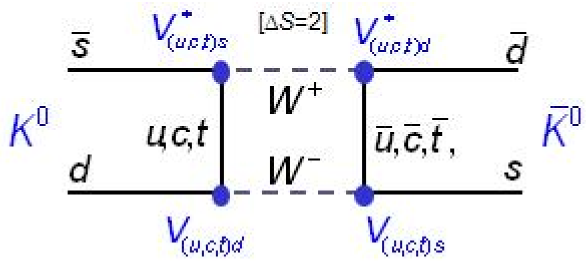

Figure 4.9: Feynman diagram of the $K^0 - \overline{K}^0$ mixing)

decays (see Figure 1.4) with the dominative top quark exchange, we see that this mixing is proportional to the $(V_{td}V^*_{tb})^2$ what is the second power of the denominator in the β definition. But K^0 and $\overline{K}^0$ are produced from the decays of B^0 and $\overline{B}^0$. Therefore for the interference of these processes must mix K^0. From the CKM elements mainly contributing to $K^0 - \overline{K}^0$ mixing see picture 4.9 is this mixing proportional to $(V_{cd}V^*_{cs})^2$.

Now is possible to theoretically put all the decays together to obtain the angle β. First B^0 transforms to $\overline{B}^0$ then it decays into $J/\psi\overline{K}^0$ which ($\overline{K}^0$) then transforms to K^0 :

$$arg\left[\frac{\text{Amplitude}(B^0_d \ \rightarrow \ J/\psi K^0_s)}{\text{Amplitude}(B^0_d \ \rightarrow \ \overline{B}^0_d \ \rightarrow \ J/\psi \overline{K}^0_s \ \rightarrow \ J/\psi K^0_s)}\right]$$

$$= arg\left[\frac{V_{cs}V^*_{cb}}{(V_{td}V^*_{tb})^2\, V^*_{cs}V_{cb}\, (V^*_{cd}V_{cs})^2}\right] = arg\left[\frac{(V_{cd}V^*_{cb})^2}{(V_{td}V^*_{tb})^2}\right] = -2\beta$$

[10] We would like to determine something as follows:

$$\text{Amplitude}(t) = \frac{\Gamma(\overline{B}^0(t) \ \rightarrow \ J/\psi K_s) - \Gamma(B^0(t) \ \rightarrow \ J/\psi K_s)}{\Gamma(\overline{B}^0(t) \ \rightarrow \ J/\psi K_s) + \Gamma(B^0(t) \ \rightarrow \ J/\psi K_s)} = sin(2\beta)\cdot sin(\Delta m_d t) \tag{4.7}$$

,where Δm_d is the oscillation frequency (like the one by B^0 mixing mentioned above). If one would like to make an experiment it is essential to identify our final CP eigenstate $J/\psi K_s$ and to determine the flavour of decaying B^0. There exist an Einstein-Podolsky-Rosen phenomenon which tells that if we produce two coherent quantum states (synchronous evolution of $B^0\overline{B}^0$ - mixed state) the measure of the flavor (or CP) of one meson (e.g. in this case from its decay products which is not the CP eigenstates) determines the flavor (or CP) of the other meson at the same proper time (it is opposite). Once the coherence is destroyed by the decay of one B^0 we need the decay time difference between the two B^0's to calculate the flavour of the tagged B^0 at the time when the second B^0 decayed. The BaBar and Belle factories use above mentioned electron-positron assymmetry-energy bunches to determine these relative decay times of the B^0's from $\Upsilon(4S)$ decay by measuring their decay vertices. We havel to know which of B^0,$\overline{B}^0$ decayed in the final state $J/\psi K^0_s$. We find this decay for example with similar trigger strategy to the one mentioned by the above mentioned decays with cuts on the reconstructed invariant masses of $J/\psi \ \rightarrow \ \mu^+\mu^-$ and $K^0_s \ \rightarrow \ \pi^+\pi^-$. It is possible to tag the flavour of the B^0_d mesons

[10]We can assume that the higher quantum contribution (loop/penguin diagrams) are very small.

from tagging the flavour of the b quark on the opposite side either with the jet charge or lepton flavour of that decay. The opposite side lepton $B - \pi$ tag has been found the most effective in this case and applicable up to ($\approx 85\%$) of all events, see section 3.1.3 or [7] . If we found for example some lepton or charged kaon we are able to identify the flavour of the B_{tagged} before it decays to them and also in the same time we know the flavour of $B_{reconstructed}$. Now we take the oscillation frequency for $B^0 - \overline{B}^0$ mixing and with use of the tiny time difference between the decays of B_{tagged} and $B_{reconstructed}$ received from vertexing (we know speed of $B_{reconstructed}$, we may fix the flavour of the $B_{reconstructed}$. Conceptually we try to measure the CP violation due to the interference of decays B^0, $\overline{B}^0$ with and without mixing. Precise measurements offered us so far a fit of $sin(2\beta) = 0.687 \ \pm \ 0.032$. Calculations with the simulated $30fb^{-1}$ of data predicted that with combination of both tagging strategies a precision on $sin(2\beta)$ could reach 0.01, see [6].

4.2.4 $B^+ \rightarrow J/\psi K^+$

$B^+ \rightarrow J/\psi K^+$ is a control sample used primarily during the pilot run mainly thank to its large branching ratio $= (10.08 \pm 0.35) \times 10^{-4}$. No CP violating asymmetry is expected to be measured but in case that there is some physics beyond the SM the forward backward asymmetry will come up in the observation of this channel also. It is used to measure the asymmetries of production, tracking, the calibration of the opposite-side flavour taggers for CP measurements in the $B_s^0 \rightarrow J/\psi\Phi$ channel (dilution factor due to mistags) and the precise measurements of B^+ mass, lifetime and differencial cross section are performed. The exclusive channel $B \rightarrow \mu^+\mu^-$ will be measured relative to this one. It was one of the first fully reconstructed channel, see also my bachelor thesis where I paid attention especially to this channel.

The dimuon trigger is used for the event selection with one muon with $p_T > 6GeV$ and a second one with $p_T > 4GeV$. Track pairs which are retained after the p_T cut are then fitted to a common vertex with the invariant mass is required to be within a mass window of $120MeV$ around the J/ψ mass. Assuming the transverse decay length cut $l_{xy} \geq 0.1\ mm$ (corresponds with the proper decay time $= 0.5\ ps$ of the B^+) is imposed in order to reduce the combinatorial background from the prompt J/ψs. All tracks with positive charge and not originating in the primary vertex are considered as K^+ candidates. The reconstructed J/ψ together with the K^+ candidate are fitted to a common vertex with $\chi^2 \leq 3.5$ per degree of freedom [11] while the momentum sum of the two has to point to the primary vertex. The total cross section is then estimated from the events selected offline in the region $p_T^{B^+} > 10\ GeV$, using a maximum likelihood fit to the invariant mass distribution. A maximum likelihood method is applied taking gaussian probability density function for the signal and linear distribution for the background. The mass resolution in this channel is estimated, for an integrated luminosity of $10pb^{-1}$, to be $= 42.2 \pm 1.3MeV$ with a total efficiency of $29.8 \pm 0.8\%$. Statistical precision at least 5% may be expected in production cross section measurements while the differential cross section can reach a precision of 10%.The systematic uncertainties are dominated by the luminosity and the branching ratio. The lifetime of B^+ is obtained by a simultaneous fit to the proper decay length and

[11] χ^2 is standard parameter of approach to fitting vertices and it has to do with the quality of the fit

the invariant mass of the reconstructed B^+ candidates taking into account the per event proper decay time error. Using the first $10pb^{-1}$ one can show that the lifetime resolution reach $0.088ps$.

Comments to the decay $B^+ \rightarrow J/\psi(e^+e^-)K^+$

J/ψ may decay also into $\rightarrow e^+e^-$ pairs. If one would like to compute the histogram of the invariant mass of J/ψ from these electron-positron pairs it could be expected that the width of the fit is larger because electrons lose its energy along the trajectory due to bremsstrahlung. I code for this analysis in unfortunately still not written, and I do not have so much time to participated on its development. But from the consultation about J/ψ invariant mass reconstruction from electron positrom pairs ensue that basically it is true that with muons we may have better results, as efficiency of reconstruction is better and resolution also, but still it might be good for an analysis to have one more approach by using electron decays. Moreover is this code important due to more reasons. Who knows what will come with first ATLAS data ? To do the muon chambers alignement etc. will take some time and for the analysis could be electrons for a while more useful. In fact the main reason is that we are interested in all $X \rightarrow e^+e^-$ resonance to study the electron reconstruction and understand calorimeter and inner detector (parts of the ATLAS detector). If we will have low background, then the fact to have the resonance favours the use of these events to study the decay product (same stands for muon decays of course). For J/ψ you have a huge amount of data produced. For electrons (also for muons) you have the Z which is the first thing to look at in first data, but electrons and muons are of high transverse momentum. The J/ψ or Υ resonance because of their low mass give low p_T electrons (or muons), so we are able to study our favourite detector at lower energies, in particular check the energy scale. That is if the J/ψ or Z mass is well reconstructed at its known value. If not we have a way to calibrate the energies, and we can do it at different energies - not only with Z. Also we can intercalibrate our detector whether is the reconstructed J/ψ or Z mass the same everywhere in the detector. If not we can correct the inhomogenities. Finally at low energies is our sensitivity to the to the amount of material in front of the calorimeter much better.

4.2.5 $\Lambda_b \rightarrow \Lambda(\rightarrow p\pi^-)J/\psi(\rightarrow \mu^+\mu^-)$

Our knowledge about the lightest b baryon Λ_b is rather basic. There are many so far hidden unexplained or estimated behavior to search for in this decay such as the direct search for CP and Time Reversal asymmetries, polarization and its saturation, lifetime measurement and so on. I would like to give a picture of how the polarization and forward backward symmetry is observed in ATLAS.

During the lifetime of ATLAS the prediction of inclusive Λ_b polarization from quark-quark scattering in proton-proton collisions. Λ_b baryons originate inclusively in p-p collisions and $\approx 30\%$ of them are polarized. This spin effect could be caused by the quark quark scattering model in which polarization of incoming u and d quarks is responsible for the spin of the baryon. Another explanation is provided by the so called Lund model in which s and $\overline{s}$ spins align with polarization of 100% to offset orbital angular momentum

Figure 4.10: Kinematics of $\Lambda_b \to \Lambda^0(\to p\pi^-)J/\psi(\to \mu^+\mu^-)$. θ is a polar angle of $\overline{p}_\Lambda$ momentum in the Λ_b rest frame relative to the normal $\overline{n}$ to the production plane. θ_1 and ϕ_2 are the angles of the proton in Λ^0 rest frame with the z axis parallel with p_Λ and the y axis parallel to $\Lambda_b \times \overline{p}_\Lambda$, θ_2 and ϕ_2 are defined for the J/ψ decay in a similar sense.

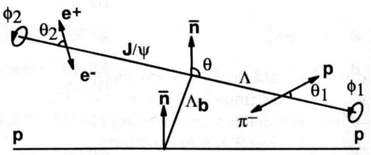

produced in color strings snapping during pair production. The u and d quarks significantly contribute to the momentum of Λ_b and the s quark contributes no net spin effect. This implicates that the proton and Λ_b polarizations can be compared with simple momentum scaling see Fig. 4.11. Nevertheless the polarization seems to be due to leading u and d quark rather than s-quark polarization and so the winner candidate in this is so far the quark-quark scattering model. One of the reasons why this effect is of interest at LHC is the Tevatron factory observation which gave us the first estimations on Λ_b polarization and as it has been shown, these predictions are found to be an order of magnitude too small polarizations on both b and s quark. Therefore significant Λ_b polarization measurement could be a sign of new physics. Lambda polarization increases linearly for transverse scattering momenta $< 1GeV$ but then achieves a plateau maintained through $3.5GeV$, see Fig 4.11. This is really dramatic and so far unexplained behaviour. Quark-quark scattering model provides only Monte carlo simulations for Λ_b polarization combinatorict without a explaining the reason of this saturation. It could be explained by the Lund model which states that the correlation between $s\overline{s}$ transverse momenta and spin polarizes the Λ_b. In more detail it assumes that the from vacuum originated $s\overline{s}$ spins are aligned in the above mentioned sense. Nevertheless measurements from 2003 give us a sign that these spins might not be necessarily correlated which would destroy the Lund explanation. Possible way to explain this could provide gluon polarization, gluon coupling[12] or better Lund Model mass dependence test. All of them need LHC for discoveries.

Information about the quark mass dependence of Λ_b polarization effects can be obtained from a polarization measurement with Λ_b baryons via the angular distributions of the cascade decay shown in Fig. 4.10.

This cascade decay is described by seven parameters including the Λ_b polarization, four helicity amplitudes, measured asymmetry parameter α_b for lambda decay, and J/ψ decay normalization amplitude. Each of three stages of this decay is described by quantum mechanical amplitude. These multiplied and squared in principle uncover the probability of observing an event like this cascade decay is. This probability is called the angular distribution function that depends on the five defined production angles see Fig. 4.10 and give us access to polarization and seven helicity amplitudes measurements and final estimations. Just to give a picture how such a distribution function looks like, it is the sum of twenty terms over the product of three functions. First of them consist of combinations

[12] Gluon polarization: The gluon in proposed to be a quanta of one unit of spin, supporting alignment of pair-produced spins. Gluon coupling describes the transverse momentum dependence of spin-flipping probability.

Figure 4.11: Forward-backward asymmetry of $Lambda_b \to \Lambda^0\mu^+\mu^-$. Left: Invariant mass distribution from Λ_b candidates identified in $b \to J/\psi\Lambda X$ Monte Carlo sample. A fit to the fully reconstructed events after vertexing requirement is shown. Center: Inclusive lambda polarization plateaus for momenta greater than $1GeV/c$. Right: Solid crosses correspond to the asymmetry predicted by the model with the positive C_7^{eff},see [17] while dashed crosses correspond to the asymmetry predicted by the standard model. Experimentally interesting points are denoted by bold points with error crosses.

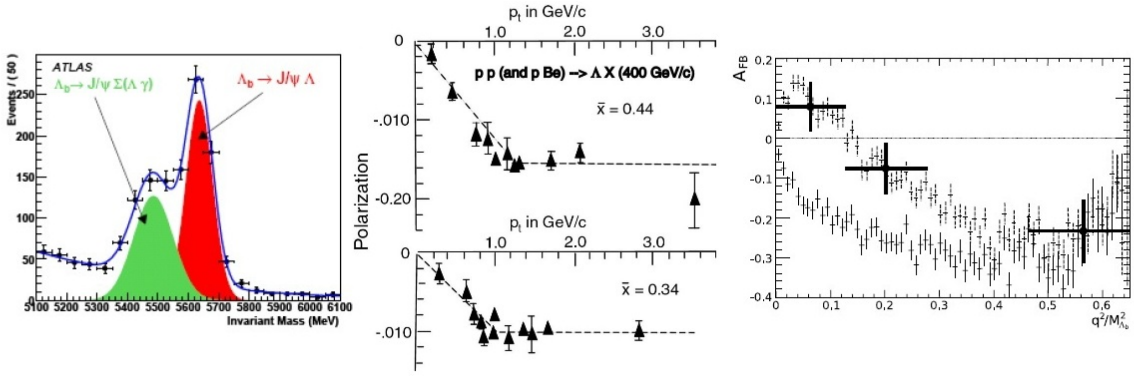

of four helicity amplitudes, second is a function of Λ_b polarization and measured parity-violating asymmetry parameter α_b and finally the orthonormal functions in terms of the five measurable angles. At the end of this picture about polarization I would like to mention that ATLAS sensitivity of measuring these spin properties of Λ_b was predicted to amount 6.1% (effectivity dimuon triger is taken into account). With an integrated luminosity of 30 fb-1, it is expected to observe 13000 signal events of this type.

In the graph 4.11 one can see the forward-backward asymmetry for this decay which leads to indirect test that will with after $30fb^{-1}$of data (providing 800 reconstructed signal events), enable clear distinction between the SM and some of it's extensions. How such a distribution exactly look like depends also on trigger and offline selection cuts especially in the low q^2 region because the detector acceptance and muon trigger are designed for higher p_T . This is a cause of A_{FB} reduction by a factor of 0.6 at $s = \frac{q^2}{M^2_{\Lambda_b}} < 0.1$. Another inconvenience is caused by the small muon opening angle that is trigger challenging. For all these reasons I will not mention how exactly is this decay triggered in ATLAS, for more information about that you can look into [8] The dimuon invariant mass $q^2 = (p_{\mu^+} + p_{\mu^-}) = M^2$ is divided into three regions. The first from $(\frac{2m_\mu}{M^2_{\Lambda_b}})$ to the so called zero point where the forward-backward asymmetry vanishes. Second range is from zero point to lower boundaries of $c\bar{c}$ resonances $(J/\psi, \Psi')$ and the last is from resonances area to $\frac{(M_{\Lambda_b} - M_{\Lambda^0})^2}{M^2_{\Lambda_b}}$ limit .

Chapter 5

Analysis of B-meson decays

What did really happened in our bunch of events ? That is what we deal with when we want to physically analyze the processes in the detector and discover the reasons of it. This is going to be more described in the last chapter of my thesis. Only the physicists decide what is reasonable to look at and whether it is something unknown to our nature understanding or not. We create histograms based on all the physically reasonable cuts and sometimes use Atlantis software to see immediately how it looked in the detector - the hits, tracks, kinematics etc.

In my case the analysis had the following two stages. The first one is the Athena framework analysis, where we can select or remove objects by writing an Athena algorithm (C++ language). It finds particles via certain parameter cuts or derive other physics data . In the second stage we go out of framework analysis. It means we use ROOT for analyze and plot histograms etc. Almost everything about Athena could be found in by me used well written paper [119].

The main B-physics analysis code is implemented as Athena tools and algorithms. Athena has a central algorithm repository for all algorithms which may be accessed via the (by me sometimes also used) web page [100]. This is not the only way how to access the code. My work has been done via the lxplus5.cern.ch server (Scientific Linux 5 installed) as my user interface. It is necessary to set up your account before you start work. One of the most general thing before whatever can be done is to set up the Configuration Manager Tool, which manages all the Athena software so that all users can use the code of all other users, which made their code part of the Athena and may benefit from common methods, functions and data types accommodated in this framework. This is only once per CMT setup and you do not need to do it often. Another thing which changes more often is the Athena release setup. The release of Athena refers to a bunch of packages that are tested and continuously developed to work together. The status is denoted by numbering. At lxplus5.cern.ch you may find different AtlasProduction releases which have the number 15.0.X and then you may set up to use the different builds from the folder /afs/cern.ch/atlas/software/builds/AtlasProduction at lxplus5.cern.ch . I used Athena release 15.6.8.9. We do this namely because the development of the algorithms is faster then the documentation and so you have to tune everything to work together properly. For that I used the following web sites: Doxygen documentation [55] and the hypernews [56]. After this is done one may 'check-out' the packages of interest using

CMT. So in this way the source code of algorithms developed by Bphysics group were copied to my home directory at lxplus and consequently compiled for the Unix system. Before compiling the user is free to make any changes in the source code. The minimum requirement is that the code has access to TrackParticles, Primary Vertices and Muons and the realistic analyses needs to use the Trigger information also. Note that analyses on Monte Carlo data use of Truth information as well. The C++ packages related to B physics are, see[57]: BPhysAnalysisObjects - accommodates some utility classes that construct objects such as BCompositeParticle or Vertex and hold information about it from vertex finding programs. BPhyAnalysisTools are suitable for use in searching of the particular decays are presented with interfaces to the vertexing programs. BPhysExamples mostly demonstrates how to use the tools in some particular cases of analysis of B events. BPhysAnalysisSkeleton are useful classes that containing two algorithms one of which, BSkeleton, is used for developing your own code and the EarlyData algorithm used for early data analysis and also for demonstration of tools for vertexing, making n-tuple files etc. JpsiUpsilonTools is a nice tool for finding quarkonia decays into two muons. This is the only part that is other-code-independent so that it may be used by the whole collaboration for various studies. And several other packages treated by the corresponding group of people developing them: JpsiUpsilonAlgs, BJpsiDecayAlgs, RareDecayAlgs, HadronicDecayAlgs and LeptonDMesonAlgs. BJpsiDecayAlgs is the package that contains two main algorithms Bplus2JpsiKplus.cxx and B2JpsiV0.cxx. the former has been developed by Christos Anastopoulos, James R Catmore, Ioannis Nomidis and Patrick Jussel and serves for analysis of $B^+ \;\rightarrow\; J/\psi K^s+$ decay. The latter comprises tools for selection decays $J/\psi \rightarrow \mu^+\mu^-$, $\Lambda \rightarrow p\pi$, $\overline{\Lambda} \rightarrow \overline{p}\pi$, $K_s \rightarrow \pi\pi$, $\Lambda_b \rightarrow \Lambda(p\pi) + J/\psi(\mu\mu)$, $\overline{\Lambda}_b\Lambda_b\overline{\Lambda}(\pi\overline{p}) + J/\psi(\mu\mu)$, $B_d \rightarrow K_s^0(\pi\pi) + J/\psi(\mu\mu)$. The Bplus2JpsiKplus.cxx and EarlyData.cxx were the algorithm of my interest. There is also some set of jobOption files (Python scripts) corresponding to each algorithm. These files can steer the C++ code after compilation. One may make cuts of the parameters of the analysis without the necessity to modify and recompile the whole code. A single Athena algorithm searches in the reconstructed AOD data for a given decay process and summarize the output is in the form of ROOT n-tuple files which contain a list of all possible candidates of the decay being sought, with full information on each part of the decay tree down to the tracks. Final analysis (including tuning cuts and all statistical analysis) should be performed on these ROOT n-tuples using ROOT scripts. The general technique is therefore to keep cuts in the Athena analysis as broad as possible.

In case you have a grid certificate from the certification authority (in my case CESNET) and you are subscribes as a member of so called ATLAS VO you are allowed to use the GRID computing resources and the really big datasets from the experiment. I was using Ganga []as a user interface for submitting jobs to grid. After the job is submitted it is distributed to the particular site for execution. When it is done the output is stored on the GRID and you may access it via DQ2 tools, see [58]

In order to analyze the real data a new tool has been developed. The Run Query Tool to find information about the latest runs and their corresponding datasets producing a MyLBCollection.xml file is used that contains information about the selected runs (numbered) and about the conditions. This file can be received via the following web page: http://atlas-runquery.cern.ch/ or using the AtlRunQuery.py script followed by the required run number and conditions, for more information see the web

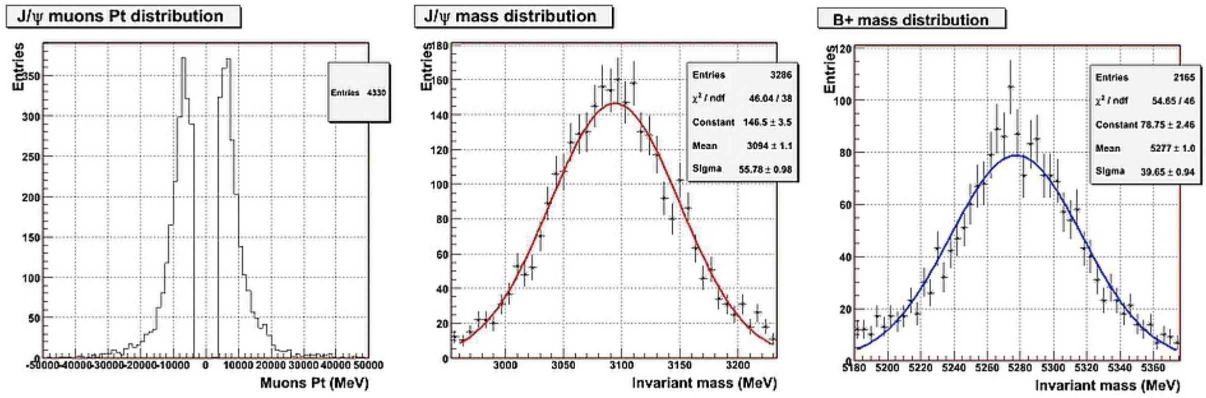

Figure 5.1: On the left: The J/ψ muons p_T distribution. Opposite sign in p_T means negative positive charge. Center:Invariant mass of J/ψ particle calculated from muon pairs p_T. On the right:Invariant mass of B^+ particle.

page. This also so called Good Run List mechanism to select lumi blocks that have been marked as containing collisions by the data quality experts is a tool of especial importance. Not all the runs are good for physics analysis, also because of the detector condition changes during the different runs and some of the detectors can be turned off etc. Another very interesting analysis approach is being developed. The TAG analysis in which you just need to find the runs in which you are interested in and at which conditions the events took place and the system will provide you a nice way for analyzing the events using your code on the GRID. The advantage of this is that you do not need to find every single dataset and write it as the input into your job options. It selects effectively just among the interesting events that took place regarding to your conditions that you required when you prompted the summarized *.root file from ELSSI gateway https://voatlas18.cern.ch/tagservices/index.htm. For selection on this web page you may again generate an MyLBCollection.xml file or use the run numbers and the tags of the datasets such as data10_7TeV_physics_MinBias_f238_m427_READ for more information please see [99]. The *.root file , usualy named with your name is than used as a reference on the important data for analysis on the Grid using this prompt: execfile('./gangaTAGPrepare.py') and after the job is completed then you put the corresponding file name with the path to it into another python script steering your analysis with your algorithm, this time execfile('./gangaWithTAG.py') will give you the output in terms of ROOT nTuples.

Just to mention what has been done by me already in the past for the monte carlo data generated for ATLAS. I used the code for reconstruction of $B^+ \rightarrow J/\psi K_s^+$ decays with the cuts mentioned in the section 4.2.4 . The only difference was the transverse momentum cut for the second muon - at that time $p_T \geq 3\ GeV$. I received the following histograms of invariant masses Fig.5.1. The width of the fitted gauss distribution is larger than it should be in reality by reason of the detector multiple scattering effects. The tails at the edges of the histograms were not possible to be fitted by gauss, because they originate from muon energy loss along its track. I used the algorithms Bplus2JpsiKplus.cxx made by the BPhysics group and with since the statistic in one run is quite low I needed to reconstruct many events. For that I choose runs from the end of March 2010 till the middle of April 2010 containing a large number of events which had the tag data10_7TeV

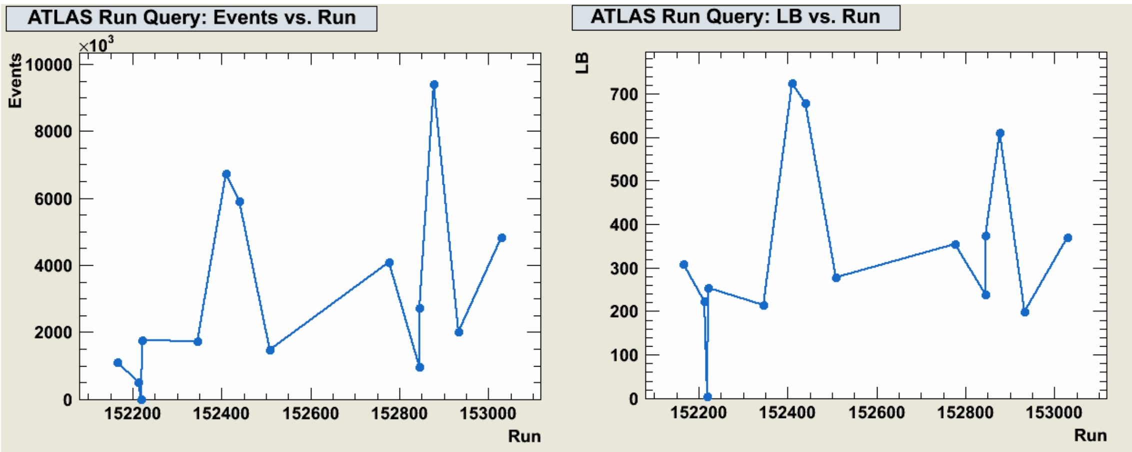

Figure 5.2: Number of events vs the run number

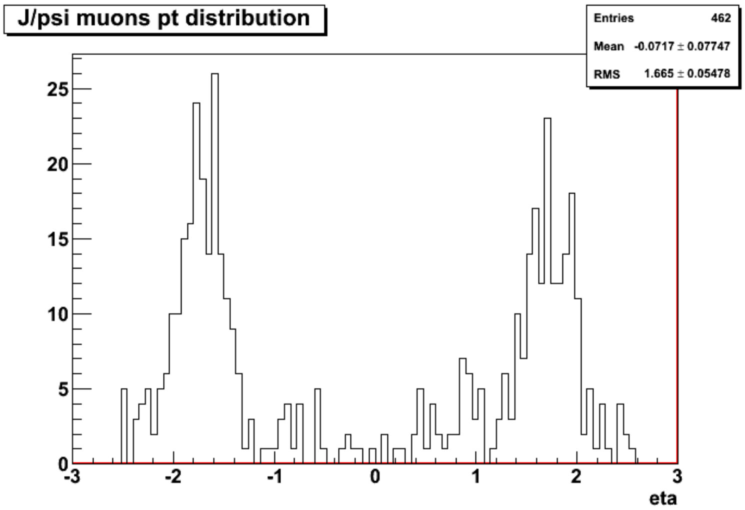

Figure 5.3: J/ψ muons p_T distribution

and were related to all detectors turned on, LHC stable beam and physics with minimum bias trigger. The picture 5.2 relates the run number with the corresponding number of events. After obtaining the results for each run the overall integrated luminosity could be calculated with the use of LumiCalc.py tool. It is rather complicated process since it requires quite an amount of information including the list of complete luminosity blocks LB - this value is implicitly given by the run number ranges and the status of the detector. Moreover, luminosity is trigger specific and requires also an estimate of the instanteous luminosity for each LB (even if there are some empty output files they carry information about these LBs !) [130] . I was able to extract only the number of LBs depending on the run number as in the Fig.5.2.I followed the above stated TAG analysis procedure to get the following histograms 5.3 , 5.4 , 5.5 .

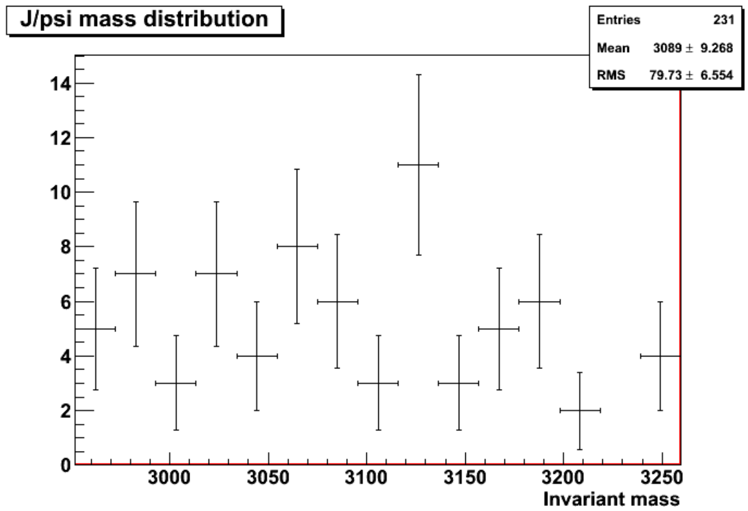

Figure 5.4: J/ψ mass distribution

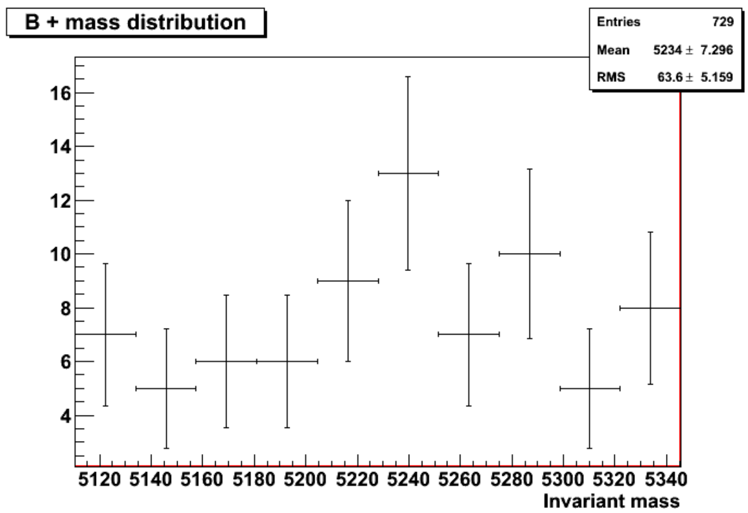

Figure 5.5: B^+ mass distribution

Chapter 6

Thesis Summary

In the first chapter of my thesis I put an effort into rather brief description the CP violation in neutral B meson decays. I started with the usual effective Hamiltonian that describes rare b decays and then reviewed some basic knowledge about the CKM matrix. The CP violation puts with its existence a unified and unbiased attack on new physics at the top of the triangle. From a sketch of all possible CP violating effects I come to $B_q^0 - \overline{B}_q^0$ oscillations and later provide something like a framework for CP violation description in neutral B meson decays.

From the theory describing the CP violation I move to the experiment in the second chapter, the half of which is focused on description of the ATLAS experiment and its major detector parts. The observation of b flavoured hadron decays with large statistics of ATLAS may offer a very fertile testing ground for the Standard Model description and eventually could extend the physical view of the reality. One of the main motivations for the CP violation experiments was the revelation of the CPV mechanism by B decays. b-physics prospects in ATLAS and especially the radiative, hadronic, purely muonic B-decays are discussed.

Dispose of more than 90 million readout channels sort over 1 billion collisions per second, that is what the ATLAS data aquisition and trigger system has to cope with. The next chapter is devoted to this system and namely to b-trigger and b-tagging strategies as a necessary tools for the analysis of b-decays. The 9 major components of ATHENA framework and the offline analysis are depicted .

I dedicated the fourth chapter to the semileptonic decays. The largest experimental equipment that have been ever built and started its operation during writing this thesis and so the early stage of this run at a low luminosity is mentioned from the b physics point of view. The expected properties of semileptonic decays of b-hadrons are stated in connection to the first years of ATLAS observation.

The principal of offline analysis are pointed out at the end of the thesis. The analysis of the real data comprises the use of a new tool- GoodRunListGenerator to pick out the dataset of interest. Since one of my interest is the practical modern physics and their tools I decided to analyze one up to now well measured decay of B^+ meson iin the new framework of TAG analysis.

Bibliography

[1] The ATLAS Collaboration *Expected Performance of the ATLAS Experiment; Detector, Trigger and Physics* CERN-OPEN-2008-020 December 2008

[2] Dimitrios Sampsonidis, ATLAS Collaboration *Early ATLAS B-physics with the first* $10 - 100pb^{-1}$,Aristotle University of Thessaloniki

[3] G.C. Branco, L. Lavoura and J.P. Silva,CP Violation, Clarendon Press, Oxford, UK, 1999.

[4] A. Policicchio, G. CrosettiB^+ Semileptonic Rare Decays in ATLASUniversity of Calabria and INFN Cosenza, ATL-PHYS-PUB-2007-017

[5] Gerhard Buchalla, Andrzej J. Buras, Markus E. Lautenbacher *Weak decays beyond leading order logarithms* arXiv:hep-ph/9512380v1 15 Dec 1995

[6] Attila Krasznahorkay Jr.[1,2] for the ATLAS and CMS collaborations, *Outlook for b Physics at the LHC in ATLAS and CMS* 1- University of Debrecen - Dept. of Experimental Physics 4010, Debrecen, Egyetem ter 1. - Hungary 2- CERN - PH Dept. CH-1211, Geneva 23 - Switzerland

[7] P.A.Booth, C.M.Buttar, M.H.Lehto Limist on the Observability of Direct CP Violation in the Decay $B_d^0 \to J/\psi K_s^0$ for ATLAS Departement of Physics and Astronomy, University of Sheffield August 9, 2001

[8] Daniel Scheirich*Development of Optimal Algorithms for the Selection of Rare Semimuonic B Decays in ATLAS*Institute of Particle and Nuclear Physics,CERN-THESIS-2008-048

[9] A. Policicchio, G. CrosettiRare Semileptonic Beauty Decays in ATLASUniversity of Calabria and INFN Cosenza, ATL-PHYS-CONF-2006-011

[10] Sebastien Viret for the LHCb,,ATLAS and CMS collaborations *Rare B decays at LHC*, LPSC, 38026 Grenoble, France

[11] Szymon Gadomski, For the ATLAS Collaboration *Overview of ATLAS B-Physics Prospects*, ATL-CONF-2002-007

[12] J.Kirk RAL on behalf of ATLAS and CMS Collaborations *B-triggers at ATLAS and CMS*ATL-DAQ-CONF-2007-007

[13] Fairouz MalekCP Violation and Rare B decays at ATLASLPSC, IN2P3-CNRS-Universit Joseph Fourier Grenoble, FR-38026 France

[14] C. DAmbrosio, T. Gys, C. Joram, M. Moll and L. RopelewskiParticle Detectors Principles and Techniques CERN PH/DT2, presentation

[15] Martin zur Nedden for ATLAS Collaboration Precise B-Decay Measurements sensitive to Beyond Standard Model Physics at ATLASHumboldt-Universitat zu Berlin, Institut fur Physik, Berlin, Germany , ATL-PHYS-CONF-2008-007

[16] Weina Ji on behalf of the ATLAS, CMS and LHCb Collaborations *B Hadron Properties at the LHC* Lund University

[17] P. Ball et al. *B DECAYS AT THE LHC* , CERNTH/2000101, arXiv:hep-ph/0003238v3 25 Mar 2000

[18] M. Beneke et al., Phys. Lett. B459, 631 (1999).

[19] The ATLAS Collaboration *Study of the rare decay* $B_s^0 \to m^+m^-$ *in ATLAS*ATL-PHYS-PUB-2006-000

[20] S. Hashimoto et al., hepph/9912318.

[21] James Catmore for the ATLAS Collaboration *ATLAS performance in B-physics channels sensitive to new physics* Lancaster University, UK

[22] James Catmore, ATLAS Collaboration *Presentations on ATLAS performance in B-physics channels sensitive to new physics*, Lancaster University, UK

[23] The ATLAS Collaboration *Charged particle multiplicities in pp interactions at* $\sqrt{s} = 7$ *TeV measured with the ATLAS detector at the LHC*April 13, 2010

[24] F. Derue B-physics overview in ATLAS ATL-PHYS-PUB-2007-002

[25] Alastair Dewhurst on behalf of the ATLAS and CMS collaborations $B_s J/\psi\Phi$ *with ATLAS/CMS*on behalf of the ATLAS and CMS collaborations, ATL-PHYS-PROC-2009-139

[26] Bruno Mansoulie, Bill Murray, Hans-Christian Schultz-Coulon, Karl Jakobs, Marzio Nessi, Tony Liss, Peppe Iacobucci *Performance of the ATLAS detector using First Collision Data* May 6, 2010 and https://twiki.cern.ch/twiki/bin/view/AtlasProtected/FirstPerfPaperWork

[27] Nikolai Nikitina, Serguei Sivoklokova, Maria Smizanskab, Danila Tlisova 4, Konstantin Tomsa *Backgrounds for rare muonic B-meson decays at ATLAS.* ATL-PHYS-PUB-2007-009

[28] Lidia Smirnova, Alexey Boldyrev on behalf of the ATLAS CollaborationPhysics with B-mesons in ATLASXXXIX International Symposium on Multiparticle Dynamics,4-9 September 2009

[29] Eduard Ebron Simioni, promotor: prof.dr. M.H.M. Merk *New physics from rare beauty*VRIJE UNIVERSITEIT, CERN-THESIS-2010-031

[30] Atlas CollaborationThe ATLAS Level-1 Calorimeter Trigger2008 JINST 3 P03001, PUBLISHED BY INSTITUTE OF PHYSICS PUBLISHING AND SISSA

[31] The ATLAS CollaborationThe ATLAS missing ET trigger performance with initial LHC runs at $\sqrt{s} = 900$GeVATL-COM-DAQ-2010-006

[32] The ATLAS Collaboration AbstractATLAS High Level Calorimeter Trigger Software Performance for First LHC Collision EventsMarch 18, 2010

[33] The ATLAS CollaborationThe ATLAS Trigger Monitoring and Operations in proton-proton collisionsATL-PUB-2010-xxx, March 9, 2010

[34] The ATLAS Collaboration1Performance study of the level-1 di-muon triggerATL-PHYS-PUB-2009-000

[35] John BainesB-trigger working group work plan - presentation

[36] Johannes HallerThe trigger system of the ATLAS experiment prezentation

[37] Srivas PrasadThe ATLAS trigger systemHarvard ATLAS weekly meeting April 04 2007, prezentation

[38] Sven menke, MPP MunchenATLAS Data & Analysis Model Seminar Uni-Wuppertal

[39] Fred WickensHigh Level Triggering presentation, Rutheford Appleton Laboratory

[40] Sebastian Fleischmannb-tagging algorithms presentation , Univ. Wuppertal

[41] The ATLAS Collaboration Tracking studies for b-tagging with 900 GeV collision data with the ATLAS detectorATLAS-CONF-2010-003 , March 8, 2010

[42] Hai-Jun Yang, Xuefei Li, Tiesheng Dai, Alex Burgers, Alan Wilson, Bing ZhouB-tagging Based on Boosted Decision Trees and Performance Comparisons of ATLAS B-taggersJuly 20, 2009

[43] Giacinto Piacquadio on behalf of the ATLAS Collaboration B-Tagging at LHC: Expected Performance and its Calibration in Data ATL-PHYS-PROC-2008-070

[44] Thomas Gopfert, on behalf of the ATLAS collaboration Tagging b-jets in ATLASATL-PHYS-PROC-2010-014, 02 February 2010

[45] Laurent VACAVANT, on behalf of the ATLAS Collaboration Prospects for b-tagging in ATLAS and tracking commissioning results with cosmic rays, ATL-PHYS-PROC-2010-015

[46] The ATLAS Collaboration Performance of the ATLAS b-tagging Algorithms ATL-PHYS-PUB-2009-018

[47] The ATLAS Collaboration Vertexing For b-tagging, ATL-PHYS-PUB-2009-019

[48] The ATLAS Collaboration Calibrating b-tagging using Dijet Events ATL-PHYS-PUB-2009-024

[49] The ATLAS Collaboration HLT b-Tagging Performance and Strategies ATL-PHYS-PUB-2009-031

[50] I. Nomidis on behalf of the ATLAS Collaboration *Preparations for precise measurements of rare muonic B-decays* May 27 - June 1 2009, Lake Placid, NY, USA Aristotle University of Thessaloniki

[51] Werner Riegler, *Summer Student Lectures 2009*, CERN

[52] P. Jussel, T. Stahl, B. Epp, E. Kneringer, W. Walkowiak Study of muon trigger scenarios for the measurement of B_s^0 oscillations in the channels $B_s^0 \to D_s^- \pi^+$ and $B_s^0 \to D_s^- a_1^+$, December 18, 2006, Institute of Astro- and Particle Physics, University of Innsbruck, Austria Department of Physics, University of Siegen, Germany

[53] H.-G. Moser * . A.Roussarie *Mathematical Methods for*$B^0\overline{B}^0$ *oscillation Analyses*, CERN-OPEN-99-030

[54] http://atlas-computing.web.cern.ch/ atlas-computing/computing.php

[55] https://twiki.cern.ch/twiki/bin/view/Atlas/ DoxygenDocumentation

[56] https://hypernews.cern.ch/

[57] https://twiki.cern.ch/twiki/bin/view/AtlasProtected/BPhysWorkingGroupAnalysisAndVertexing

[58] http://www-zeuthen.desy.de/technisches_seminar/texte/dq2.pdf

[59] G. Altarelli, M. Mangano (Eds.) *Proceedings of the workshop on the Standard Model physics (and more) at the LHC*, CERN 2000-004

[60] The ATLAS Collaboration *Expected Performance of the ATLAS Experiment, Detector, Trigger and Physics* CERN-OPEN-2008-020

[61] The ATLAS Collaboration *The ATLAS B-physics Trigger*Simon George, University of London, Surrey TW20 0EX,UK

[62] ATLAS Collaboration.*ATLAS DETECTOR AND PHYSICS PERFORMANCE,Technical Design Report,Volume I and Volume II)* CERN/LHCC 99-14,25 May 1999

[63] C. Amsler et al. *Physics Letters B667, 1 (2008)* Particle Data Group, www.iop.org/journals/jphysg

[64] Dan Green *The Physics Of Particle Detectors*Cambridge University Press 2000

[65] James D. Bjorken, Sidney D. Drell *Volume I: Relativistic Quantum Fields,Volume II: Relativistic quantum mechanics* McGraw Hill Book Company, New York 1964

[66] Jaroslav Guenther*Study of b-quark production in decay channels with J/ψ on ATLAS at LHC, Bachelor Thesis*, Faculty of Nuclear Science and Physical Engineering, prom. fyz Václav Vrba, CSc., 2007 Institute of Physics, 1994

[67] J. Blank, P. Exner, M. Havlíček, *Hilbert-Space Operators in Quantum Physics*, American Institute of Physics, 1994

[68] Pavel Jez Early physics at LHC with the detector ATLAS Czech Technical University 2008

[69] J. Chýla, *Quarks, partons and Quantum Chromodynamics*, lecture notes, http://www-hep2.fzu.cz/Theory/notes/text.pdf

[70] S. F. Novaes, *Standard model: An introduction*, 10th Jorge Andre Swieca Summer School: Particle and Fields, Sao Paulo, Brazil, 31/1 - 12/2 1999, hep-ph/0001283

[71] Mikio NAKAHARA *GEOMETRY, TOPOLOGY AND PHYSICS, Second Edition*, Department of Physics Kinki University, Osaka, Japan, 2002.

[72] B.R.Martin& G.Shaw *Particle Physics, SECOND EDITION*, Department of Physics and Astronomy, University College London, Department of Theoretical Physics, University of Manchester, reprinted March 2003.

[73] N. Cabibbo, Phys. Rev. Lett. 10, 531 (1963).

[74] M. Kobayashi and T. Maskawa, Prog. Th. Phys. 49, 652 (1973).

[75] C. Jarlskog, Phys. Rev. Lett. 55, 1039 (1985); Z. Phys. C29, 491 (1985).

[76] R. Aleksan, B. Kayser and D. London, Phys. Rev. Lett. 73, 18 (1994).

[77] Guy D.Coughlan, James E.Dodd, Ben M.Gripaios *The Ideas of Particle Physics An Introduction for Scientists, Third edition*, Cambridge University Press, 2006.

[78] I. Bigi et al., hepph/9401298.

[79] Yuval NE'EMAN and Yoram Kirsh *The Particle Hunters, Second edition*, Cambridge University Press, 1996.

[80] W-M Yao et al 2006 *J. Phys G: Nucl. Part. Phys.* 33 1 http://stacks.iop.org/JPhysG33/1

[81] *Determination of the* $B_d^0 \rightarrow D^* l\nu$ *Decay Width and* $|V_{cb}|$,arXiv:hep-ex/0210040 v1 16 Oct 2002

[82] *A measurement of the* $B^0\overline{B}^0$ *oscillation frequency and determination of flavor-tagging efficiency using semileptonic and hadronic* B^0 *decays* ,BABAR-CONF-00/08, SLAC-PUB-8530, August 8, 2000

[83] *Measurement of the* $B_d^0 - \overline{B}_d^0$ *Oscillation Frequency* ,CERN-EP/98-28 (revised), March 23, 1998

[84] B. Blok, M. Shifman and D.-X. Zhang, Phys. Rev. D57, 2691 (1998); (E) Phys. Rev. D59, 019901 (1999).

[85] I. Bigi et al., Phys. Rev. D59, 054011 (1999); I. Bigi and N. Uraltsev, Phys. Rev. D60, 114034 (1999); Phys. Lett. B457, 163 (1999).

[86] B. Grinstein and R. Lebed, Phys. Rev. D57, 1366 (1998); Phys. Rev. D59, 054022 (1999).

[87] *Writing B-physics analysis code in Athena* ,CERN-EP/98-28 (revised), March 23, 1998

[88] http://documents.cern.ch/cgi-bin/

[89] S. Eidelman *et al.*, Physics Letters B592, 1 (2004)

[90] *Rare B Decays into States Containing a J/ψ Meson and a Meson with $s\overline{s}$ Quark Content*, BABAR-PUB-02/07, SLAC-PUB-9262, hep-ex/0000000

[91] *Exclusive Semileptonic and Rare B-Meson Decays in QCD*, arXiv:hep-ph/9805422 v2 10 Jul 1998

[92] *Standard model matrix elements for neutral B-meson mixing and associated decay constants*, arXiv:hep-ph/0011086 v2 28 Feb 2002

[93] *CP Violation and B Physics at the LHC*,arXiv:hep-ph/0703112v1 12 Mar 2007

[94] C. DAmbrosio, T. Gys, C. Joram, M. Moll and L. Ropelewski Particle Detectors Principles and Techniques CERN Academic Training Programme 2004/2005

[95] *Flavour Dynamics: CP Violation and Rare Decays*, arXiv:hep-ph/0101336 v1 30 Jan 2001

[96] *RARE B DECAYS AT BELLE*, arXiv:hep-ex/0205033 v3 21 May 2002

[97] *J/ψ Production at LEP: Revisited and Resummed*, arXiv:hep-ph/9810364 v2 19 Oct 1998

[98] http://atlas-computing.web.cern.ch/atlas-computing/projects/twikiUtils/

[99] https://twiki.cern.ch/

[100] https://svnweb.cern.ch/trac/atlasoff/browser

[101] http://castor.web.cern.ch/castor/DOCUMENTATION/

[102] http://pdg.lbl.gov/

[103] http://glite.web.cern.ch/glite/

[104] https://gus.fzk.de/pages/home.php

[105] http://grid-deployment.web.cern.ch/grid-deployment/documentation/

[106] http://lcg.web.cern.ch/LCG/

[107] http://gridui02.usatlas.bnl.gov:25880/server/pandamon/

[108] http://dashb-atlas-data.cern.ch/dashboard/request.py/site

[109] http://www.slac.stanford.edu/xorg/hfag/rare/index.html

[110] http://atlas.ch/

[111] http://aliceinfo.cern.ch/

[112] http://cms.cern.ch/

[113] http://lhcb.web.cern.ch/lhcb/

[114] I. Nomidis on behalf of the ATLAS Collaboration, Preparations for precise measurements of rare muonic B-decays Aristotle University of Thessaloniki

[115] http://agenda.cern.ch/tools/SSLPdisplay.php?stdate=2006-07-03&nbweeks=6

[116] https://twiki.cern.ch/twiki/bin/view/Atlas/TriggerDAQ

[117] http://www.hep.ucl.ac.uk/atlas/atlantis/

[118] http://www.thep.lu.se/ torbjorn/Pythia.html

[119] http://atlas-computing.web.cern.ch/atlas-computing//documentation/swDoc/

[120] http://root.cern.ch/

[121] Erez Etzion on behalf of the ATLAS Collaboration B-Physics and Quarkonia studies with early ATLAS data Tel Aviv University

[122] http://proj-gaudi.web.cern.ch/proj-gaudi/

[123] https://twiki.cern.ch/twiki/bin/view/Atlas/DistributedAnalysisUsingGanga

[124] http://projects-docdb.fnal.gov/cgi-bin/ShowDocument?docid=91

[125] https://twiki.cern.ch/twiki/bin/view/Atlas/GangaWithAtlantis

[126] http://ganga.web.cern.ch/ganga/presentations/index.html

[127] http://ganga.web.cern.ch/ganga/documents/index.html

[128] http://en.wikipedia.org/wiki/Main_Page

[129] https://twiki.cern.ch/twiki/pub/Atlas/AtlasComputingOperationsCZ/DDM_Shift_Instructions.pdf

[130] https://twiki.cern.ch/twiki/bin/view/Atlas/CoolLumiCalcTutorial